NORTHWESTERN UNIVERSITY

The Modulation of Magnetic Properties in Magnetic Resonance Imaging Contrast Agents using Enzymes

A DISSERTATION

SUMBITTED TO THE GRADUATE SCHOOL
IN PARTIAL FULFILLMENT OF THE REQUIREMENTS

for the degree

DOCTOR OF PHILOSOPHY

Field of Chemistry

By

Paul June Hyung Lee

EVANSTON, ILLINOIS

December 2008

Abstract

THE MODULATION OF MAGNETIC PROPERTIES IN MAGNETIC RESONANCE IMAGING CONTRAST AGENTS USING ENZYMES

Paul June Hyung Lee

Magnetic resonance imaging (MRI) is an advanced imaging modality that is experiencing increasing popularity in clinical and experimental settings. MRI enjoys the benefit of high-resolution, the use of non-ionizing radiation, and the ability to distinguish between soft tissues. MR imaging is enhanced with the use of Gd^{3+} chelated contrast agents; however the current commercially available contrast agents for MRI are low relaxivity, monomeric vascular agents. A new generation of MR contrast agents has been developed that addresses the need for these agents to respond to localized biological environments. This thesis expands upon a family of enzyme-activable MR contrast agents.

This thesis concerns the design, synthesis, and characterization of lanthanide complexes that change relaxivity in response to hydrolyzing enzymes. Chapter 2 describes a MR contrast agent with a pendant galacto-D-pyranose sugar attached to a Gd^{3+} chelator via a self-immolative linker that is sensitive to β-galactosidase. Chapter 3 introduces a phosphatase activatable MR contrast agent that uses an inter- and intra-molecular binding to inhibit inner sphere water molecules from coordination to the lanthanide. Chapter 4 describes the use of an alkyl bridge to block water access to the macrocyclic Gd^{3+} chelator. The addendum presents a nitrogen mustard alkylating agent conjugated to a Gd^{3+} chelate to slow the tumbling rate once attached to DNA.

Acknowledgements

Graduate school has been a trying time for me. It is only with the support of wonderful people in my life that I have mustered enough courage to continue with my studies. It is said that the important object lesson is not what one does in life, but with whom one does it.

I would first like to thank my lovely wife, Page Hayton Lee, who has been my support and encouragement throughout my time in graduate school. She has brought much perspective to my life at the times when I have most needed it. She graces my life with wisdom and enriches it beyond measure.

I would like to acknowledge my family, who has been a constant source of strength and love. My father, John Jung Hoon Lee, and my mother, Grace Soon Woo Lee, have given me counsel about life and school. They have given to me without any reservations or motive. My sister, Esther Lee, has been a patient ear and a voice of reason. To my family, I would like to dedicate this thesis.

I would like to thank Dr. Thomas J. Meade, my principal investigator. I appreciate his advice and he has been patient through my many moments of self-doubt. He has allowed me to pursue my intellectual curiosity, and he is generous with his time and resources. His unrelenting work ethic is an inspiration to me.

There are many members of the Meade lab who have taught me so much about chemistry. From my early years, I would like to acknowledge Dr. Frank Femia, Dr. Matthew Allen, Carrie Allen, and Dr. Joseph Duimstra. They have been patient with my shortcomings and have lent me wise counsel. I would especially like to thank Dr. Luca Frullano, who has set the standard of what great chemists should be. I admire him as a

scientist and as a friend. Dr. Amanda Eckermann has helped me become a better writer and I want to thank her for her help in preparing some of my manuscripts, and certainly this thesis. Other notable people in the Meade lab whose expertise and friendship have made my graduate school worthwhile are Dr. Ji Youn Lee, Keith Macrenaris, Brad Ulrich, Ying Song, and Dr. Paul Endres.

I would like to extend my appreciation to the number of high-quality professors I have encountered here. Dr. Kenneth Spears is an example of a great instructor with the heart and knowledge to help young students along. I respect him much for his humility and intelligence. I would also like to thank Dr. Chad Mirkin, for whom I had the privilege to TA. He drove me hard, but I learned so much from his management style and his personality. I also appreciate the two members of my committee. Dr. Mark Ratner is a truly wise and knowledgeable professor. He is the model of a decent person, who does not let prestige or power change how he treats others. If I ever become famous, he is the person I would most like to emulate. Dr. Thomas O'Halloran has given me new viewpoints and wise counsel through my challenging academic journey. Dr. Richard Silverman, I just like you; you are tough but fair. All of you have taught me much.

And last but not least, I would like to thank all my friends outside of graduate school who have made my life interesting and enjoyable. It is true that graduate students need a life outside of their studies. Thank you.

Abbreviations

Abbreviations	Definition
Units	
^{o}C	celsius
nm^{-1}	wavenumber
cm	centimeter
s	second
m	minute
h	hour
d	day
K	kelvin
M	molar
MHz	megahertz
mM	millimolar
mmol	millimole
mol	mole
mV	millivolt
nm	nanometer
ns	nanosecond
μm	micrometer
μmol	micromole
Chemicals	
BSA	bovine serum albumin
CAM	cerium ammonium molybdate
CDI	carbonyl diimidazole
cyclen	1,4,8,10-tetraazacyclotetradodecane
DMAP	N,N-dimethylamino pyridine
DMF	N,N-dimethylformamide
DMSO	dimethyl sulfoxide
ACN	acetonitrile
DNA	deoxyribonucleic acid
DO3A	N,N',N"-ticarboxymethylene cyclen
DOTA	N,N',N",N"'-tetracarboxymethylene cyclen
DTPA	diethylenetriaminepentaacetic acid
Et_2O	diethyl ether
EtOAc	ethyl acetate
EtOH	ethanol
HSA	human serum albumin
Gd	gadolinium
Eu	europium
Tb	terbium
AP	alkaline phosphatase
IPA	isopropyl alcohol

Ln	lanthanide
MeOH	methanol
MOPS	3-(N-morpholino)propanesulfonic acid
NBS	N-bromosuccinimide
Ph	phenyl
Ox	oxalate
PNG	*p*-nitrophenyl-β-D-glucuronide
DBU	Diaza(1,3)bicyclo[5.4.0]undecane
THF	tetrahydrofuran
pNPP	*p*-nitrophenyl phosphate
ONPG	*o*-nitrophenyl-β-D-galactoside
PPh_3	triphenylphosphine
TFA	trifluoroacetic acid
TEA	triethylamine
TMS	tetramethylsilane
CH_2Cl_2	dichloromethane/methylene chloride
β-gal	beta-D-galactosidase
MMP	matrix metallo-protease

General

RT	room temperature
EA	elemental analysis
EPR	electron paramagnetic resonance
ESI	electrospray ionization
MS	mass spectrometry
FT	Fourier transform
FTIR	Fourier transform infrared
HPLC	high performance liquid chromatography
ICP-MS	inductive coupled plasma mass spectrometry
LC-MS	liquid chromatography mass spectrometry
MR	magnetic resonance
MRI	magnetic resonance imaging
NMR	nuclear magnetic resonance
ParaCEST	paramagnetic chemical exchange saturation transfer
PMT	prodrug monotherapy
UV-Vis	ultraviolet – visible spectroscopy

Symbols

br	broad
d	doublet
$E_{1/2}$	half reaction potential
H_o	applied magnetic field
$\mathbf{H_o}$	applied magnetic field vector
I	nuclear angular momentum quantum number
J	NMR coupling constant

k_B	Boltzmann constant
L	orbital angular momentum quantum number
M	magnetization magnitude
$\boldsymbol{M}$	magnetization vector
m	multiplet
m/z	mass to charge ratio
M_o	equilibrated magnetization vector
Pm	mole fraction of contrast agent
δ	chemical shift
k_{cat}	catalysis rate
q	number of inner sphere water molecules
r_1	longitudinal relaxivity
r_{1P}	corrected longitudinal relaxivity
R_f	retention factor
s	singlet
S	spin quantum number
T	temperature
t	triplet
T_1	longitudinal nuclear relaxation time
T_e	longitudinal electronic relaxation time
T_2	transverse nuclear relaxation time
T_{2e}	transverse electronic relaxation time
V_{max}	maximum velocity
γ_H	proton gyro-magnetic ratio
ε	molar absorptivity
λ_{em}	emission wavelength
λ_{ex}	excitation wavelength
$\boldsymbol{\mu}$	magnetic moment vector
μ_B	Bohr megneton
τ_c	total correlation time
τ_D	diffusional correlation time
τ_m	water residency lifetime
τ_r	rotational correlation time
χ	magnetic susceptibility
ω_H	proton Larmor frequency

Table of Contents

List of Figures

List of Tables

List of Schemes

Chapter 1:

Introduction

Introduction:

Magnetic Resonance Imaging: A historical prospective:

The foundations of magnetic resonance imaging (MRI) are found in the discovery of nuclear spin. In 1922, nuclear spin phenomenon was discovered by two German physicists, Otto Stern and Walther Gerlach. They were able to measure the effect of nuclear spin by deflection of a beam of hydrogen molecules in an inhomogenous magnetic field.[1] This experiment demonstrated the basic principles of quantum mechanics, in which the deflections were found to have discrete values. The Stern-Gerlach experiment revealed that the distribution of possible angular momenta was not continuous; rather that spin angular momentum was quantized. Otto Stern became professor of physics at Carnegie Institute of Technology and was the sole recipient of the 1943 Nobel Prize in Physics. The award never mentioned the Stern-Gerlach experiment, as Walther Gerlach was working in Nazi Germany.

Cornelis Gorter from the Netherlands began experimenting with relaxation properties of paramagnetic salts using a calorimetric method in 1931. Gorter attempted to observe transitions in two Zeeman states by passing a magnetic wave into highly anisotropic environments and measuring minute temperature shifts from ^{1}H in $K[Al(SO_4)_2]\cdot 12H_2O$ salts and ^{7}Li in LiF crystals.[2] These experiments were carried out in liquid hydrogen, with a 20 MHz alternating field, in strong magnetic fields (B_1), as high as 1 mT. Gorter first described paramagnetic relaxation in 1936, but his caloric method missed the nuclear spin resonance.

Isidor Isaac Rabi received a fellowship to study with some eminent physicists, among them Otto Stern. Afterward, Rabi became a physics professor at Columbia University,

where he began his investigations into the nature of the forces which bind protons to atomic nuclei. In September 1937, Gorter made history when visiting Rabi's lab. Gorter suggested that the beam should pass thorough a region with a constant magnetic field with weak radio frequency at right angles by coils at the resonance frequency to observe nuclear-spin resonance experimentally.[3] After this conversation, Rabi demonstrated how to measure the nuclear magnetic moment. This led to the publication of 'A New Method of Measuring Nuclear Magnetic Moment' in 1938.[4] Rabi discovered that spin state transitions could be induced using time-varying radio frequencies (RF).

The Rabi oscillations are the working mechanism for the nuclear magnetic resonance (NMR) instruments used for chemical analysis today. Gorter was the physicist who came up with idea and spoke in haste at his Columbia visit. Rabi manifested Gorter's idea as a tangible experiment and showed how nuclear moments can be observed empirically. Rabi received the Nobel Prize in Physics in 1944 for the atomic and molecular beam magnetic resonance method of observing atomic spectra.

The next step in the evolution toward MRI was the discovery of NMR. Felix Bloch, born in Zurich in 1905, taught at the University of Leipzig. He joined the faculty of Stanford in 1934, where he discovered NMR phenomenon with water and worked out the equations necessary for the NMR.[5] Independently, Edward Purcell of Harvard University discovered the NMR phenomenon while experimenting with solid state NMR using paraffin in 1946.[6] The two scientists were awarded the Nobel Prize in Physics in 1952 for their development of new methods for nuclear magnetic precision measurements. Their pioneering work led to the construction of the first commercial NMR, called Varian A-60, in 1958. Although NMR spectra are commonplace today for chemical

characterization, it was during the 1950s and 1960s that NMR was being developed as an analytical tool. E.J. Corey was one of the first organic chemists to begin to publish his compounds with NMR characterization.[7]

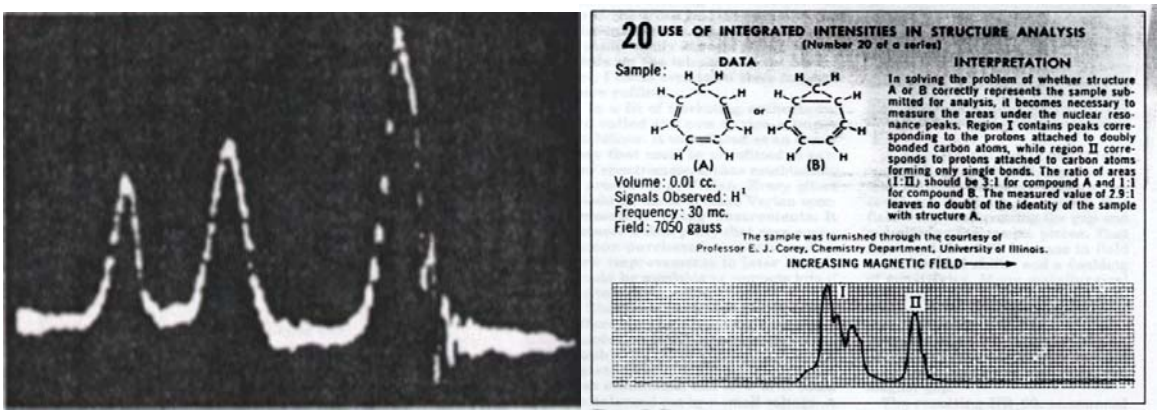

Figure 1-1: a) One of the first spectra taken on the Varian A-40 of ethanol. The methyl, methylene, and alcohol peaks are observed. b) E.J. Corey NMR characterization of cyclohexadienone.[7]

The invention of MRI soon followed. Paul Lauterbur is given credit for introducing the gradient field to NMR that allowed for spatial resolution for two-dimensional images. Legend has it that Lauterbur came up with the idea for MRI at a local sandwich shop and wrote it on a napkin as a graduate student in 1962. He later became a professor at University of Illinois Urbana-Champaign. Some of the first images that Lauterbur took with his new imaging modality were of a clam his daughter collected from a beach, a green bell pepper, and two test tubes of heavy and normal water. Lauterbur called his technique Zeugmatography, which in Greek means “yoke,” or “joining together.” By analysis of the characteristics of the emitted radio waves, he could determine their origins

in space. This made it possible to build up two-dimensional pictures of structures using the concentration of water protons in a voxel, which is a volumetric pixel. Lauterbur first submitted his findings to *Nature* in 1973, describing the fundamental principles of MRI, but his paper was rejected because his images of heavy and ordinary water were too "fuzzy."[8] After much cajoling by Lauterbur, the editors of *Nature* eventually capitulated and published his two-page essay, which became an article that changed the way we image the human body today.

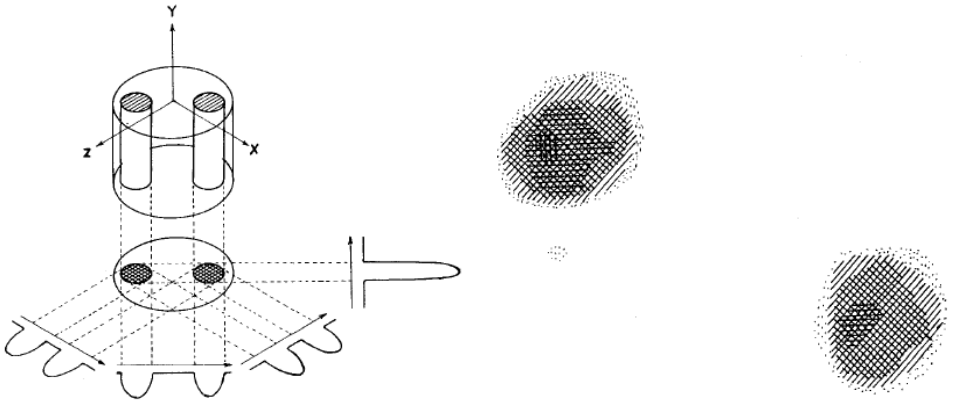

Figure 1-2: From *Nature* paper describing Zeugmatography using cylinders of normal and heavy waters. Lauterbur describes the relationship between the three-dimensional object and the two-dimensional images, made possible with the use of gradient fields.[8]

In 1975, Richard Ernst took Lauterbur's back projection and used switched gradient fields in the time domain. Ernst developed the methodology of short, intense pulses of radio-frequency for nuclear magnetic resonance (NMR) spectroscopy, which allowed for faster acquisition of MRI data and multidimensional processing of NMR. That same

year, Ernst published "NMR Fourier Zeugmatography," the basic reconstruction of MR imaging still used today.[9] The faster processing allowed for the massive amounts of data from a single MRI scan to be feasibly processed into an image. Ernst in 1991 was awarded a Nobel Prize in Physics for his work in Fourier transform and multi-dimensional NMR of Lauterbur's back projection.

Taking Lauterbur's initial work one step further, Peter Mansfield of the University of Nottingham developed a mathematical process to speed the image reading. The first image of a human body part, taken in 1976, was of his finger.[10] Mansfield developed echo-planar imaging reduces which reduces influences of field inhomogeneity in static magnetic fields utilizing gradients field. He developed a new imaging trajectory that allows for faster mathematical analysis, which allows for MRI to become practical for faster imaging.[11] This led to new techniques such as fMRI and MR angiography.

In 1977, Raymond Damadian, a medical doctor at Downstate Medical Center Brooklyn, came up with an apparatus and method for detecting cancer using the T_1 and T_2 relaxation times and MRI technology. He found that cancerous rat tissue had longer relaxation times than normal tissues using his Field Focusing NMR (Fonar) system. The Fonar methodology never had the capacity to see images, only looked at relaxation times of tissues. Damadian accused the Nobel committee of overlooking his contributions when Lauterbur and Mansfield were awarded the 2001 Nobel Prize in Physiology and Medicine for the progress they made in magnetic resonance imaging. Despite Damadian's protest, commanding a full page of the *New York Times*, the Nobel committee did not change their decision.[12]

The bold research of many creative thinkers in the field of MRI has laid the groundwork for current clinical imaging. With this foundation laid, the remainder of this thesis will explicate my doctoral research on novel MRI contrast agents.

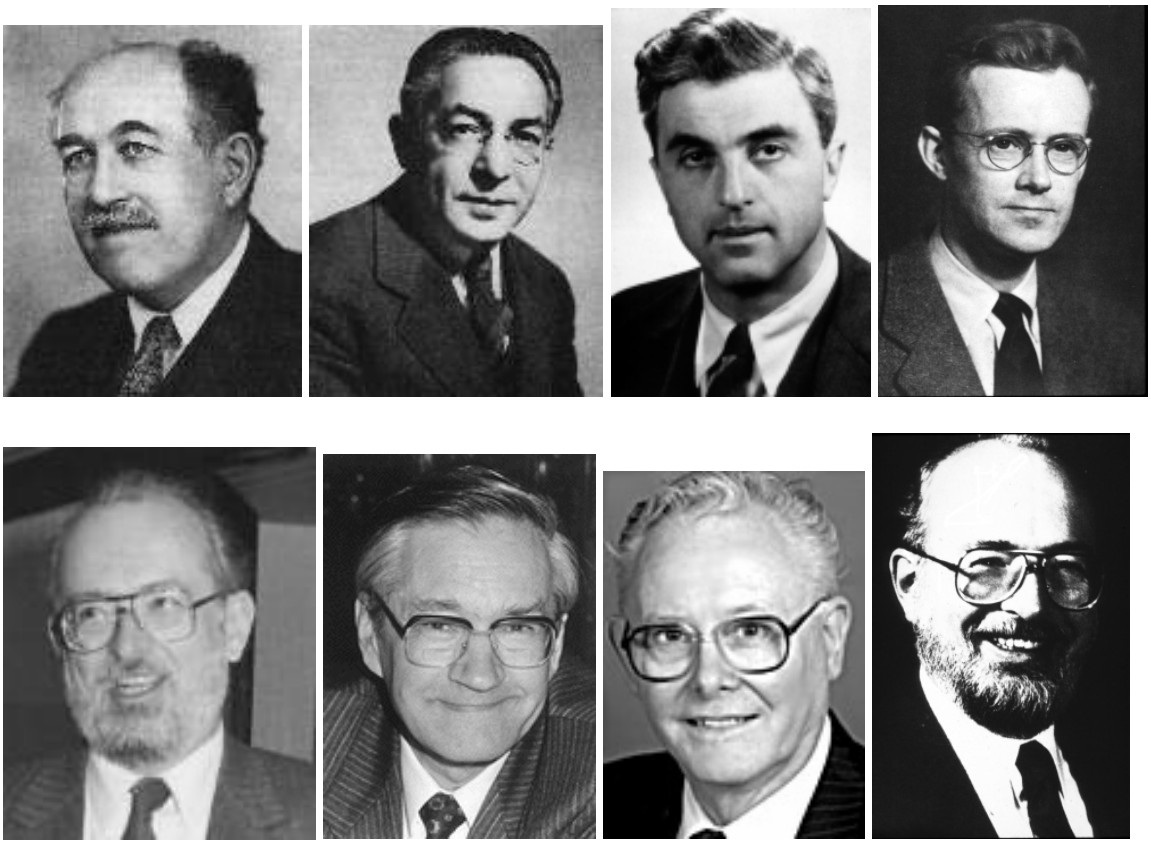

Figure 1-3: Photographs of important figures in the development of magnetic resonance imaging. (From left to right) Top row: Otto Stern, Rabi, Felix Bloch, Edward Purcell. Bottom row: Paul Lauterbur, Richard Ernst, Peter Mansfield, Raymond Damadian.

Magnetic Resonance Imaging Fundamentals:

Atomic nuclei have quantized angular momentum. The nuclei can be visualized as a vector rotating around an axis through its center. Nuclei with an even mass number (equal numbers of neutron and protons) have spin quantum numbers that are even multiples of $^1/_2$ (I = 0, 1, 2,…), while nuclei with odd mass numbers have spin numbers as odd multiples of $^1/_2$ ($I = {}^1/_2, {}^3/_2, {}^5/_2, \ldots$).[13] Nuclei with a spin quantum number of $I = 0$ cannot be studied with NMR because they are unresponsive to magnetic fields. The most common nuclei studied in NMR are those with $I = {}^1/_2$. (i.e. ^{1}H, ^{13}C, ^{31}P, ^{17}O, ^{19}F, ^{29}Si, ^{15}N, ^{14}N, ^{113}Cd, ^{195}Pt, ^{10}B, ^{11}B, ^{23}Na, ^{35}Cl.) Odd quantum spin values allow nuclei to be sensitive to magnetic fields. The spin characteristic of nuclei is intrinsic with a magnitude $\boldsymbol{I}$, which can be defined as a vector:

$$|\boldsymbol{I}| = \hbar \sqrt{I\ (\ I+1\ )}\quad ,\quad \hbar = h/2\,\pi \qquad \textbf{Equation 1.1}$$

where h is Plank's constant and I is the spin quantum number.

Although these nuclei are not in physical rotation per se, the nuclei are treated as classical particles, with individual nuclei possessing a vector $\boldsymbol{I}$. With the introduction of an external magnetic field $\boldsymbol{B}_o$, a certain population of spin vectors will align with the magnetic field N_{up}, while others will align opposing it N_{down}.[14]

$$\frac{N_{up}}{N_{down}} = \exp\left(\frac{\gamma\hbar\boldsymbol{B}_0}{k_B\ T}\right) \qquad \textbf{Equation 1.2}$$

The population difference is determined by a Boltzmann distribution k_B, expressed in **Equation 1.2**, with a slightly higher population of spin vectors in the lower energy state aligned with B_o. The ensemble of I results in a net magnetic moment M, along the axial magnetic field which process at the Larmor frequency that is correlated with strength of the magnetic field.[13]

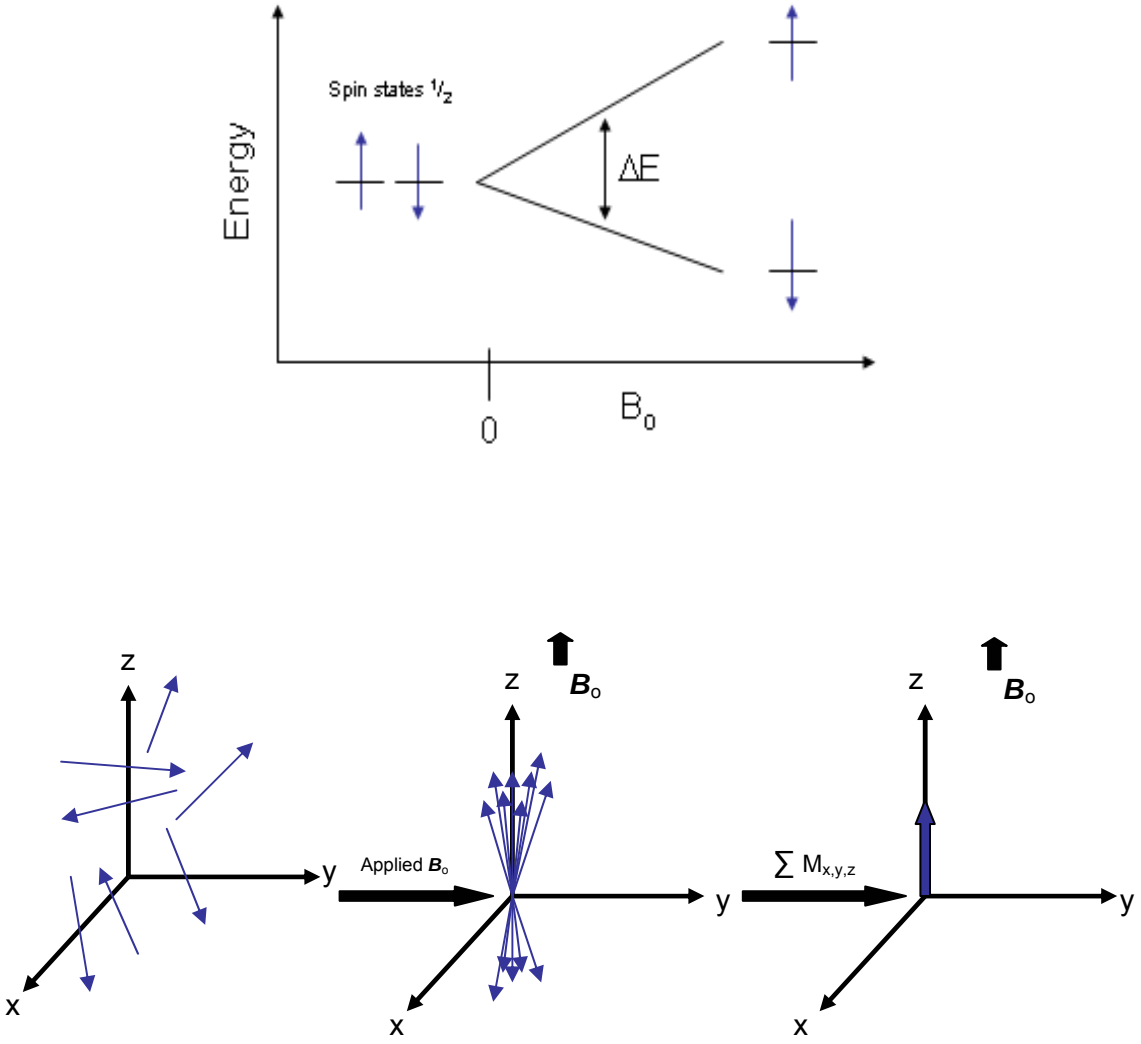

Figure 1-4: a) The Zeeman Effect of nuclei with ½ spin states. One spin state aligns with the magnetic field B_o, which is the lower energy state. The other spin state aligns

against the magnetic field, which is depicted by the spin state in the higher energy state.

b) The spin vectors in an anisotropic environment become organized once they encounter an applied magnetic field $\boldsymbol{B}_o$. The bulk magnetization $\boldsymbol{M}$, results from the ensemble of unequal population of spins in different energy states. The nuclei are constantly spinning at the Larmor frequency, ω_L.[15]

The two spin states are separated by the magnetic field via the Zeeman Effect (**Figure 1-4**). The Zeeman Effect stipulates that a dynamic equilibrium is held between the energy of the two spin states. The energy difference is defined as ΔE. Electromagnetic radiation with the exact ΔE can induce transitions between the spin states. The Zeeman states are temperature dependent as seen in **Equation 1.2** depicted as variable *T*. For room temperature, the transitions between $\pm^1/_2$ spin states can be induced using radio frequency waves (RF).[14] Super-conducting magnets require energy in the microwave range for the nuclei spins to change energy states. Furthermore, the energy difference (ΔE) between the neighboring states is directly correlated with the magnetic field strength as given by: $\Delta E = \gamma \hbar \boldsymbol{B}_o$, where the constant γ is the gyromagnetic ratio and $\hbar$ is derived from Plank's constant. Thus, the ΔE is directly proportional to the strength of the applied magnetic field.

$$\boldsymbol{M} = \sum \gamma I \qquad \textbf{Equation 1.3}$$

$$\boldsymbol{M} = M_x + M_y + M_z \qquad \textbf{Equation 1.4}$$

A net magnetization observed in the direction of $\boldsymbol{B}_o$, termed $\boldsymbol{M}$, represents the ensemble of magnetic moments of spin states parallel and anti-parallel with the applied magnetic field. **Equation 1.3** and **Equation 1.4** demonstrate the sum of all the spin vectors I with M_x, M_y, and M_z components to collectively form the net magnetization $\boldsymbol{M}$. The individual magnetic moments have a precessing rotation with the Larmor Frequency that is dependent on the strength of the magnet.

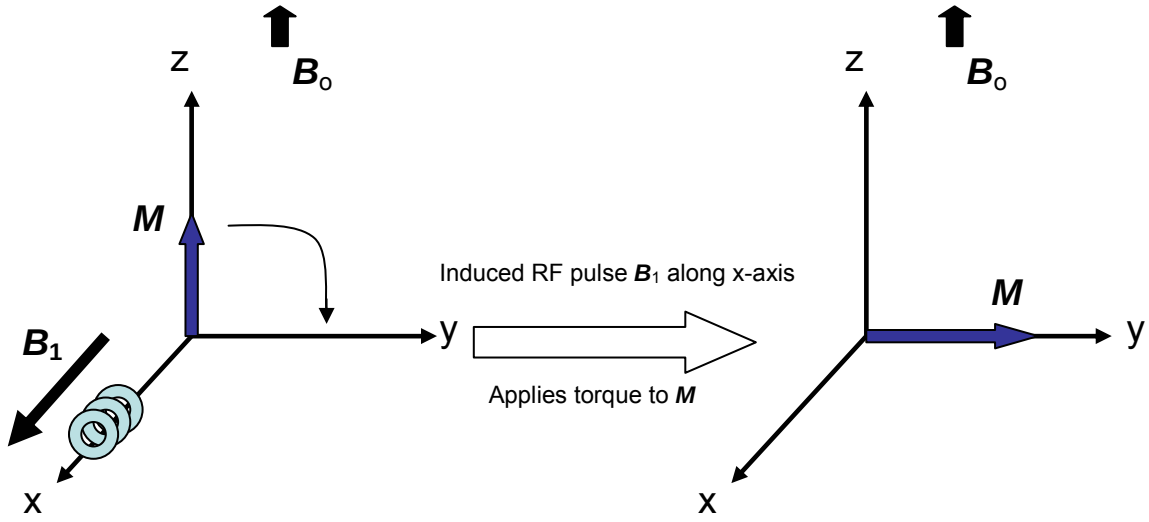

Figure 1-5: a) The RF coil generates a magnetic field along x-axis. This excitation turns the $\boldsymbol{M}$ to an angle (α) during the RF excitation. This example demonstrates a 90 degree torque with the application of the RF pulse into the xy plane.

During the excitation process, a coil is placed perpendicular to the applied magnetic field, $\boldsymbol{B}_o$ (**Figure 1-5**). This coil is fed a sinusoidal current with angular frequency (Ω), which causes the perpendicular magnetic field $\boldsymbol{B}_1$ to be introduced into the

environment. The net magnetization vector $\boldsymbol{M}$ will torque toward the xy plane in the presence of the new magnetic field $\boldsymbol{B}_1$. The induced RF ($\boldsymbol{B}_1$) causes the magnetization to flip, and a magnetization angle (α) is observed. Once the RF is turned off, the $\boldsymbol{M}$ will return to its original equilibrium state, which is aligned with the $\boldsymbol{B}_o$.

After the RF excitation with a 90^o pulse, $\boldsymbol{M}$ displays a detectable rotating magnetization $\boldsymbol{M}_{xy}$. The detection pulse is in the plane of the xy domain, and only the magnetization in the direction perpendicular to $\boldsymbol{B}_o$ will be observed. Signals measured with the receiver coil produce free induction decay (FID), which is deconvoluted using the Fourier Transform, to give a NMR spectrum. The nuclear spins will interact with the lattice and other spins states while returning to their ground state that alters the time taken to get the system back into equilibrium in a process called relaxation.

There are two categories of relaxation processes: the spin-lattice and spin-spin relaxation. The spin-lattice relaxation time (T_1) is the amount of time for the net magnetization to return longitudinally along the z-axis to equilibrium after the perturbation by 180^o RF pulse. The spin-lattice relaxation cannot be measured directly because the detection from the receiver coils can only measure resonance signals at perpendicular angles to the applied magnetic field $\boldsymbol{B}_o$. The pulse sequence to measure T_1 is shown in **Figure 1-6a**. Applying an 180^o (inversion) pulse to the system tips $\boldsymbol{M}$ in the opposite direction of $\boldsymbol{B}_o$. At this moment, there is no xy planar component, thus giving a zero signal. Shortly thereafter, a 90^o pulse is given that torques the resonance signal in the xy plane, which allows for the detection of $\boldsymbol{M}$. A variable delay time (tau) is used between the 180^o and 90^o pulses to measure its effect on magnitude of $\boldsymbol{M}_{xy}$. From the

plot seen in **Figure 1-6b**, the longitudinal relaxation (T_1) is extrapolated from the inversion recovery spectra.

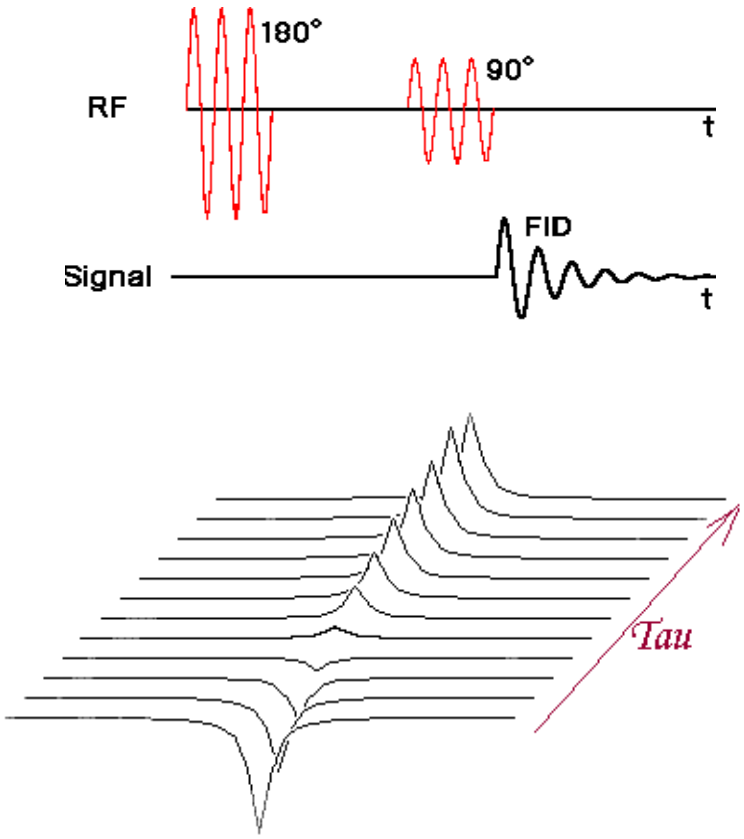

Figure 1-6: **a) TOP** The basic pulse sequence to measure the longitudinal relaxation time (T_1). **b) BOTTOM** A series of RF pulse sequences with varying Tau between the 180^o and 90^o pulse give the trajectory of the pulse signal. This gives the longitudinal proton relaxation time.

The second category of relaxation is called spin-spin relaxation (T_2). This magnetization property describes the transverse relaxation of $\boldsymbol{M}_{xy}$ as it loses phase

coherence. The pulse sequence used to measure T_2 is shown in **Figure 1-7**. After the 90° pulse, the $\boldsymbol{M}_{xy}$ begins to experience phase dispersion because of the random fluctuations of the angular velocities of each nuclear spin. This magnetization, presented in the xy-plane after the 90° pulse, measures T_2, which essentially is a dispersion time constant. Shortly after a variable delay time (Tau), an 180° pulse is given to the system. Interestingly, the coherence process briefly after the 180° pulse of the T_2 sequence is one of the known cases where the entropy of the system without additional energy decreases for a moment; an instance that violates the third law of thermodynamics.[16] The phase incoherence induced from the first delay time returns to phase on the opposite side after the 180° pulse. T_2 values are generally much less dependent on field strength ($\boldsymbol{B}_o$) than T_1 values because the de-phasing time constant is independent of $\boldsymbol{B}_o$. However, time constant T_2* is dependent on field strength and measures the actual decay rate of the observable NMR signal.[13] T_2* represents the rephasing time from all the field inhomogeneities, which are actually spin-echo gradient measurements.

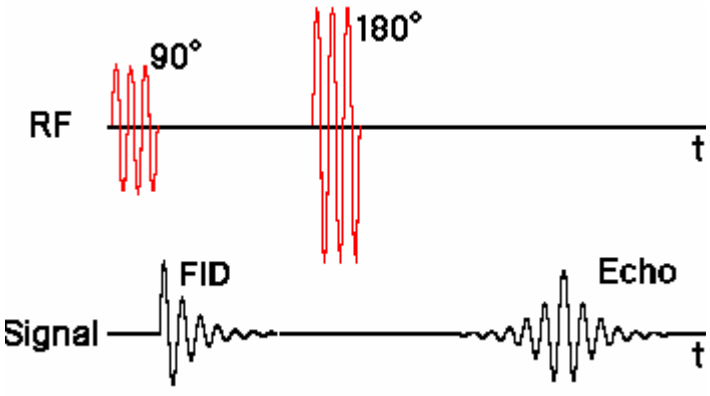

Figure 1-7: The pulse sequence of T_2 transverse relaxation rates, which determine the phase coherence in the $\boldsymbol{M}_{xy}$.

The relaxation T_i (i =1, 2) values can be correlated to an image seen with magnetic resonance imaging (MRI). Gradient fields of the x, y, and z components ($\boldsymbol{G}_{x,y,z}$) in the $\boldsymbol{B}_o$ allow for each region of nuclear spin to experience a unique magnetic field. The distinct magnitudes of rotating nuclear frequencies vary along the desired field and ultimately allow imaging of their position in space (**Figure 1-8**). The "slice" or the position of two-dimensional image can be selected with specific frequency (Ω) along a gradient field using a particular RF pulse. The thickness of the image is dependent on the strength of $\boldsymbol{B}_o$ and the gradient field $\boldsymbol{G}_{x,y,z}$. The stronger gradient fields and applied magnetic fields allow for better resolution of MR images.

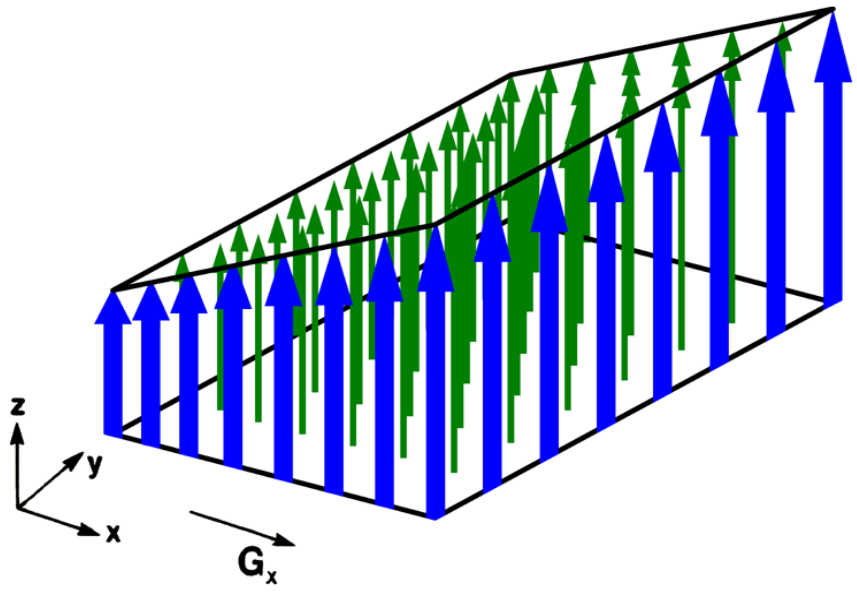

Figure 1-8: Gradient fields ($\boldsymbol{G}_{x,y,z}$) that allow for spatial positioning for resolution used for obtaining MR images.

The spatial resolution induced with gradient fields has a slightly different α angle for $\boldsymbol{M}_{xy}$, depending on their position along the combined magnetic fields. Each position in space corresponds to a k-space, which is a temporary time-domain space. MRI collects successive samples of different k-spaces and connects them to values using Fast Fourier Transform (FFT). FFT deconvolutes resonance signals from a rectangular Cartesian grid and correlates them back to the gradient frequency where they originated. This process matches different T_i (i = 1, 2) values to each k-space that is in the gradient field. The FFT approach has given way to new, more time-efficient methods that can sample multiple fields for each RF excitation.[17] Spiral FT imaging is a faster reconstruction algorithm that is a pattern strategy to sample the k-space within a single excitation sequence. Additionally, echo-planar imaging combats the field inhomogeneity and allow for tissue-specific factors into the acquired images. The T_i (i = 1,2) values from each k-space are related to a pixel on a gray scale; with the short T_1 values appearing as brighter pixels and shorter T_2 signals as darker pixels. Thus, the k-space can be correlated to an image where the spatially resolved unit is called a voxel. In practical terms, T_1-weighted images for MRI show the cerebral spinal fluid (CSF) as dark and T_2-weighted images show CSF as bright (**Figure 1-9**).

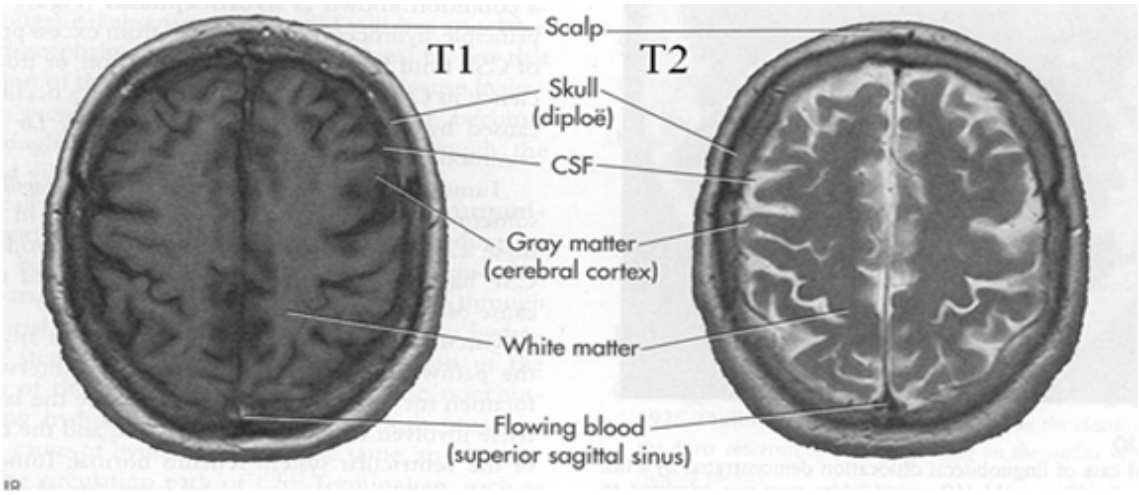

Figure 1-9: T_1 and T_2 weighted MR image of an axial section of the cranial region.[18]

A variety of parameters can influence intrinsic contrast in tissues for MR images. Tissues such as muscles and adipose have dissimilar T_i (i = 1,2) values because they have differing water proton densities and hydrocarbon/water concentrations. Pathologies can have altered values of T_i (i = 1,2), which might allow them to be distinguished from normal tissues. A good example is where MRI can distinguish between pathologic soft tissue is in the case of multiple sclerosis. Diffusion and flow of a fluid in the body can alter signals from MRI. A liquid flowing through a slice can experience an RF pulse and then flow out of the slice by the time the signal is recorded. Additionally, the magnet strength varies the image resolution. The resolution for current experimental MR imaging has reached regimes in the micrometer range, while clinical magnets are in the millimeter resolution range. Finally, temperature variations can alter the outcome of imaging.[19] Therefore, because of all the variability from one scan to the next, it is difficult to make true comparisons between two MR images. To make an accurate

association between T_1/T_2 values using MRI, a reference of known value must be taken in the same scan as the sample.[20]

Contrast-enhancing agents, which are the subject of this thesis, improve the signal to noise ratio (SNR) thereby enhancing the contrast observed in the MR image. MR contrast agents function by reducing the longitudinal and transverse relaxation times for T_1 and T_2, respectively. MR contrast agents are described as "T_1 agents" or "T_2 agents" depending on their relative reduction in relaxation times. Gadolinium (Gd^{3+}) is the lanthanide of choice for most T_1 relaxation agents.[17] Gd^{3+}-based agents are the most widely used for T_1 contrast because Gd^{3+} is the most paramagnetic, stable element with a spin state of $^7/_2$. Gd^{3+} lanthanides also possess a long electronic relaxation time (T_{1e}). This feature is ideal for quantum transfer of spin information to bulk water molecules, which results from the symmetric S state of the ion. A dipolar interaction between the surrounding water molecules and the lanthanide allows for transfer of faster relaxation rates for the protons on the surrounding water molecules.

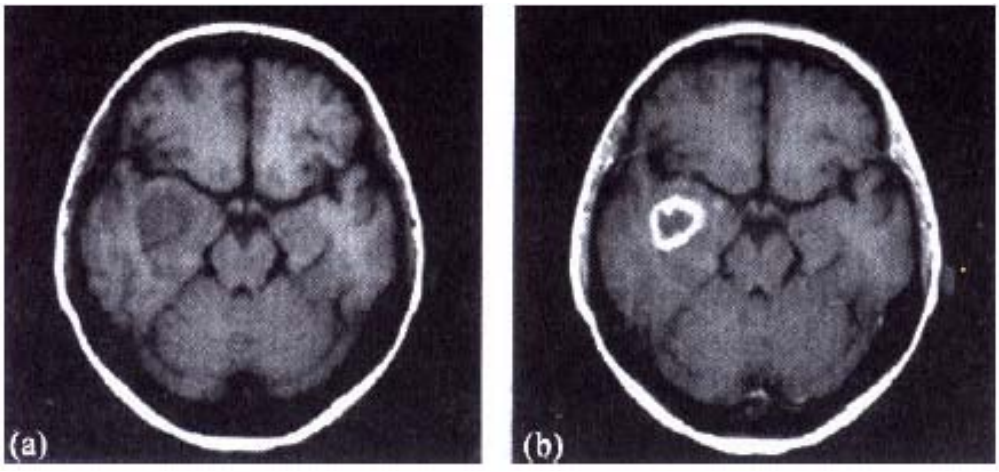

Figure 1-10: **a) LEFT** T_1-weighted axial slice of a cranium with mass lesion on the left temporal lobe **b) RIGHT** Identical T_1-image with MR contrast agent. Note the bright ring, which identifies the boundary of the tumor.[13]

Iron oxide particles are examples of MR contrast agents that influence T_2 more efficiently than T_1 and are thus labeled a T_2 agent. These T_2 relaxation agents are super-paramagnetic agents and are more efficient in affecting the transverse relaxation and accelerating the phase coherence dephasing time. This thesis will focus on T_1 MR contrast agents. For more information on T_2 agents, please refer to the review references at the end of this chapter.

The paramagnetic ion Gd^{3+} is known to be toxic and cannot be used as contrast agent in this aqua form. The ion must be chelated by a ligand; otherwise they would cause undesirable bio-distribution in vivo. It is believed that unchelated Gd^{3+} ions are cytotoxic because of their interaction with calcium channels. This interaction disrupts normal cellular function and results in deleterious biological consequences.[21] Lanthanide ions found in neurons can regulate synaptic transmission, as well as block some glutamate receptors.[22] Recently, Gd^{3+}-based MR contrast agents have been demonstrated to precipitate as crystals in the organs of a small percentage of the population.[23] The incidences of renal failure were especially high in the patients with kidney insufficiencies.[24]

Manipulations of the Gd^{3+}-chelators allow for enhanced relaxivity by modulating many of the parameters involved with contrast agents. The chelator can affect parameters to increase relaxivity, which is the efficiency of the contrast agents to relax the

surrounding water protons. Gd^{3+} based contrast agents shorten T_1 allowing for faster scans, which directly correlate with higher spatial resolution and sensitivity. More scans become possible with a given time, because not much time is needed between scans to get the proton spins back to equilibrium. Without paramagnetic species in solution, the relaxation times of a voxel are in the regime of seconds, but with MR contrast agents, T_i (i = 1, 2) can be diminished to milliseconds. Theoretical models were performed on the concentration needed for a satisfactory contrast enhancement in magnetic resonance images.[25] Contrast agents help elucidate structures in the MRI and enhance differences between tissues.

Role of Different Parameters in MR Contrast Agent Theory

MR contrast agents are molecules that shorten the relaxation times in the NMR time scale. Gd-based complexes have a more prominent effect on T_1 in relation to T_2 and are thus considered T_1 agents. The observed relaxation rate $(^1/T_1)_{obs}$ of the bulk water in MRI can be distributed into the diamagnetic component (subscript 'dia') and paramagnetic (subscript 'para') component in **Equation 1.5**. The diamagnetic component is the intrinsic relaxation property of the water voxel without any relaxation agents. Different biological tissues have inherently different T_1 values based on the proton densities of water and its interactions with its local environment. The paramagnetic component represents the effect of the Gd-complex on the longitudinal relaxation rates of the bulk water.

$$\left(\frac{1}{T_1}\right)_{obs} = \left(\frac{1}{T_1}\right)_{dia} + \left(\frac{1}{T_1}\right)_{para} \qquad \textbf{Equation 1.5}$$

$$\left(\frac{1}{T_1}\right)_{obs} = \left(\frac{1}{T_1}\right)_{dia} + r_1\ [\mathrm{Gd}] \qquad \textbf{Equation 1.6}$$

The paramagnetic component is directly proportional to the relaxivity (r_1) and the concentration of the Gd^{3+} complex [Gd], as demonstrated in **Equation 1.6**. The relaxivity is defined as the effectiveness of the paramagnetic substance to enhance the relaxation rate of the surrounding water protons.[26] The concentration of the Gd^{3+} complex is limited to the voxel in the MR image and restricted to the tissue distribution to where they are located.

$$\left(\frac{1}{T_1}\right)_{para} = \left(\frac{1}{T_{1\,para}}\right)^{IS} + \left(\frac{1}{T_{1\,para}}\right)^{OS} \qquad \textbf{Equation 1.7}$$

$$\left(\frac{1}{T_1}\right)^{IS} = \frac{cq}{55.5}\left(\frac{1}{T_{1m} + \tau_m}\right) \qquad \textbf{Equation 1.8}$$

The paramagnetic contribution to the overall T_1 relaxation is divided into the inner sphere (superscript 'IS') and outer sphere water (superscript 'OS') components (**Equation 1.7**). Inner sphere water, defined as *q*, is the number of water molecules that are directly coordinated to the Gd^{3+} center. The translational motion of inner sphere water diffuses to areas surrounding the complex becoming second and outer sphere

waters. The outer sphere contributions are from water molecules exterior to the first coordination shell of the Gd^{3+} complex that have diffused to the bulk water. This outer sphere contribution to relaxivity is a difficult parameter to modulate and remain as a constant background to the overall relaxivity.[14]

The inner sphere water contribution to the overall proton T_1 relaxivity is in **Equation 1.8**, where q is the hydration number of the complex, c is the molal concentration of Gd-complex, τ_m is the water exchange rate, and T_{1m} is the longitudinal proton relaxation rate. Longitudinal relaxivity ($1/T_1$) is directly proportional to parameters q and c, while other parameters do conduct such a linear correlation.

$$\left(\frac{1}{T_{1\,m}}\right) = \left(\frac{1}{T_1}\right)^{DD} + \left(\frac{1}{T_1}\right)^{SC} \qquad \textbf{Equation 1.9}$$

$$\left(\frac{1}{T_1}\right)^{DD} = \frac{2}{15}\left(\frac{\gamma_I^2\ g^2\ \mu_B^2}{r_{GdH}^6}\right) S(S+1) \left(\frac{\mu_0}{4\ \pi}\right)^2 \left(7\frac{\tau_{c2}}{1+\omega_s^2\ \tau_{c2}^2} + 3\frac{\tau_{c1}}{1+\omega_I^2\ \tau_{c1}^2}\right)$$

Equation 1.10

The longitudinal proton relaxation rate ($1/T_{1m}$) in **Equation 1.9** takes into consideration both dipole-dipole (DD) and scalar (SC) mechanism of relaxation. In images taken with MR instruments that use greater than 10 MHz, the inner sphere scalar component quickly diminishes to become insignificant due to its field dependency. The scalar interaction is mainly influenced by electron spin relaxation (T_{1e}) and by water exchange rates (τ_m).[13] Dipole-dipole coupling represents the interaction between the

lanthanide and the inner sphere water protons. The nuclear spins of the water protons interact with the regional fluctuating magnetic field caused by the 7 unpaired electrons of the Gd^{3+} ion. This interaction between water protons and the Gd^{3+} lanthanide demonstrates thorough-space character that diminishes at a rate of $1/r^6$ (r = distance) in relation to distance as demonstrated in **Equation 1.10**. The relaxation rates are expressed in the modified Solomon-Bloembergen equation in **Equation 1.10**, which includes: μ_B – the Bohr magneton, r_{GdH} – the electron spin proton distance, g – the electron g factor, ω_I – nuclear Larmor frequency, and ω_s - electron Larmor frequency.[17]

$$\left(\frac{1}{\tau_{c1}}\right) = \left(\frac{1}{\tau_R}\right) + \left(\frac{1}{T_{1e}}\right) + \left(\frac{1}{\tau_m}\right) \qquad \textbf{Equation 1.11}$$

The overall correlation time (τ_{c1}) included in **Equation 1.10** is the parallel sum different parameters in **Equation 1.11**. The parameters important in influencing the overall correlation time (τ_{c1}) of the Gd-complexes are the following: the rotational correlation, τ_R; the electronic relaxation time, T_{1e}; and the water exchange rate, τ_m. For the small molecular weight (>600 MW) MR contrast agents, such as Gd^{3+}- 1,4,7,10-tetraazacyclododecane (DOTA), the rotational correlation time dominates (~10^{-12} s).[20] However, the electronic relaxation time and the water exchange of Gd^{3+}-DOTA are in the range of μsec and nsec, respectively. The rate-limiting parameter that prevents Gd^{3+}-DOTA from reaching higher relaxivity values is the rotational correlation time. The optimization of these three parameters simultaneously will lead to a maximum relaxation for MR contrast agents seen in **Figure 1-13**. When two parameters are optimized, the

remaining factor will be limiting factor. The current commercially available contrast agents have relaxivities of 4-5 $mM^{-1}s^{-1}$ in 25 MHz, and they are far from the theoretical ~100 $mM^{-1}s^{-1}$, due to their fast rotation and slow water exchange rate.[13]

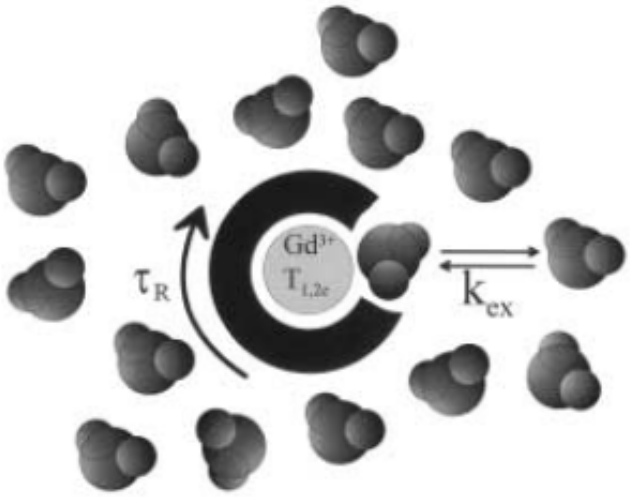

Figure 1-11: Schematic of the MR contrast with the Gd^{3+} center that is enclosed in a ligand. Water molecules, depicted in the space filling model, are shown in exchange with the inner and outer sphere waters.[17]

Inner sphere water (*q*) – This parameter represents the hydration number of the MR contrast agents or is the total number of inner sphere water molecules bound to the lanthanide center. *q* is a dominant component of overall r_1 in high relaxivity agents. Some methodologies to measure *q* include europium luminescence decay and dysprosium induced shifts (DIS). Luminescence decay studies can help determine the hydration value of Eu^{3+} analogs of contrast agents.[27] Europium luminescence is quenched in an H_2O environment, because the $^7F_o \rightarrow {}^5D_o$ transitions for europium match the energy of -HO oscillations of the solvent H_2O.[28] However, the Eu^{3+} luminescence is not quenched

in deuterium oxide (D_2O) because the –OD oscillations do not correlate with the correct energy transitions. The comparison of the luminescence decay rates in H_2O and D_2O can be made with an empirical equation from Horrocks et al. to give a reliable value for the hydration state of the lanthanide complex.[29]

Another methodology using dysprosium analog of the contrast agent can be used to determine q. The lanthanide-induced shift of the ^{17}O NMR peak from dysprosium will be proportionally to the concentration of the dysprosium analog in solution. The slope of the DIS vs. dysprosium complex concentration plot the ratio is compared with the ratios of other known complexes, and q of the desired lanthanide complex can be inferred indirectly.[30]

Mean Water Residence Lifetime (τ_M) – Water exchange rate is the time designated for an inner-sphere water molecules to switch positions with second-sphere water molecules. The determination of water exchange rate (τ_M) can be made using a variable temperature ^{17}O NMR technique. The transverse ^{17}O NMR of a 1% ^{17}O water-enriched solution of Gd^{3+} contrast agent is recorded at variable temperature environments.[31] The spectra of the transverse ^{17}O rates are subtracted relative to the line width of ^{17}O solution without Gd-complexes. The principle behind this method is that the kinetic energy of the solvent molecules increases when the temperature of solutions is raised. At low temperatures, the reduced transverse relaxation rates increase with temperature, in a region of the parabolic curve that is considered the "slow exchange region". At high temperatures, the reduced transverse relaxation of ^{17}O NMR decreases with increasing temperature in what is considered the "fast exchange region".[32] The transition from slow to fast exchange

regions is the inflection point that allows to determine the overall exchange rate of the Gd^{3+} complex. This curve is fit to the Swift-Connick equation to determine the water exchange rate, τ_M.[33] Additional information about the mechanism of water exchange can be determined using variable pressure ^{17}O NMR to help elucidate an associative or dissociative water exchange mechanism.[34] An optimal water exchange rate exists for paramagnetic complexes. If the exchange is too slow or too fast, inefficient quantum transfer occurs between the water solvent and the lanthanide complex. The optimal exchange rate from theoretical models is calculated to be in the low nanosecond range (~36 ns).[31]

Rotational Correlation time (τ_R) – The rotation of the Gd^{3+} complexes affect the overall relaxivity, because the tumbling rate of the contrast agent modify how effectively the lanthanide center can interact with the bulk water. Additionally, the rotational correlation time can change how efficiently the inner sphere water can exchange with the bulk water.[86] Monomeric small contrast agents rotate in the ps range, and the rotational correlation time is the limiting factor the higher proton relaxivity.[14] The fast rotation of small molecular weight contrast agents does not allow for optimal water-lanthanide interaction because the coordination site for water is rotating too quickly. Unlike water exchange rates, which have a parabolic optimal exchange rate seen in **Figure 1-12**, the rotational correlation time (τ_R) is optimized at any time slower than 10^{-9} seconds.[17] The slowing of the rotational correlation times can be achieved by attaching the contrast agent to a large molecular weight structure. The main method for determining the rotational correlation time for MR contrast agents is with the use of nuclear magnetic resonance

dispersion (NMRD).[35] By plotting relaxivity (r_1) in varying magnetic fields, a dispersion curve can be created. The dispersion curve is fitted to the Debye-Stokes equation, and the estimation of τ_R can be made, assuming a spherical molecule.[36] The general shape of the dispersion curve gives insight into the rotational behavior of the contrast agent. With slow tumbling rates, at higher field values, the dispersion curve will give a characteristic peak. However, small monomeric contrast agents will experience marked decrease in r_1 at higher fields, implying a fast tumbling rate. This feature is important, as the trend for MRI is to move to higher magnetic fields. In order to take advantage of the more powerful magnets in clinical settings, MR contrast agents must have reduced tumbling rates to be more efficient.

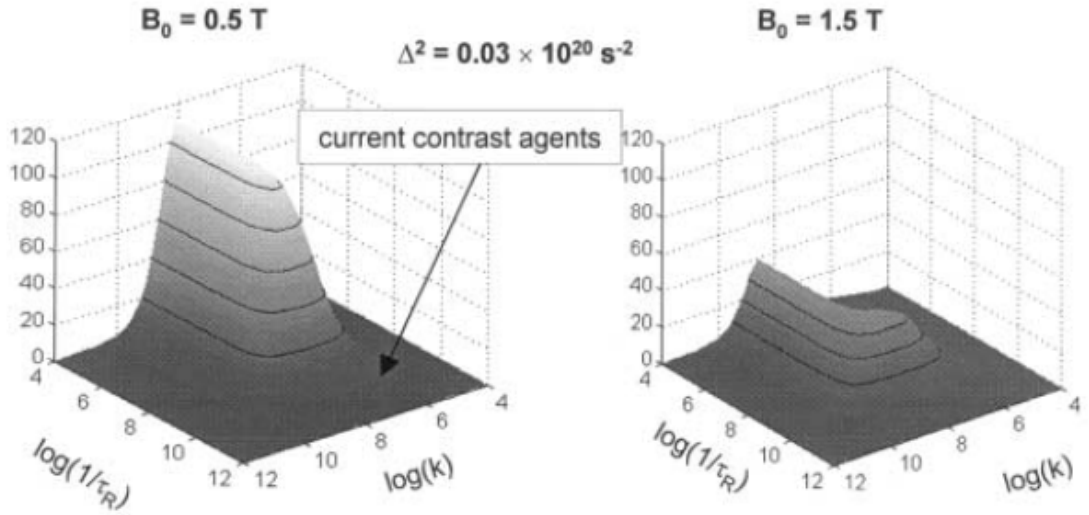

Figure 1-12: These three-dimensional plots correlate the theoretical relaxivity (r_1) with rotational correlation time (τ_R) and water exchange rate (τ_M) in the x and y axis respectively. The two graphs represent topographical maps in two different magnetic

field strengths. The arrow in the first graph represents the location of commercially available MR contrast agents. The highest point represents the theoretical maximum of the efficiency of contrast agents.[17]

Electronic Relaxation time (T_{1e}) - The electronic relaxation parameter is challenging to modify because the T_{1e} is an intrinsic property of the lanthanide. The electronic configuration for Gd metal is [Xe] $6s^2$ $5d^1$ $4f^7$. However, lanthanides tend to lose three electrons, usually $5d^1$ and $6s^2$, to attain their most stable oxidation state as trivalent ions. This leaves Gd^{3+} paramagnetic complexes with a $4f^7$ sub-shell shielded by the $5s^2$ and $5p^6$ closed sub-shells. Gd^{3+} has an electronic spin-state of $^7/_2$ which can be described by static zero field splitting (ZFS) and transient ZFS.[37] The static ZFS measures the random rotational motion of the lanthanide, and the transient ZFS describes fast distortion of the valence electrons. In the Redfield limit of theory of electronic spin relaxation, the $1/T_{1e}$ the longitudinal relaxation function G(t) has a quasi-monoexponential decay and demonstrates a dependence on variables: applied magnetic field ($\boldsymbol{B}_o$), ZFS values, and vibrational/rotational correlation times of Gd^{3+} complexes.[38] Recent efforts have been made to change the ground states of MR contrast agents by effectively shutting off the T_{1e} by taking advantage of scalar and dipolar coupling of hetero-nuclear complexes.[39-41]

Radius (r) – The lanthanide-proton distance of Gd^{3+} to coordinated water proton is defined as $r_{Gd\text{-}H}$. The dipole-dipole relaxation experiences a $1/r^6$ dependence. The closer the water protons are to the lanthanide, the higher the relaxivity. The range distance observed for $r_{Gd\text{-}H}$ is between 2.5-3.3 Å with the average distance 3.1±0.1 Å.[42] This

distance was determined using the anisotropic hyperfine constant T determined from pulsed ENDOR spectroscopy.[42] The radius, however, is not studied frequently, because it is difficult parameter to modulate.

MR contrast agents:

Type of Contrast Agent	**Approved**	**Yet to be Approved**
Extracellular Agent	Dotarem Magnevist Omniscan ProHance	Gadovist MultiHance OptiMARK
Orally Administered	Abdoscan Ferriseltz Imagent GI LumenHance Lumirem/GastroMARK Magnevist Enteral	Gadolite
Organ Specific (Liver)	Endorem/Feridex MultiHance Teslascan	Eovist Resovist
Organ Specific (Lymph Nodes)		Sinerem/Combidex
Blood Pool Agents (Extended Residence Intravascular Agents)	Clariscan	AngioMARK (MS-325) Sinerem/Combidex MultiHance NC-100150
Non-1H Agents		Hyperpolarised Gases

Table 1-1: Commercially available MR contrast agents and agents that are in clinical trials.[14]

Contrast agents are currently being used in clinical settings. Some of the commercial available agents that are currently available are listed in **Table 1-1**. Most of these MR contrast agents use Gd^{3+} ions because of its characteristic long T_{1e} and high

magnetic moment.[43] The chelation of Gd^{3+} ion to a ligand is necessary to combat toxicity and provide safe passage of the lanthanide through the patient in vivo. These agents need to kinetically inert and thermodynamically stable to prevent the lanthanide from being sequestered into the patients. The two basic ligand sets available for commercial use as MR contrast agents are based on diethylenetriaminepentaacetic acid (DTPA) and 1,4,7,10-tetracarboxymethyl-1,4,7,10-tertaazacyclododecane (DOTA) with slight variability on the pendant arms.

These intravenous agents are non-specific and only travel through the vessels and chambers where they are injected.[44] They are used to preferentially image blood streams because they are hydrophobic and do not leak into the interstitial space. They are quickly removed from circulation through the kidneys within a couple of hours. However, these first generation MR contrast agents need improvement in the fields of efficiency, targeting, activatable, and responsive to a variety of biological environments. Current research in MR contrast agents hopes to change MRI from being used imaging modality to a diagnostic tool with the use of advanced MR contrast agents. MRI can be used for disease identification without biopsies or other invasive surgeries. The distinctive property of the new generation of agents, outlined in this chapter, relies on the relaxivity (r_1) difference seen upon an exposure to a microenvironment with specific physiochemical characteristic of the desired tissue when compared with normal tissue. The following section is a brief survey of categories describing such new MR contrast agents.

pH Responsive Contrast Agents – These T_1 MRI contrast agents change relaxivity based on pH. The imaging of pH is deemed vital because tumors display a slightly lower pH. Activating a contrast agent with pH gives promise to highlighting areas with cancers and the possibility of discovering evasive, smaller tumors.

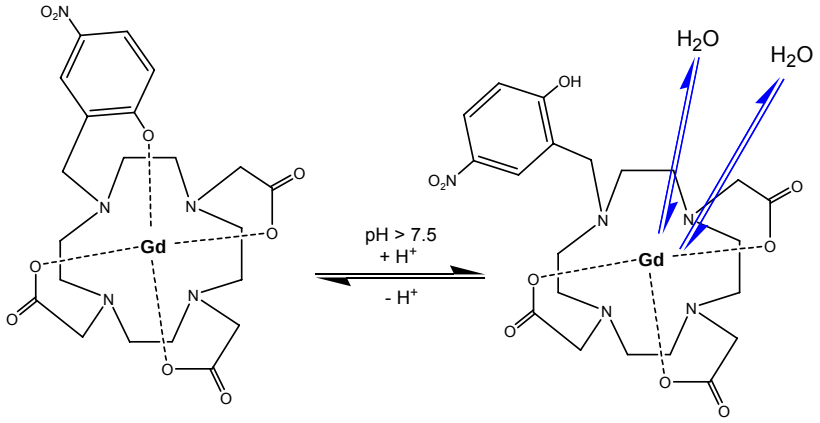

Figure 1-13: The pH sensitive MR agent Gd(NP-DO3A) has a ligating group for intramolecular ligand binding to coordinately saturate the Gd-complex. [45]

The Gd^{3+}-DO3A tetraamide derivative Gd(NP-DO3A) in **Figure 1-13** changes relaxivity in different pH environments.[45] The relaxivity increases from 4.1 $mM^{-1}s^{-1}$ at pH 9 to 7.0 $mM^{-1}s^{-1}$ at pH 5, as a result of acid catalyzed dissociation of the nitro-phenol from the lanthanide. In basic conditions, the *p*-nitro-phenol pendant arm coordinates to the lanthanide and does not allow for inner sphere water to bind to the complex. The luminescence increase was correlated with the decrease in relaxivity at higher pH values. Thus, the addition of a water blocking moiety as one of the linker arms of the DOTA derivative can be used to make a pH sensitive MR contrast agent.

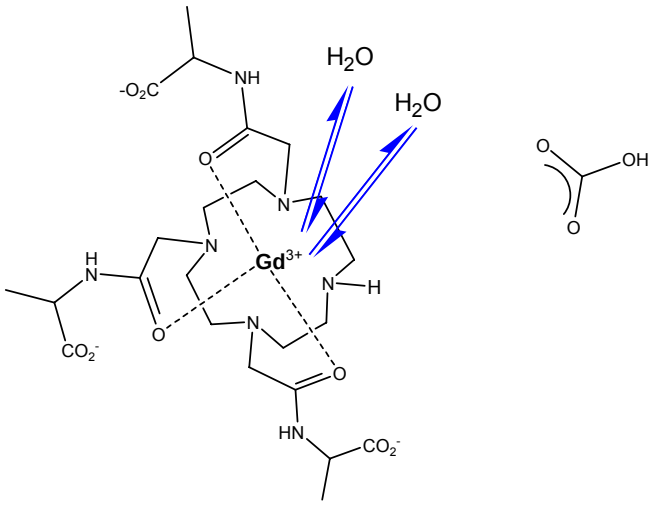

Figure 1-14: A hydrogencarbonate pH sensitive MR contrast agent.[46]

A Gd^{3+}-cyclen based derivative with three pendant (2-acetylamino)-propionic acid arms from Aime et al.[47] demonstrates the ability to replace two waters in the first coordination sphere with carbonate (**Figure 1-14**). The relaxivity of this hepta-dentate Gd^{3+}-complex in a sodium hydrogenocarbonate solution changes from high relaxivity (r_1 = 7.5 $mM^{-1}s^{-1}$) at low pH value to low relaxivity (r_1 = 1.9 $mM^{-1}s^{-1}$) at high pH. This pH phenomenon is attributed to the formation of a ternary complex between the Gd^{3+}-complex and hydrogencarbonate, thereby inhibiting the inner-sphere water contribution that leads to the low relaxivity values.[48]

A pH responsive MR liposome-based contrast agent was synthesized with with low molecular weight Gd^{3+} chelate (Gd-DTPA-BMA) encapsulated within the pH sensitive liposome.[49] The liposome with dipalmitoyl-phosphatidyl ethanolamine and palmic acid demonstrated a strong pH dependency. At lower pH values, the r_1 of the liposome increases sharply by 6-7 fold due to liposome destabilization and the release of the entrapped Gd-DTPA-DMA.

Metabolite Chelating Contrast Agents – Metabolites are ubiquitous in virtually every process in our bodies. They help regulate cellular function and are especially crucial in signal transmission along nerve tissue. The ability to detect changing metabolite concentrations enable the tracking of many otherwise MR silent processes, and may elucidate tissue pathologies in vivo.

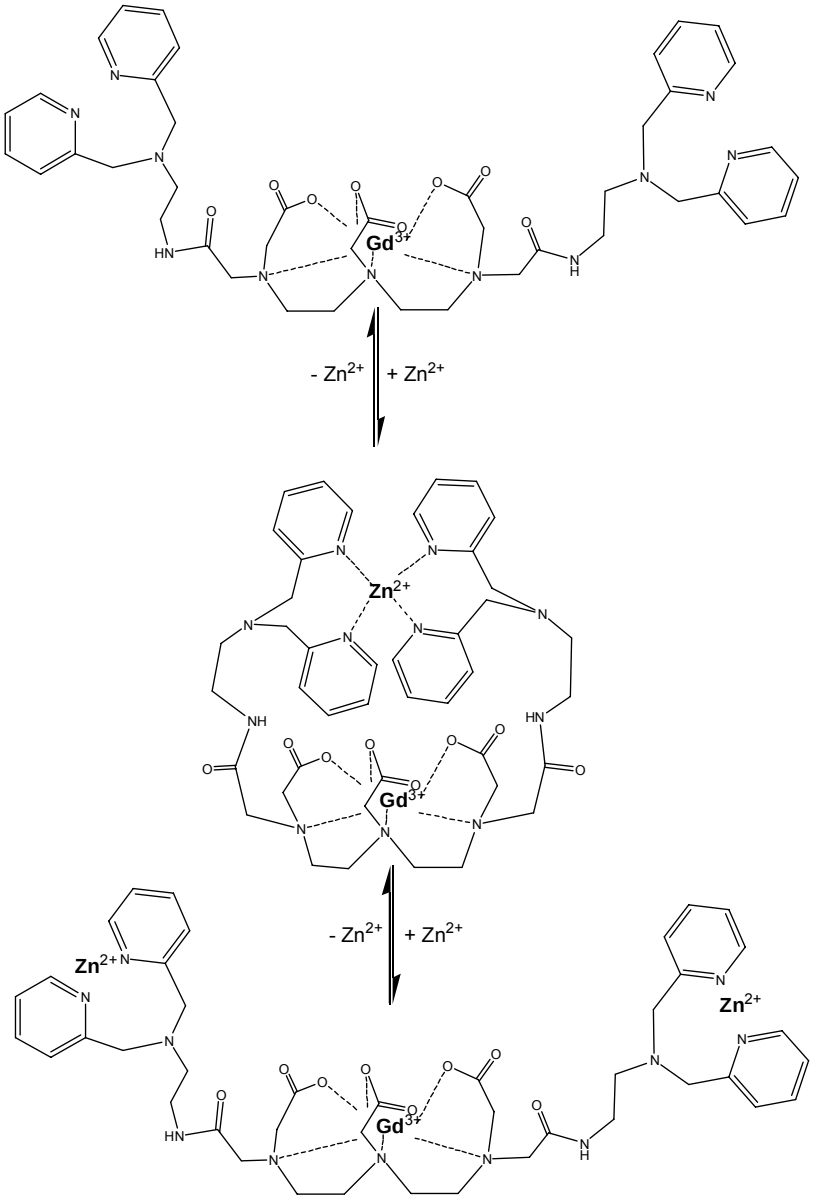

Figure 1-15: A zinc-sensitive MR-agent that modulates inner sphere water in different zinc concentrations. [50]

Gd^{3+}-DTPA derivative with pyridyl-Zn^{2+} binding group synthesized by Nagano et al. has demonstrated to change relaxivity in the presence of zinc (**Figure 1-15**).[51] Before activation by zinc, these agents have its pyridyl arms in an open conformation so water has access to the lanthanide center. However, upon Zn^{2+} activation, r_1 decrease because the pyridyl arms fold up and bind zinc which effectively makes the contrast agent into a q = 0 complex. The bound zinc inhibits inner sphere water access to the lanthanide. As zinc concentration increases, the each pyridyl arm is proposed to bind a single zinc ion and the agent is reopened to observe original relaxivity. The zinc concentration has to equal the concentration of the agent; otherwise it would be difficult to gauge the true concentration of zinc in solution.

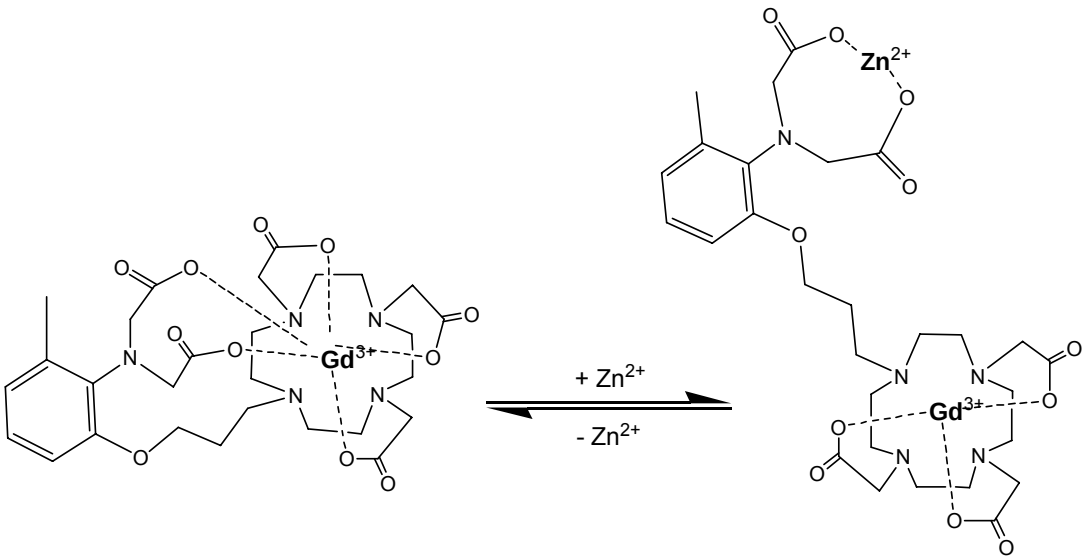

Figure 1-16: A zinc-sensitive contrast agent using a resorcinol backbone. [52]

Another zinc-responsive MR contrast agent was recently published from the Major et al. (**Figure 1-16**).[52] The zinc-binding component is based on half-1,2-bis(o-aminophenoxy)ethane-N,N,N',N'-tetraacetic acid (BAPTA), which has its structural origin from a fluorescence agent. This contrast agent demonstrates selective chelation for zinc over calcium or magnesium. Before zinc is present in solution, free acetate arms are bound to the lanthanide center and coordinatively saturate the complex ($q = 0$). After the introduction of zinc ions, the acetate arms on the resorcinal have a stronger affinity for the zinc, and the acetate arms dissociate from the complex allowing inner sphere coordination of water to the lanthanide-chelator. This selective binding motif increases in r_1 after the acetate arms coordinate to the zinc.

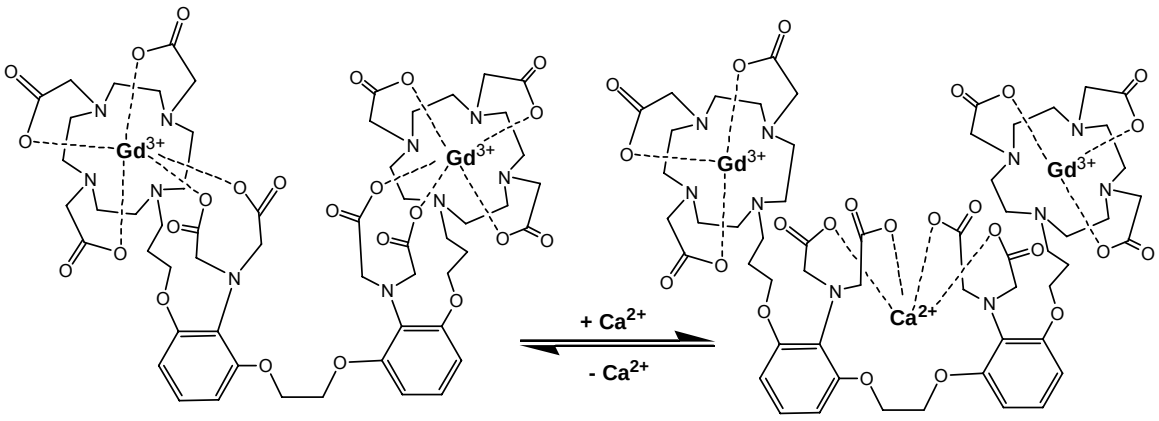

Figure 1-17: Calcium-activated MR contrast agent based on BAPTA using two DO3A derivatives. [53]

A Ca^{2+}-activated MR contrast increases in relaxivity (r_1) in the presence of Ca^{2+} metabolite **(Figure 1-17)**.[53] The acetate arms are proposed to be in a fluxional process

between coordination to the Gd^{3+}-DO3A derivative and Ca^{2+} ion. Before the addition of Ca^{2+}, the closed conformation has a relaxivity of 3.3 $mM^{-1}s^{-1}$ with zero inner sphere waters ($q = 0$). However, in a physiological Ca^{2+} solution, a conformational shift of the acetate arms to bind Ca^{2+} allow for water access to Gd^{3+} and an increase in relaxivity by 75% is observed.[54] This MR agent demonstrates promise to image neuronal activity which uses Ca^{2+} metabolites to modulate synaptic transduction. It may also image the activation of second-messenger system of the intracellular IP_3-DAG-calmodulin pathway.[55]

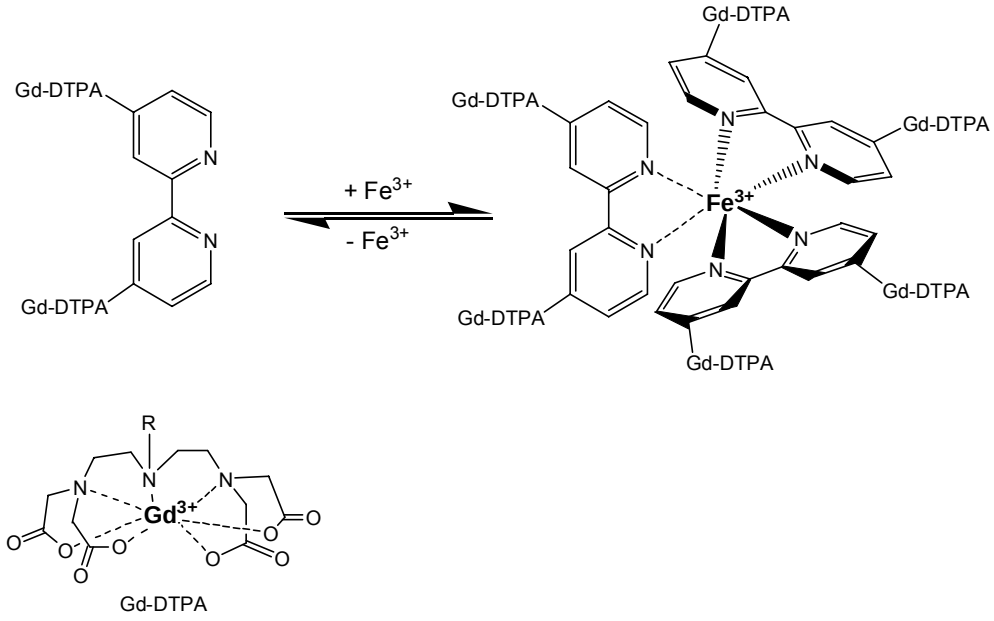

Figure 1-18: Iron-sensitive MR contrast agent using a τ_R strategy for activation. [13]

Iron is a transition metal that is ubiquitous in the body and performs many important functions such as O_2 transport, redox reactions, and electron transport. A MR contrast agent using a bis-Gd-DTPA derivative attached to a bipyridyl ligand

demonstrates an increase relaxivity in the presence of Fe^{3+} ions (**Figure 1-18**).[13] In the presence of iron, three bipridyl ligands coordinate to a single iron to create a supramolecular structure. The increase in molecular weight of the multimeric complex slow the rotational correlation time thereby increasing relaxivity by 145%. This complex, however, is short-lived as the ligands are labile and sequestered by macrophage cellular mechanisms. Similar agents using a Gd-PhenHDO3A instead of DTPA are known agents as well.[56] Iron responsive agents can help image free iron distributions in vivo.

Enzyme Activated Contrast Agent – The ability to image enzyme activity becomes very useful as much pathology like cancer exhibit unique enzyme concentrations that are different from normal tissue.

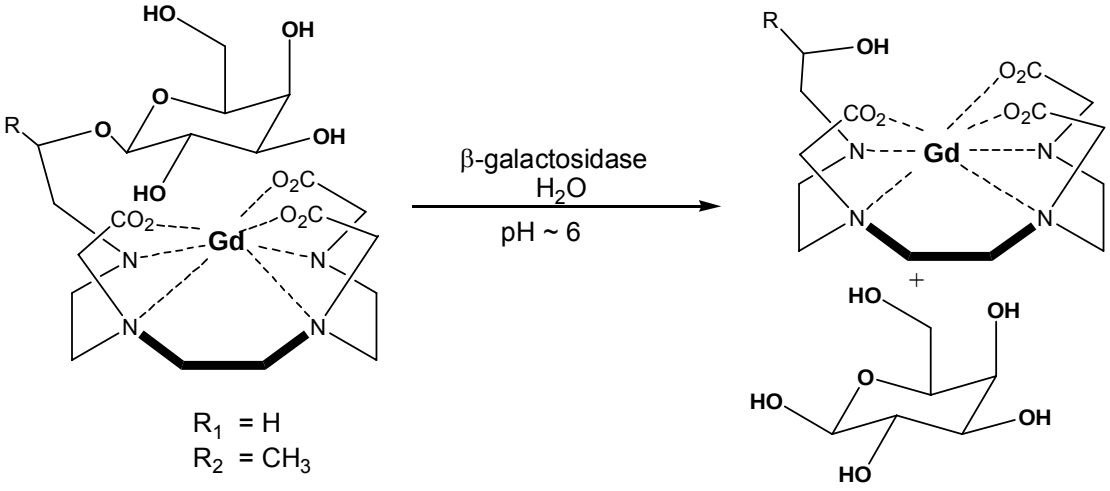

Figure 1-19: The structure of the MR contrast agent EGad (R = H) and EGadMe (R = CH_3).

The first enzyme-responsive MR contrast agent was published by Meade et al.[57], which was a DO3A derivative with an ethyl-β-D-galactopyranoside sugar as the pendant arm called EGad (**Figure 1-19**).[58] The hydroxyls on the galactopyranose sugar are believed to coordinate to the lanthanide center and block the coordination of water. Additionally, the methyl group added on the α carbon further restricts the fluctuation of the sugar and anchors the sugar in a blocking position preventing water from accessing the lanthanide. In the presence of enzyme in vivo, the enzyme β-galactosidase (β-gal) cleaves the sugar to release the blocking moiety from the lanthanide center, which increase relaxivity (r_1) and allow for visualization of the presence of enzymes in vivo. EGad was used in Zebra fish embryos to map gene expression using the addition of LacZ operon. In a cellular model that expresses β-gal, EGad demonstrates a 20% increase in relaxivity. NMR structural studies were performed to confirm the sugar over the ninth coordination site.[59] EgadMe was determined to improve the change in relaxivity with enzyme cleavage because it exhibits a steric methyl on the α position of the arm with the sugar to restrict the sugar to position over the coordination site.

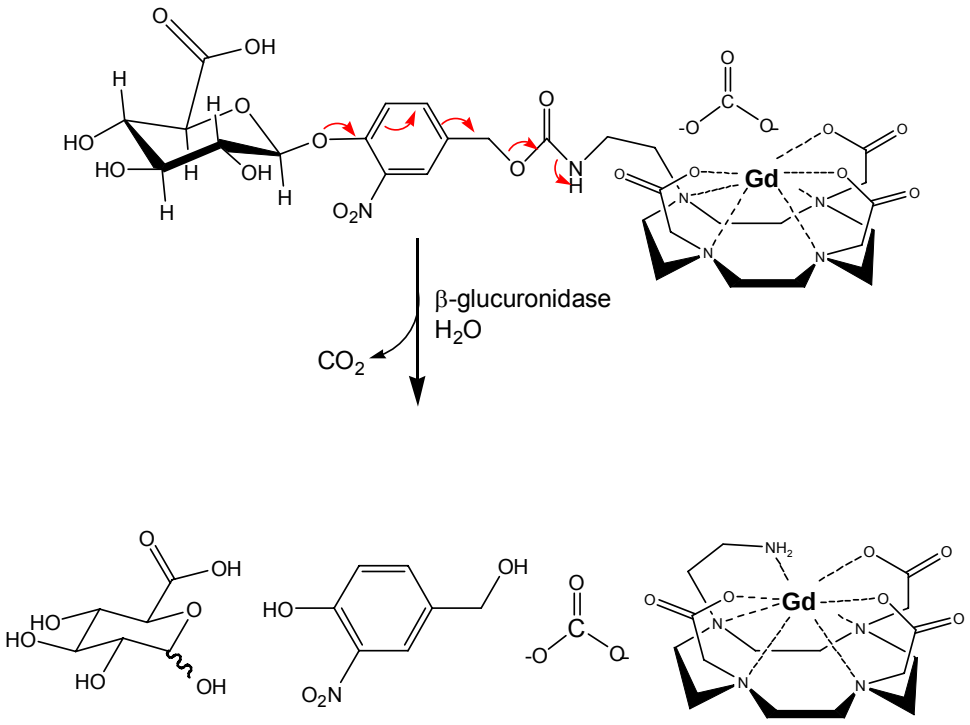

Figure 1-20: A β-glucuronidase responsive MR contrast agent that uses a self-immolative linker. [60]

A new MR contrast agent sensitive to β-glucuronidase was published by Dumistra et al.[60] that utilizes a glucuronic acid sugar substrate attached to an amine-ethyl Gd-DO3A via nitro-phenyl carbamate linker (**Figure 1-20**). Prior to cleavage by β-glucuronidase, the anion carbonate binds to the hepta-coordinate Ln-DO3A component in a bidentate fashion to coordinatively saturate the complex to effectively make the complex q = 0. Upon exposure to the enzyme β-glucuronidase, the β-D-glucopyronuonate acid sugar is hydrolyzed to induce electrons to cascade along the nitro-phenolic backbone to generate carbon dioxide, 4-hydroxymethyl-2-nitro-phenol, and 2-aminoethyl-GdDO3A. The irreversible activation of the self-immolative linker, leaves the agent in the "on" state leaving the Gd-complex with one inner sphere water. The

glucuronidase-responsive agent was designed with a self-immolative linker between the Gd(III)-chelator and the sugar moiety to improve enzyme kinetics from EGadMe. This "self-destructive" linker demonstrated faster enzyme turnover by 2-3 orders of magnitude. This MR contrast agent has potential use for imaging tumors, as cancerous tissues express β-glucuronidase at concentrations higher than normal tissue.

.

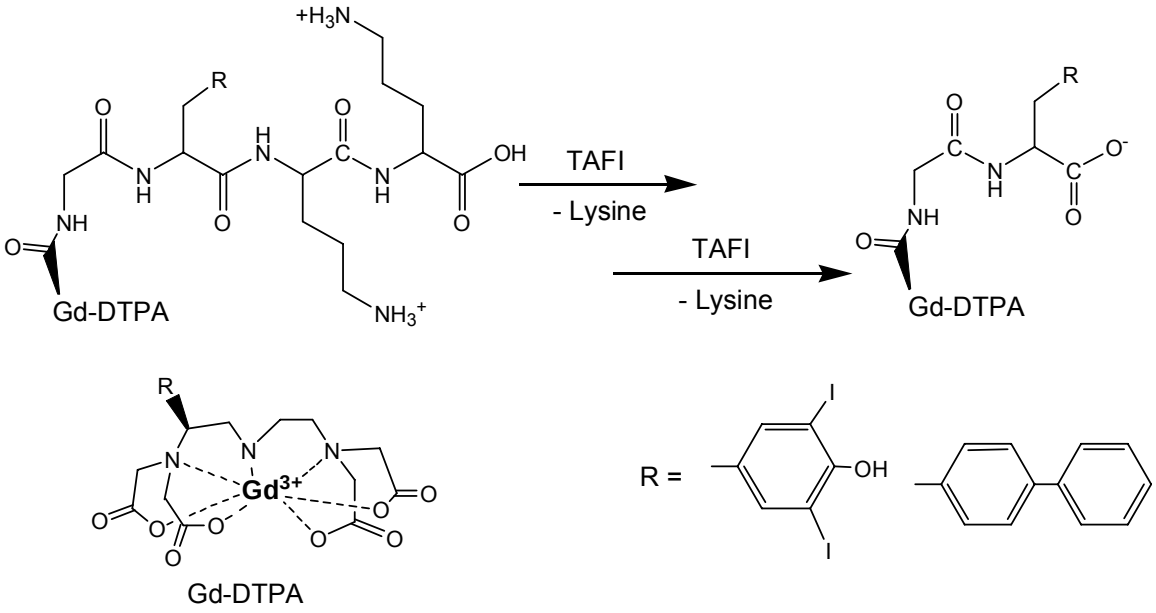

Figure 1-21: A MR contrast agent sensitive to human carboxypeptidase B called thrombin activatable fibrinolysis inhibitor (TAFI).

A MR contrast agent sensitive to thrombin activatable fibrinolysis inhibitor (TAFI) exhibits the ability to modulate relaxivity (r_1).[61] In the presence of TAFI, successive terminal lysines are hydrolyzed by a carboxypeptidase to reveal a hydrophobic group, such as diphenylalanine or 3,5 diiodotyrosine group (**Figure 1-21**). Hydrophobic moieties demonstrate a high affinity for human serum albumin (HSA). The non-specific

binding slows the tumbling rate (τ_R) of the MR contrast agent, thereby increasing the overall proton relaxivity (r_{1P}). This TAFI MR contrast agent potentially can be used in vivo to image the endovascular system, specifically at sites of platelet coagulation.

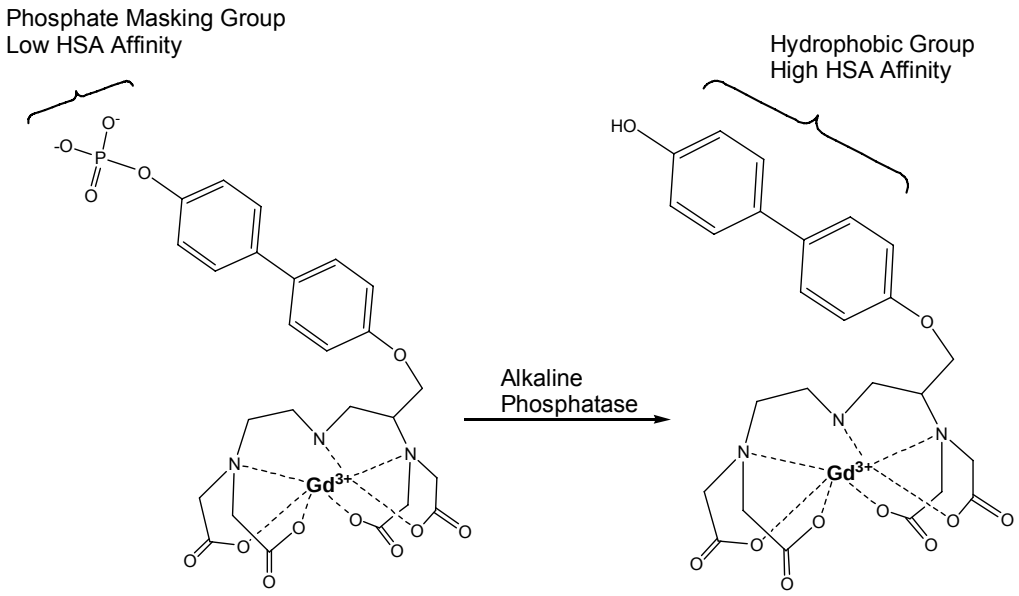

Figure 1-22: An MR contrast agent responsive to alkaline phosphatase.

A phosphatase-responsive MR contrast agent was demonstrated by Lauffer et al. with the synthesis a Gd^{3+}-DTPA chelate with a hydrophobic bi-aryl sidearm with a phosphate group at the terminal end (**Figure 1-22**). The ionic phosphate masking group prevents the hydrophobic group from interacting with human serum albumin (HSA). After hydrolysis of the phosphate group by alkaline phosphatase, the hydrophobic linker is revealed and the agent gains the ability to bind non-specifically to lipophilic serum proteins like HSA. The complexation of the agent post-cleavage with HSA increases the relaxivity (r_1) of the agent by 70%. This non-covalent binding results in slowing of the

tumbling rate of the contrast agent.[62] This strategy for activating MR contrast agent is an effective strategy for increasing relaxivity, because the fast rotational correlation time of smaller monomeric complexes is the limiting factor for implementing high efficient spin quantum transfer with bulk water. Phosphatase agents demonstrate promise to image specific tumors and areas bone of resorption.

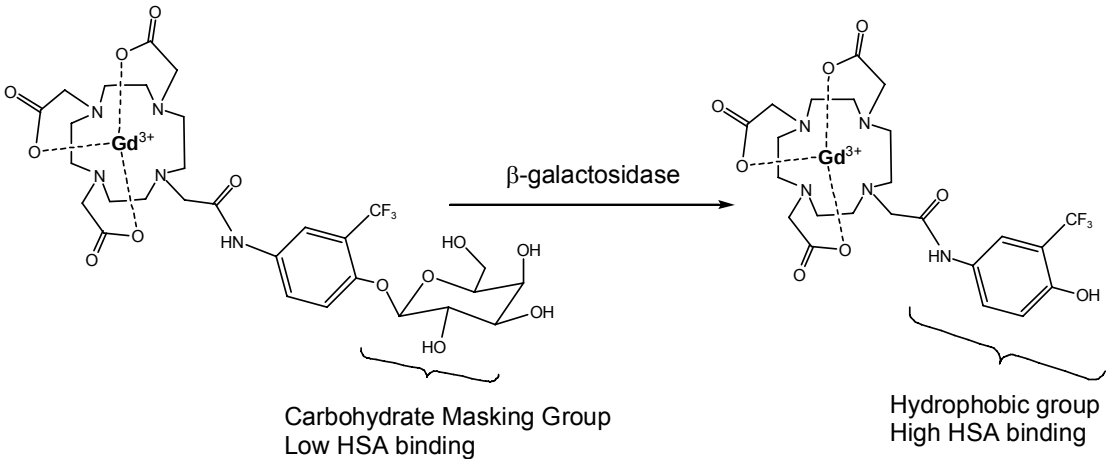

Figure 1-23: A β-galactosidase responsive MR contrast agent that uses the τ_R activation strategy,

This β-galactosidase responsive MR contrast agent by Chang et al. has a -β-D-galactopyranoside sugar attached to a Gd^{3+}-DO3A derivative with a trifluoro-phenyl-galactopyranose carbohydrate (FPG) linker (**Figure 1-23**).[63] Upon cleavage of the sugar by β-galactosidase, the relaxivity (r_1) of the agent increase by 60% in the presence of HSA. The galactopyranose sugar moiety is cleaved to reveal a hydrophobic moiety that will nonspecifically bind to lipophilic, extracellular proteins such as HSA. MR imaging studies demonstrate a higher signal intensity of the samples that contained the agent

along with HSA and β-galactosidase when compared to the agent itself. In vitro cell studies conclude this MR agent demonstrates low toxicity and has the ability to permeate cell membranes. This β-galactosidase MR contrast agent demonstrates potential for use in bioactivatable gene mapping experiments.

Cell Permeable Contrast Agents – Cells regulate activity with compartmentalization. Many cellular activities are localized in specific organelles and used for regulation of cellular function. Intracellular fluid contrasts with extracellular matrix and demonstrates different concentrations of metabolites, pH, enzyme activity, and regulation. It is important for contrast agents to penetrate the cellular membrane to image and report on the intracellular functions using MRI. Cell membranes demonstrate selective behavior for discreet molecules to transducer into cells. In the case of the blood-brain–barrier, this discriminatory gate-keeper role allows for the brain to function properly.[18]

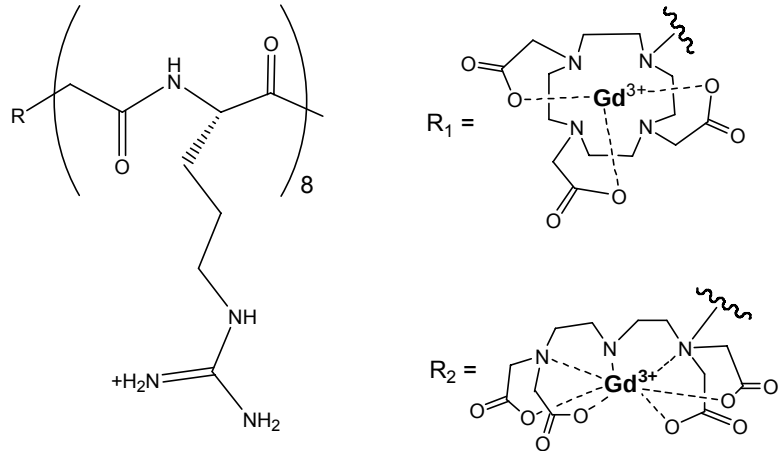

Figure 1-24: A poly-arginine conjugated MR contrast agent, which is designed to transduce cellular membranes.

A poly-arginine peptide sequence (8 mer) was conjugated to MR contrast agents, which demonstrates the ability to transduce with the cellular membrane (**Figure 1-24**). The multivalence polyarginine peptides associate to cells along side their plasma membrane, which causes an electronic imbalance along the membrane surface. This signals the cell to invaginate and internalize the poly-arginine residue and the MR contrast agent. The receptors next to the cellular membrane facilitate the process the endocytosis. X-ray fluorescence studies are used to get high resolution images of the contrast agents associating with different cell lines. The other enzyme and metabolite responsive agents, described thoroughout this introduction can only determine extracellular biological environment, and require the cell-penetrating peptide coupled to MR contrast agents to report on the intracellular function.

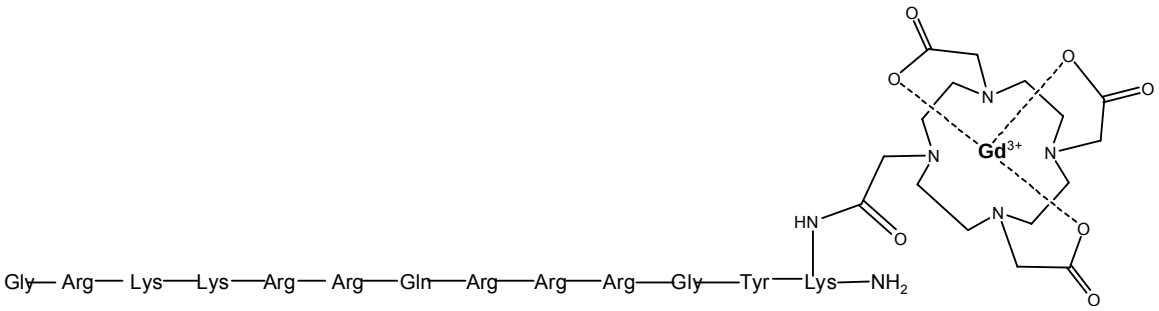

Figure 1-25: A Tat-peptide labeled Gd^{3+}-DO3A chelator designed to tranduce plasma membranes.[64]

A Tat-peptide labeled coupled to DOTA derivative chelator was synthesized to be internalized into cells (**Figure 1-25**).[64] Tat-peptide is a translocase peptide designed to encourage cellular uptake of the MR contrast agent into cells. The Tat-peptide-Gd^{3+}-DOTA complex demonstrated higher relaxivity in aqueous solution at $r_1 = 4.1\ mM^{-1}s^{-1}$,

while after incubation. However, the contrast agent inside cells demonstrated a lower relaxivity of 2.2 $mM^{-1}s^{-1}$. This is attributed to the slow water diffusion rate inside cells.

Another MR contrast agent Gd^{3+}-DOTA was coupled to the transduction domain stillbene. Stillbene has demonstrated the ability to cross the blood brain barrier (BBB), with its hydrophobic planar functional group. The ability to cross the membrane is believed to allow the MR contrast agent to cross the BBB. This agent may be used to selectively image intracellular plaques in the brain such as those associated with Alzheimer's disease.

Targeted Contrast Agents – A targeted MR contrast agent is beneficial to imaging because it can highlight specific areas of interests. The localization of the contrast agent with specific cellular receptors allow for imaging specific tissues and organs.

Monoclonal antibody coupled MR contrast agents demonstrate efficient receptor targeting and can label a variety of receptor sites. Antibodies are protein structures part of the humoral adaptive immunity that recognize foreign substances (antigens) encountered in the environment.[65] An antibody labeled MR contrast agent specifically attachs to anti-antibody antigens, which include bacteria and aggregate around sites of infections. An anti-carcinoembryonic (anti-CEA) immunoglobulin γ (IgG) coupled to a Gd^{3+}-DTPA was reported to have no measurable loss of antigen binding.[66] The in vivo efficacy was unsuccessful because not high enough concentration of IgG-Gd^{3+}-DTPA agent localized at the tumor site. However, this agent was the first antibody-targeting contrast agent. Subsequent antibody-labeled MR contrast agents have been published that targeted cardiac myosin[67], human colon adencarcinoma[68], anti-human T-cells[69],

angiogenesis[70], and biotin-streptavidin[71]. All of these monoclonal antibody agents suffer from low concentration at the receptor site for MRI.

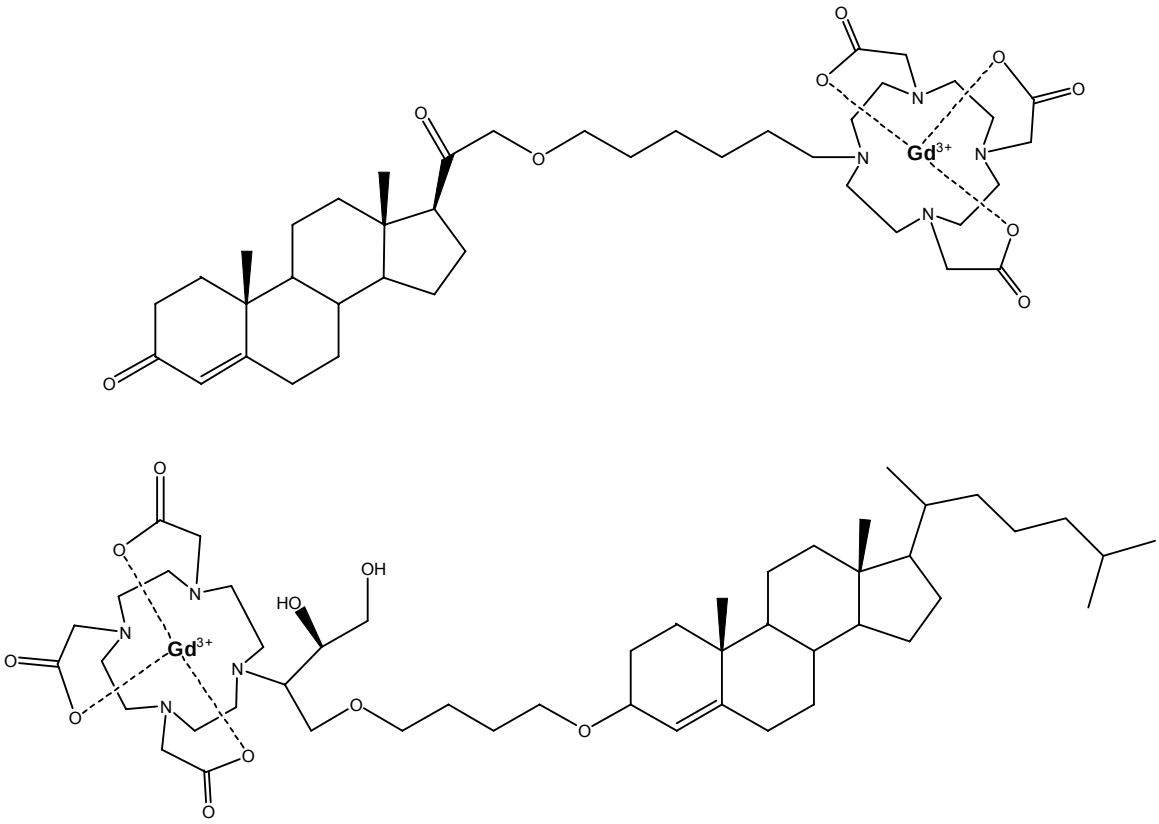

Figure 1-26: Steroid substituted Gd-DO3A MR contrast agents. **a) TOP:** a progesterone conjugated MR-contrast agent[72] **b) BOTTOM**: cholesterol-conjugated MR contrast agent. [73]

Cholesterol conjugated MR contrast agent have demonstrated efficacy to attach to nuclear receptors and affect transcription of DNA. A low molecular weight Gd^{3+}-DO3A with a conjugated steroid synthesized by Lee et al. have demonstrated to bind with progesterone receptors and enhance contrast in MRI (**Figure 1-26a**).[72] Several linkers and attachment points for the steroid were explored. All conjugated agents demonstrated

low binding affinity due to modification of the progesterone. This agent has potential use in diagnosing breast cancers which have elevated levels of progesterone receptors. A Gd^{3+}-DO3A conjugated to cholesterol has been synthesized by Muhler (**Figure 1-26b**).[73] Cholesterol is the serves as precursor for mineralocorticoids, androgens, and glucocorticoids synthesized in the adrenal cortex.[55] The accumulation of the agent at the adrenal gland resulted in a 162% increase in MRI signal.

High Relaxivity Contrast Agents – High efficiency MR contrast agents require a lower concentration of the agent to observe a contrast in the MR image. An optimized hydration number (q), water exchange rate (τ_m), and rotational correlation time (τ_R) contribute toward high relaxivity. Lower concentration for imaging anatomical difference aids other research fields like targeting, where agents suffer for poor localization.

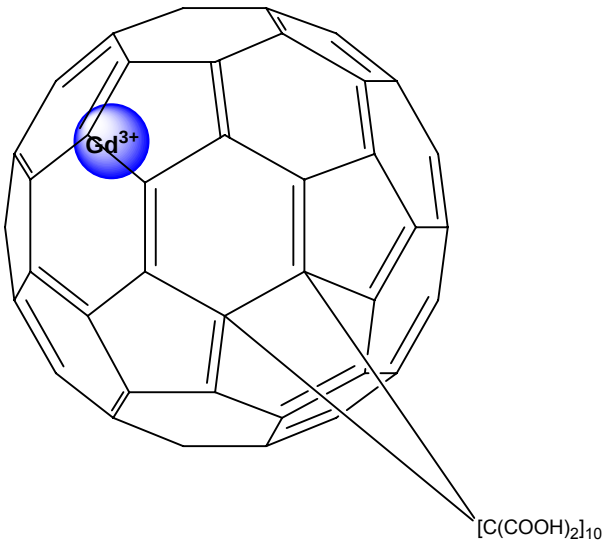

Figure 1-27: A metallofullerene-based MR contrast agent demonstrates high relaxivity properties.[74]

Lanthanoid entrapped endohedral metallofullerenols were used for MRI contrast agents (**Figure 1-27**).[74-76] The Gd^{3+}-fullerenols were found to have extremely high r_1 = of 73 $mM^{-1}s^{-1}$, which are attributed to dipole-dipole relaxation combined with a decrease in the molecular rotational motion. Curie-Spin relaxation is also high, and helps relax a wide number of water molecules thorough a second-sphere exchange mechanism. Although water molecules are not directly coordinated to the lanthanide, metallofullerenes has intrametallofullerenol electron transfer which can affect the relaxation spins of a large number of surrounding water protons at a single moment.

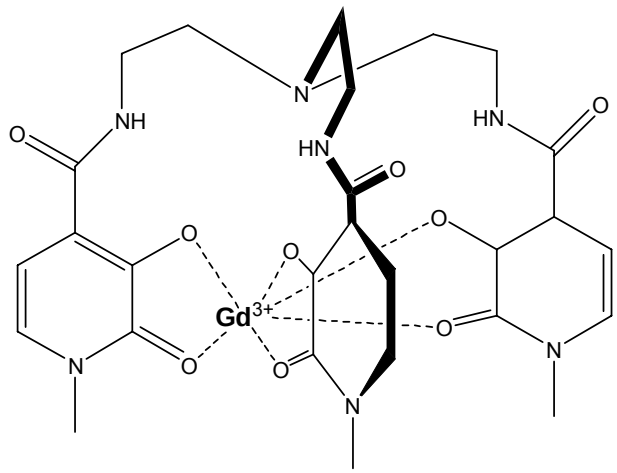

Figure 1-28: A high relaxivity MR contrast agent based on hydroxypyridinone (HOPO).[77]

A novel chelator based on hydroxypyridinone (HOPO), synthesized by Xu et al., demonstrates to become a high relaxivity monomeric Gd-based MR contrast agent (**Figure 1-28**).[78] The water exchange rate (τ_m) for HOPO is near optimal while having two inner-sphere waters (q). However, HOPO suffers from lower stability constants and

demonstrates poor water solubility. Substitution efforts have made HOPO more soluble while retaining its desirable τ_m.[79] HOPO introduces a new platform for high relaxivity MR contrast agents.

Polymer Contrast agents – Multimeric MR contrast agents has benefits of high relaxivity based on large number of Gd^{3+} ions and taking advantage of the higher molecular weights for slower tumbling rates.

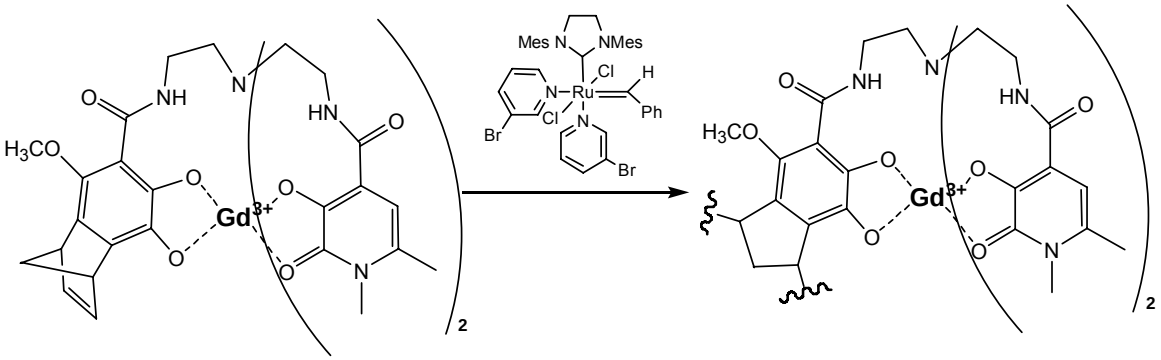

Figure 1-29: A polymer synthesized using ring-opening metathesis polymerization and HOPO. [80]

An MR contrast agent polymer using ring-opening metathesis polymerization (ROMP) has been used on a Gd^{3+}-HOPO chelator (**Figure 1-29**).[80] The τ_m optimized chelator HOPO was integrated into the backbone of ROMP to increase the rotational correlation time (τ_r) of the resulting macromolecule. Solubility was addressed by incorporating guanidinium amines between the insoluble HOPO monomers. Relaxivity values as high as 111 ± 1.5 $mM^{-1}s^{-1}$ was observed for each polymer. The benefit of this

ROMP polymer is the interchangeable functional monomers that are possible with can be readily polymerized with reasonable control into the backbone.

A dendrite MR contrast agent coined Gadomer has been synthesized by Schering AG. [81] The dendritic agent has a core of 1, 3, 5 benzene-tricarboxylic acid which is coupled to a shell of lysine residues. Gd^{3+}-DO3A monoamide chelates are on the surface of the dendrimer. An estimated number of Gd^{3+}-chelator units on the surface of the 4th generation dendrimer is 24. Larger multimeric polymers are expected to increase relaxivity (r_1) with increasing molecular weight as predicted with the Debye formula. However, it is not necessarily the case for Gadomer, which exhibits high internal flexibility of the linking group that attaches Gd^{3+}-chelator to the macromolecule.[36] This causes the local rotation of the Gd^{3+}-chelate to be much faster than the global rotation of the macromolecule. The internal rotation is responsible for much of the lower effective rotational correlation times, and subsequently the lower relaxativity values of many macromolecular agents.

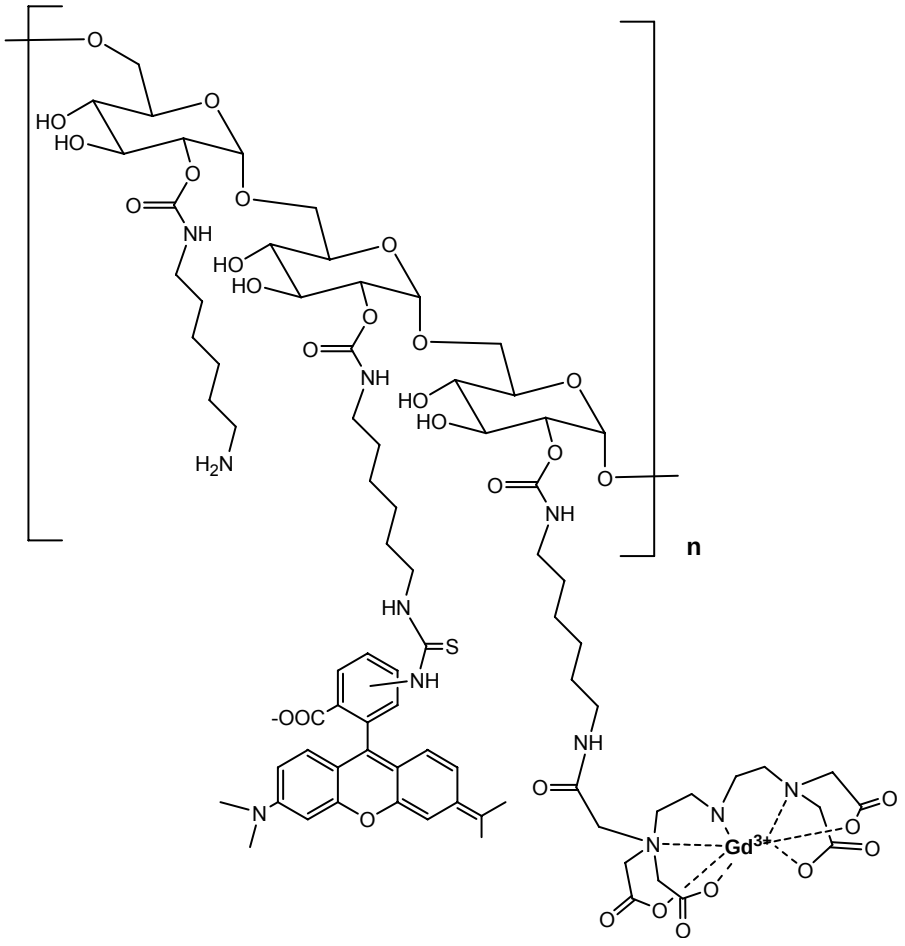

Figure 1-30: GRID is a multimodal MR contrast agent with a chromophore to co-register the MR image with the fluorescence image.

Another class of large polymeric Gd^{3+} complexes is multimodal MR contrast agents. These agents provide opportunities to co-register imaging with an orthogonal technique. The imaging information is corroborated from two imaging modalites. This is especially helpful for fate-mapping of embryological tissue. An example of such multimodal contrast agent is GRID, which incorporates a chromophore and Gd^{3+}-DTPA chelator into a carbohydrate backbone (**Figure 1-30**).[82] Dextran is useful as a backbone because it is biologically tolerated and has good hydrophilic solubility characteristic.

Some issues with dextran-based multimodal agents are that the optical functional group has a 4 orders of magnitude higher sensitivity than the magnetic component. It is difficult to quantify how much of rhodamine chromophore to Gd^{3+}-chelator is actually on dextran. These multimodal contrast agents, because of their high molecular weights, can be helpful in use as blood-pool agents.

T_2 Agents - Iron oxide superparamagnetic particles exhibit large magnetic moments and demonstrate the ability to have a predominant T_2 relaxation effect. The particle consists of a core of one or more iron oxide crystals embedded in a coating that prevents agglomeration. The relaxivity of these superparamagnetic colloids depend highly on their size, chemical composition, and the coating.[83] Dextran-coated particles have demonstrated to associate with high affinity to the surface of cells.[84]

The relaxation theory of iron-oxide crystals deviates from the Solomon-Bloombergen theory that governs T_1 agents. The electron spin-lattice relaxation does not effect the paramagnetic enhancement of proton spin relaxation. The anisotropy energy for the iron-oxide nanoparticles is size-dependent and vary with the density of the iron core.[13] At higher fields, the transverse relaxation effect of iron-oxide particles becomes more prominent and is relevant for MRI as clinical magnets are moving to more powerful magnets.

The biodistribution of these iron oxide particles is relatively benign. Iron is ubiquitous in the human body, and the particles get sequestered by heptaocytes or Kupffer cells and are cleared by the liver.[85] These macrophages incorporate the excess iron into the body or it is excreted via the digestive or urinary tract.

Other reviews and resources:

Many reviews have been published with a wide survey of recent second-generation MR contrast agents. Please look to these references for more information:

Bertini, I.; Luchinat, C.; Parigi, G. *Concepts in Magnetic Resonance* **2002**, *14*, 259-286.

Bottrill, M.; Kwok, L.; Long, N. J. *Chemical Society Reviews* **2006**, *35*, 557-571.

Aime, S.; Dastru, W.; Crich, S. G.; Gianolio, E.; Mainero, V. *Biopolymers* **2002**, *66*, 419-428.

Kobayashi, H.; Brechbiel, M. W. *Molecular Imaging* **2003**, *2*, 1-10.

Caravan, P.; Ellison, J. J.; McMurry, T. J.; Lauffer, R. B. *Chemical Review* **1999**, *92*, 2293-2352.

Caravan, P. *Chemical Society Reviews* **2006**, *35*, 512-523.

Aime, S.; Botta, M.; Fasano, M.; Terreno, E. *Chemical Society Review* **1998**, *27*, 19-29

Pautler, R. G.; Fraser, S. E. *Current Opinions in Immunology* **2003**, *15*, 385-392.

Stiriba, S.; Frey, H.; Haag, R. *Angewandte Chemie Internation Edition* **2002**, *41*, 1329-1334.

Peters, J.; Raber, D. J. *Progress in Nuclear Magnetic Resonance Spectroscopy* **1996**, *28*, 283-350.

Corsi, D. M.; Platas-Iglesias, C.; Van Bekkum, H.; Peters, J. *Magnetic Resonance in Chemistry* **2001**, *39*, 723-726.

Meade, T. J.; Taylor, A. K.; Bull, S. R. *Current Opinions in Neurobiology* **2003**, *13*, 597-602.

Lauffer, R. B. *Chemical Review* **1987**, *87*, 901-927.

Raymond, K. N.; Pierre, V. *Bioconjugate Chemistry* **2005**, *16*, 3-8.

Bogdanov, A. A.; Lewin, M.; Weissleder, R. *Advanced Drug Reviews* **1999**, *37*, 279-293.

Aime, S.; Botta, M.; Fasano, M.; Terreno, E. *Chemical Society Review* **1998**, *27*, 19-29

Scope of Thesis:

Chapter 1 is an introduction into magnetic resonance imaging (MRI) and the role of contrast agents in MRI. It begins with a historical perspective describing the different characters that were involved with the evolution of MRI. All the different personalities contributed to making MRI possible including some people who were denied recognition of their achievements based on their political views. The next section describes how MRI functions, and there is a cursory description for how images are rendered from magnetic fields. The third section is describes MR contrast agent theory. It expounds on the variable parameters that affect the overall relaxivity of agent. It mainly focuses on T_1 agents. The final section is a survey of interesting second-generation MR contrast agents

that have been developed and explores strategies for activation, targeting, and responsiveness to a variety of biological environments. A list of reviews is available at the end of the introduction.

Chapter 2 focuses on the biochemical activation of a MR contrast agent that is sensitive to the enzyme β-galactosidase. This research is based on previous work involving Egad and EGadMe (**Figure 1-19**). The EGadMe system utilizes a galactopyranoside sugar to cover the ninth coordination site of the Gd(III)-DO3A complex. Relaxation of EGadMe is modulated by the catalytic cleavage of β-galactopyranoside by β-galactosidase. With the hydrolysis and removal of the blocking sugar moiety, the r_1 increases, accompanied with an increase in q. However, the enzyme turnover for EGadMe was too slow to study real-time gene-expression. A glucuronidase-responsive agent was designed with a self-immolative linker between the Gd(III)-chelator and the sugar moiety to improve enzyme kinetics. (**Figure 1-20**) This "self-destructive" linker demonstrated faster enzyme turnover by 2-3 orders of magnitude. Chapter 2 discusses the β-galactosidase sensitive MR contrast agent using the self-immolative linker. The synthesis and characterization of this agent is described, along with the in vitro testing of the β-galactosidase responsive compounds. This chapter explores the use of exogenous anions to coordinate to β-galactosidase agent and its effect on overall relaxivity. The pH profile vs relaxivity of the β-galactosidase agents are demonstrated in this chapter. Variable temperature ^{17}O NMR and fluorescence decay studies were performed to determine the hydration state of the agent. The electronic effects of the nitro-adduct on the phenolic linker were investigated with relation to enzyme kinetics. The effect of β-galactosidase was studied on the relaxometric and colormetric properties

of the agents. Cell viability and transduction studies were performed to determine toxicity and the efficiency of these agents to cross cell membranes.

Chapter 3 examines the modulation of q of a phosphatase sensitive MR contrast agent. This project aims to prove that the self-immolative mechanism can be activated by alkaline phosphatases. Two phosphatase sensitive agents were designed, synthesized and tested in vitro. One phosphatase agent utilizes a self-immolative linker connecting an inorganic phosphate and gadolinium-chelator DO3A. The other agent is similar in structure but exhibits a dangling acetate group on the pendant phosphate arm to coordinate back to the lanthanide. The effects of exogenous anions such as carbonate and phosphates were studied in relationship to relaxivity for each complex. The effect of pH on relaxivity is explored for both these phosphatase MR agents. Variable temperature ^{17}O NMR and luminescence decay studies enlighten us as to the hydration state of these complexes. Preliminary phosphatase kinetics studies are reported to demonstrate that the rate of hydrolysis for this phosphatase system is desirable for practical applications in MRI. Molecular dynamic studies were performed on the both these compounds, and initial computational calculations are presented in this chapter.

Chapter 4 is the bridged macrocycle project. The bulk of my graduate research was performed on this activatable contrast agent, which has been designed with an alkyl linker that bridges over a pseudo-trans-DO2A derivative. The alkyl-bridge was designed to block the access of water to the inner sphere water molecules to the paramagnetic gadolinium ion in the macrocycle. The hydrolysis of galactopyranose sugar induces a cascade of electrons which releases the alkyl-bridge from the contrast agent, ultimately increasing the relaxivity of the processed agent. All the schemes and different strategies

attempted to the final bridged complex are reported in this section. Under the conditions tested in this addendum, the lanthanide metal ions were not able to chelate into the macrocycle pocket.

The final chapter (addendum) concerns the DNA alkylation project. This agent uses a mustard alkylating agent to attach to DNA or other electrophilic biomolecules. This alkylating event slows the rotational correlation time of the agent, with the ultimate effect of increasing the overall relaxivity. An agarose gel electrophoresis was performed to determine the ability of the contrast agent to alkylate and cross-link DNA. This was shown with the loss of activity of the restriction enzyme and the increased molecular weight of the DNA strands.

Chapter 2:

Magnetic Resonance Imaging Contrast Agents Sensitive to β-Galactosidase via Self-immolative Linker

ABSTRACT

Bioactivatable MRI contrast agents that respond to physiological conditions such as pH, secondary messengers, and enzyme activity are of current interest. We previously reported a new class of enzyme-activated MR contrast agents that use a self-immolative mechanism. We have expanded the family of self-immolative MRI contrast agents by two new members, **5** and **15**, comparing the electronic effect of substituents on the linker. **5** is a dual chromogenic and relaxometric probe for β-galactosidase detection and has been synthesized by linking β-D-galactopyranoside with a self-immolative linker to Gd(III)DO3A, (DO3A = 1,4,7-tricarboxymethylene-1,4,7,10-tetraazacyclododecane). The linker of **5** contains a nitro group, whereas the linker for **15** does not. The coordination chemistry of these complexes has been extended to include determination of q, t_m, and the relationship of relaxivity to pH. Further, Eu analogs of these complexes, **6** and **16,** transduce cells and have greater than 95% viability in NIH/3T3 cells. Enzyme kinetics studies show the enzyme cleaves **5** and **15** generating 2-aminoethyl-GdDO3A (**9**). The rate for **15** is slower, likely due to the lack of nitro group. The enzymatic cleavage of **5** was followed by UV-vis and the kinetics fit the single site Michael-Menten model with a K_{cat}/K_m = 118.2 ± 6.3 $M^{-1}s^{-1}$. The relaxivity of **5** decreases 25% upon incubation with the enzyme in PBS. However, in buffer mimicking in vivo concentrations of anions such as carbonate, the relaxivities of **5** and **15** are lower than that of **9**.

KEYWORDS: β-galactosidase, magnetic resonance imaging, activatable contrast agent, enzyme responsive contrast agent, smart contrast agent, cell transduction, self-immolative linker, chromogenic probe, relaxometric, DOTA, DO3A.

Introduction:

The differentiation of embryonic cells into their respective tissue is a result of a complex arrangement of gene regulation.[1] This concert of genotypic controls ultimately determines the phenotypes of cells.[2] Biochemical investigations into the genetic origins of diseases become possible when investigators are able to track gene expression in vivo, such as the genesis of cancer.[3] A strategy for monitoring the regulation of a gene in whole animals is the in situ hybridization of a gene marker to a specific allele of interest.[4-6] Lac Z is one of the most frequently used reporter genes in transfection experiments, because it encodes for the protein β-galactosidase (β-gal) that enzymatically hydrolyzes lactose.[7] Mammalian cells cannot endogenously process galactopyranose sugars such as lactose. β-gal expression is visualized histochemically through the hydrolysis of X-gal yielding a blue precipitate.[7] Furthermore, fluorescent probes have proven effective for following gene expression.[8] However, the two main limitations of these optical techniques are: that they are limited to topical imaging in whole animals due to the light scattering properties of tissue, and they necessitate animals to be dispatched in order to do stop-point histology of the deep tissue samples. Investigations into the use of μPet (micro-positron emission tomography) and SPECT (single-photon emission computed tomography) have demonstrated potential to render spatial imaging of gene transduction.[9] However, these imaging modalities suffer from low resolution (cubic millimeter range) and necessitate the use of ionizing radiation.[10,11]

Magnetic resonance imaging (MRI) provides an alternative approach with the benefits for temporal, whole animal imaging at cellular resolution (~10 μm) without the use of high-energy radiation.[12,13] MR images are an array of gray scale pixels with intensities

that correspond to the relaxation times (T_1 spin-lattice relaxation times and T_2 spin-spin relaxation times) of water protons in tissue.[14,15] Clinical, extracellular Gd(III)-based contrast agents are used to highlight anatomic features by shortening the local water relaxation times, ($R_i = 1/T_i$ (s^{-1}), i = 1, 2), thereby shortening acquisition times and improving contrast.[14,16-18] Relaxivity (r_{1P}) is a measure of how efficiently of MR contrast agents to shortens the longitudinal relaxation times of surrounding water protons.[19] Current efforts in MR contrast agent research aim to develop agents that report on the biochemical functions of tissues, beyond mere anatomy.[20,21] The relaxation properties of these second-generation "activatable" MR contrast agents change in response to specific biochemical conditions such as pH, or the presence of specific metabolites or enzymes.[22] MR imaging using these bio-activatable contrast agents provides a way to track gene expression in vivo in high-resolution spatial mapping with real-time registration of gene activation of the whole animal.

EgadMe is a MR contrast agent with Gd(III) ion chelated to a 1,4,7-tricarboxylmethylene-1,4,7,10-tetraazacyclododecane (DO3A) with a pendant β-D-galactopyranoside sugar positioned over the ninth coordination site effectively blocking water from the inner-sphere.[23-25] This β-gal sensitive contrast agent has demonstrated ability to modulate the water T_1 relaxation rates upon the hydrolysis of the galactopyranose sugar ($r_{1\ cleaved} = 2.72$, $r_{1\ uncleaved} = 0.90$). However, the cleavage of EgadMe by β-gal in vitro is more than 2 orders of magnitude slower than the cleavage of a known chromogenic substrate, 2-nitrophenyl β-D-galactopyranoside (ONPG), by the enzyme β-gal.[26,27]

To improve enzyme turnover of the activatable agent, a β-glucuronidase activated MR contrast agent was developed using a self-immolative linker.[28] Derived from a strategy employed for a β-glucuronide prodrug,[29] this agent is comprised of a β-glucuronic acid moiety connected with a *para*-2-nitro-phenyl-carbamate linker to Gd(III)-DO3A. Marked improvements in kinetic properties were observed with even faster cleavage rates than the standard β-glucuronidase substrate, *para*-4-nitrophenyl-β-D-glucuronide (PNG).

We present new members to the family of enzyme-activated MR contrast agents that use the self-immolative mechanism. The agents are designed to change their coordination chemistry in upon the hydrolysis of the β-D-galactopyranoside moiety (Figure 1), which in turn changes their effect on water proton T_1 relaxation rates. The electronic effects on enzyme kinetics have been explored by introducing a nitro group was on the self-immolative linker. The kinetics for this agent are compared to the kinetics for an agent with no modifications to the linker. The synthesis, characterization, and in vitro enzyme kinetics experiments of these complexes are reported in this paper. Cell transduction and viability studies were performed to examine in vitro efficacy.

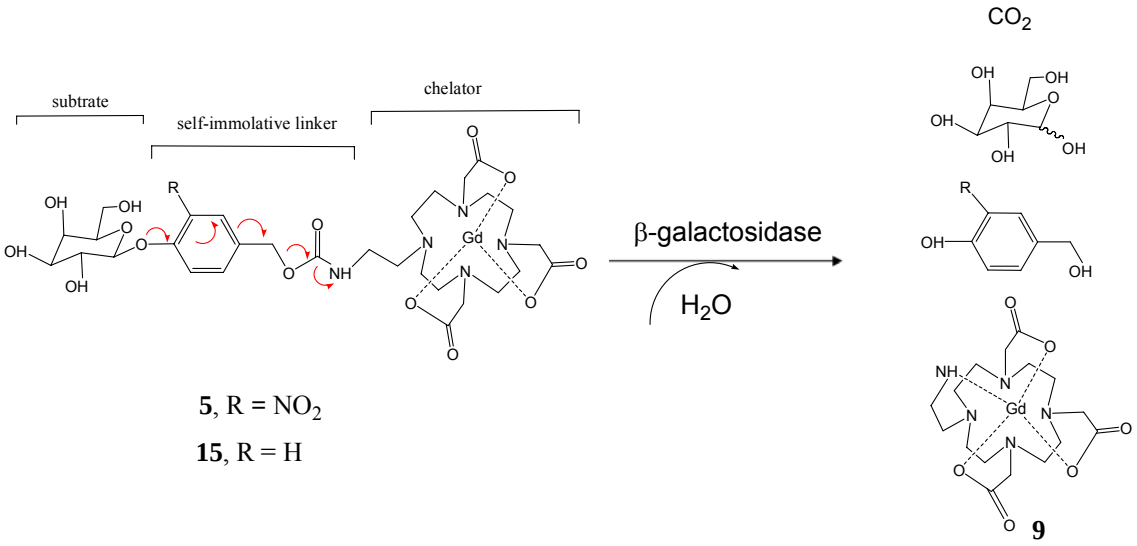

Figure 2-1. β-galactosidase catalyzed hydrolysis of MR contrast agents **5** and **15**.

Experimental Section:

General Methods: All the reactions were performed under dry N_2 atmosphere unless otherwise indicated. All anhydrous solvents were from GlassContours solvent systems. All the compounds used in the reactions were available from Aldrich (Milwaukee, WI) and Fisher (Hanover Park, IL). 1,4,7,10-Tetrazacyclododecane (cyclen) was purchased from Strem. The β-galactosidase enzyme, from bovine liver, was purchased from Sigma-Aldrich. The enzyme substrate *ortho*-nitrophenyl-b-D-galactopyranoside (ONPG) was purchased as a kit from Promega, and the procedure provided in Technical Bulletin No. 097 was followed to determine the enzyme kinetics of the bovine β-gal. Water was purified using a Millipore Milli-Q Synthesis purifier. The ^{1}H NMR spectra were obtained on either a Varian Mercury 400-MHz or Varian INOVA 500-MHz NMR spectrometer. The ^{17}O NMR spectroscopy were performed on the Varian INOVA-400 using a 1% ^{17}O enriched solution with an external D_2O standard to lock. All the ^{13}C NMR spectra were

performed on the Varian INOVA 126 MHz NMR using a 10mm broadband carbon probe. All deuterated solvents were obtained from Aldrich (Milwaukee, WI). The spectra obtained in $CDCl_3$ were referenced to 0.01% TMS internal standard, otherwise all other deuterated solvents were referenced to the solvent peak. Mass spectrometry was performed on Varian 1200L quadrapole MS using electrospray ionization (ESI). The elemental analyses were performed at Desert Analytics (Tucson, AZ). The UV-Visible spectroscopy was performed on a HP5452 diode array spectrometer thermostated at 37^{o}C. The fluorescence measurements were performed on a Hitachi F4500 fluorometer. ICP-MS measurements were performed on a VG Elemental PQ Excell spectrometer standardized with eight concentrations from 0-50 ppb Gd(III). An internal standard of 1 ppb In(III) was used in all of the ICP samples.

LC-MS and Preparative LC – The analytic LC-MS was performed on a Varian Prostar model 210 with a 410 autosampler on a 100 μl sample loop. Two 210 pump heads pumped the eluent at 5 ml/min to split to a 363 fluorescence detector and a 330 photodiode array (PDA) detector, connected to a 1200L quadrupole ESI-MS. A 3:1 split valve was used to direct the column-separated sample to 3 parts series connected light detectors and 1 part MS. All runs used a 1 ml/min flow rate on a ThermoElectron 4.6 * 150 mm 5 μm Aquasil C18 column. The mobile phase was millipore purified water and HPLC grade acetonitrile.

The preparative LC is the Varian Prostar model 210 consisting of two 210 pumps with 25 ml/min heads with a 5 ml manual injection sample loop. The Prostar system has a 2 channel UV-Visible detector tandem to a HP-1046A fluorescence detector. The mobile phases were under the same conditions used on the analytical LC-MS. The preparative

concentrations ranged between 25 mg – 150 mg dissolved in 3 ml of water. The preparative runs used a 15 ml/min on Atlantis Prep T3 10 μm 19 x 10 mm guard column.

Acetic acid 3,5-diacetoxy-2-acetoxymethyl-6-(4-formyl-2-nitro-phenoxy)-tetrahydro-pyran-4-yl ester (1) – A flask was charged with 4-hydroxy-3-nitrobenzylaldehyde (15 g, 36.4 mmol), potassium carbonate (18 g, 130 mmol), and anhydrous dimethylformamide (250 ml) and stirred for 1 h. at 40 ^{o}C. A solution of α-bromo-acetylgalactopyranose (37 g, 221.4 mmol) in anhydrous dimethlyformamide (250 ml) was added dropwise to the mixture over a period of 6 h. The orange solution was stirred overnight at 40 ^{o}C and turned to a dark brown solution. The solvent was removed under reduced pressure. The remaining oil was extracted from the remaining solids in dichloromethane (200 ml) and water (200 ml). The organic layer was dried over sodium sulfate, and concentrated to an oil. The oil was purified using silica gel chromatography (1:1 ethyl acetate:hexane). The solvent was removed to give an oil which was triturated in Et_2O. A solid crystalline formed and was filtered. The solid was washed with cold Et_2O and dried. Yield = 13.83 g (76.4%). ^{1}H NMR (500 MHz, $CDCl_3$/TMS): δ = 2.17 (12H, m), 4.19 (2H, m), 4.22 (1H, q), 5.13 (1H, dd), 5.22 (1H, d), 5.51 (1H, d), 5.62 (1H, dd), 7.50 (1H, d), 8.09 (1H, d), 8.33 (1H, s), 9.99 (1H, s). ^{13}C NMR (125 MHz, $CDCl_3$/TMS): δ = 188.77, 170.45, 170.35, 170.28, 169.36, 153.65, 141.38, 134.18, 131.62, 127.05, 118.91, 100.23, 71.98, 70.52, 67.75, 66.76, 61.54, 20.86, 20.81, 20.78, 20.75. ESI-MS *m/z* $(M+Na)^+$ 520.1 Anal. Calcd for $C_{22}H_{25}NO_{12}$: C 50.71, H 4.66, N 2.82. Found: C 50.98, H 4.90, N 2.60.

Acetic acid 3,4,5-triacetoxy-6-(4-hydroxymethyl-2-nitro-phenoxy)-tetrahydro-pyran-2-ylmethyl ester (2) – A flask was charged with **1** (5.25 g, 10.5 mmol), anhydrous

methanol (20 ml), and anhydrous dichloromethane (20 ml). Sodium borohydride (1.1 g, 30.6 mmol) was added in portions at –78 ^{o}C using an acetone/dry ice bath. The solution turned yellow after stirring for 6 h, after which water (2 ml) was used to quench the reaction. The solvent was removed under reduced pressure. The resulting residue was dissolved in CH_2Cl_2, washed with water, dried using sodium sulfate, and the remaining organic solvent was removed under reduced pressure. The remaining oil was purified on a silica gel column using a 0%-66% ethyl acetate:hexanes gradient. The fraction containing the product were concentrated and dried in vacuo to leave a yellow solid. Yield = 4.33 g (82.5%). ^{1}H NMR (500MHz, $CDCl_3$/TMS): δ = 2.07 (12H, m), 4.17 (3H, m), 4.71 (2H, s), 5.06 (2H, m) 5.48 (2H, m), 7.34 (1H, d), 7.51 (1H, d), 7.79 (1H, s). ^{13}C NMR (125 MHz, $CDCl_3$/TMS): δ = 170.34, 170.18, 170.14, 169.48, 148.41, 141.29, 137.25, 131.82, 123.29, 119.99, 100.95, 71.57, 70.73, 68.05, 66.92, 63.60, 61.56, 21.00, 20.98, 20.91. ESI-MS *m/z* $(M+Na)^+$ 522.2 Anal. Calcd for $C_{22}H_{27}NO_{12}$: C 50.50, H 5.05, N 2.80. Found: C 50.39, H 5.11, N 2.76.

Acetic acid 4,5-diacetoxy-6-acetoxymethyl-2-[4-(2-bromo-ethylcarbamoyloxymethyl)-2-nitro-phenoxy]-tetrahydro-pyran-3-yl ester (3) – A solution of **2** (1.57 g, 3.14 mmol), 1-bromo-2-isocyanato-ethane (0.34 ml, 3.76 mmol), DMAP (0.46g, 3.76 mmol), and dichloromethane (20 ml) was stirred at RT for 48 h. The solvent was removed and the resulting oil purified on a silica gel column using a gradient from 30%-70% ethyl acetate:hexanes. The fractions containing the product were dried in vacuo overnight to give a white glass. Yield = 1.048 g (51.4%). ^{1}H NMR (500 MHz, $CDCl_3$/TMS): δ = 2.11 (12H, m), 3.49 (2H, m), 3.63 (2H, m), 4.14 (3H, m), 5.11 (4H, m), 5.25 (1H, b), 5.47 (1H, d), 5.55 (1H, q), 7.35 (1H, d), 7.52 (1H, d), 7.82 (1H, s). ^{13}C

NMR (125 MHz, $CDCl_3$/TMS): δ = 170.38, 170.25, 170.16, 169.44, 155.83, 149.01, 141.07, 133.26, 132.66, 124.61, 119.53, 100.58, 71.44, 70.52, 67.83, 66.79, 64.93, 61.42, 42.79, 32.18, 20.67. ESI-MS *m/z* $(M+Na)^+$ 672.9 with Br isotope pattern.

(**4,7-Bis-ethoxycarbonylmethyl-1,4,7,10tetraaza-cyclododec-1-yl)-acetic acid ethyl ester (8)** – A flask was charged with cyclen (4.0 g, 23.2 mmol), sodium bicarbonate (6.0 g, 71.4 mmol), and anhydrous acetonitrile (200 ml). While stirring vigorously, ethyl-bromoacetate (5.8 ml, 52.3 mmol) was added dropwise over 6 h at RT and stirred for 48 h. The solution changed from clear to orange. The solvent was removed under reduced pressure, and the resulting residue was extracted in dichloromethane (200 ml) and water 150 (ml). The organic layer was collected and washed with brine and washed with additional 2x deionized water (100 ml). The organic layer was concentrated, and further purification was performed using silica gel column chromotography (4% methanol in dichloromethane). The product was triturated twice in Et_2O and refrigerated for 3 d at – 20 ^oC resulting in solid plates. The product was filtered and dried in vacuo overnight to leave a fine white powder. Yield = 3.618 g (36.2%). ^1H NMR (500 MHz, $CDCl_3$/TMS): δ = 1.27 (9H, t), 2.82 – 3.51 (22H, b), 4.16 (6H, q), 10.01 (1H, b). ^{13}C NMR (125MHz, $CDCl_3$/TMS): δ = 171.32, 170.49, 94.94, 60.96, 57.44, 54.58, 51.55, 51.41, 49.47, 47.57, 14.41. ESI-MS *m/z* $(M)^+$ 430.6.

(4,7-Bis-ethoxycarbonylmethyl-10-{2-[3-nitro-4-(3,4,5-triacetoxy-6-acetoxymethyl-tetrahydro-pyran-2-yloxy)-benzyloxycarbonylamino]-ethyl}-1,4,7,10tetraaza-cyclododec-1-yl)-acetic acid ethyl ester (4) – A flask was charged with **3** (1.04 g, 1.60 mmol), **8** (0.67 g, 1.56 mmol), potassium carbonate (0.26 g, 1.88 mmol) and anhydrous acetonitrile (30 ml). The yellow solution was stirred for 3 d at RT. The solvent was

removed under reduced pressure, and the resulting solution was extracted using dichloromethane (50 ml) and water (50 ml). The organic layer was washed with sat. bicarbonate solution (50 ml). The organic layer was collected and concentrated in vacuo. The resulting oil was purified using silica gel column chromatography (5% methanol in dichloromethane). The resulting product is a yellow oil. Yield = 0.234 g (15.0%). ^{1}H NMR (500 MHz, $CDCl_3$/TMS): δ = 1.24 (9H, m), 2.07 (12H, m), 2.25-3.83 (26H, b), 4.10 (9H, m), 5.06 (3H,m) 5.45 (1H, d), 5.51 (1H,q), 6.55 (1H, b), 7.38 (1H, d), 7.57 (1H, d), 7.75 (1H, s). ^{13}C NMR (125 MHz, $CDCl_3$/TMS): δ = 173.67, 173.45, 173.29, 170.79, 170.26, 170.03, 169.86, 169.28, 157.01, 148.64, 140.61, 133.06, 124.27, 123.78, 119.21, 100.14, 71.23, 70.41, 67.74, 66.73, 64.33, 61.70, 61.37, 61.16, 60.62, 55.68, 55.13, 54.50, 52.48, 50.12, 37.63, 30.18, 29.51, 20.54, 14.10 ESI-MS *m/z* (M) 999.4, $(M+Na)^+$ 1021.4.

Gadolinium -(4,7-Bis-carboxymethyl-10-{2-[3-nitro-4-(3,4,5-trihydroxy-6-hydroxymethyl-tetrahydro-pyran-2-yloxy)-benzyloxycarbonylamino]-ethyl}-1,4,7,10tetraaza-cyclododec-1-yl)-acetic acid (5) – Compound **4** (0.136 g, 0.136 mmol) was dissolved in tetrahydrofuran (0.2 ml). A solution of 0.25M NaOH solution (5 ml) was added to the reaction mixture and stirred at RT for 3 h. The pH was adjusted to 5.0 using a 0.5 M HCl solution, and a color change was observed at pH 8.0. A solution of anhydrous $GdCl_3$ (0.045 g, 0.171 mmol) dissolved in deionized water (1 ml) was added to the solution. The pH was monitored. As the pH began to decrease, a 0.25 M NaOH solution was used to adjust the pH to 5.0. The solution became cloudy after 1 h. The solution was stirred for 4 d. A 1 M NaOH (1 ml) was added to change the pH to ~10. The cloudy solution was filtered through a 0.25 μm syringe filter. Further purification was performed using HPLC. The product was lyophilized to give a fluffy yellow solid. Yield

= 65.2 mg (53.2%). ESI-MS *m/z* $(M)^+$ 898.4 with Gd isotope pattern. Anal. Calcd for $C_{31}H_{45}GdN_6O_{15}$: C 39.99, H 4.81, N 9.33. Found: C 40.40, H 5.07, N 9.38.

Europium -(4,7-Bis-carboxymethyl-10-{2-[3-nitro-4-(3,4,5-trihydroxy-6-hydroxymethyl-tetrahydro-pyran-2-yloxy)-benzyloxycarbonylamino]-ethyl}-1,4,7,10tetraaza-cyclododec-1-yl)-acetic acid (6) – A flask was charged with **4** (0.0482 g, 0.0482 mmol) and 0.25 M NaOH solution (1.75ml). The solution was stirred at RT for 3 h. The pH was adjusted to 5.0 using a 0.5 M HCl solution, and a color change was observed at pH 8.0. A solution of $EuCl_3$ (0.0117 g, 0.0453 mmol) dissolved in deionized water (1 ml) was added to the ligand solution and the pH monitored. As the pH began to decrease, a solution of 0.25 M NaOH solution was used to adjust the pH back to 5.5. The solution became cloudy after 1 h. The solution was stirred for 4 d. A solution 1 M NaOH (1 ml) was added to change the pH to ~10. The solution was filtered through a 0.25 μm filter. Further purification was performed using HPLC. The product was lyophilized to give a fluffy yellow solid. Yield = 12.0 mg (27.8%). ^{1}H NMR (500MHz, D_2O, at 25.3^{o}C): δ = -23.5--0.3 (mb), 3.7 (m), 4.9 (b), 7.6 (m), 8.3-30.1 (mb) ESI-MS *m/z* $(M)^+$ 895.7 with europium isotope pattern. Anal. Calcd for $C_{31}H_{45}EuN_6O_{15}\cdot 4H_2O$: C 37.23, H 5.31, N 8.68. Found: C 37.18 H 5.25 N 8.43.

Acetic acid 3,4,5-triacetoxy-6-(4-formyl-phenoxy)-tetrahydro-pyran-2-ylmethyl ester (10) – A flask was charged with 4-hydroxylaldehyde (4.0 g, 37.75 mmol), cesium carbonate (10.5 g, 32.2 mmol), and anhydrous dimethylformamide (65 ml) and was stirred for 30 min. The solution was cooled to 0 ^{o}C and a solution of dichloromethane (100 ml) and of α-bromo-acetylgalactopyranose (12.5 g, 30.4 mmol) added dropwise to the reaction mixture. The solution was allowed to warm to RT and stirred overnight. The

reaction was washed with water (200 ml) and brine (200 ml). The organic layer was collected and concentrated under reduced pressure. Further purification was performed using silica gel column chromatography (1:1 ethyl acetate:hexane). The solvent was removed under reduced pressure and the remaining solid was dried in vacuo overnight to a give fluffy white solid. Yield = 11.1g (80.6%). ^{1}H NMR (500 MHz, $CDCl_3$/TMS): δ = 2.15 (12H, m), 4.19 (3H, m), 5.17 (2H, m), 5.50 (2H, m), 7.11 (2H, d), 7.85 (2H, d), 9.92 (1H, s). ^{13}C NMR (125 MHz, $CDCl_3$/TMS): δ = 189.51, 170.24, 170.07, 169.98, 169.221, 161.198, 191.81, 116.76, 98.62, 71.46, 70.80, 68.54, 66.99, 66.90, 61.54, 20.99, 20.945, 20.91, 20.85, 20.82. ESI-MS *m/z* $(M+Na)^+$ 475.1. Anal. Calcd for $C_{22}H_{26}O_{10}$: C 55.75, H 5.35, N 0. Found: C 55.56, H 5.32, N<0.05.

Acetic acid 3,4,5-triacetoxy-6-(4-hydroxymethyl-phenoxy)-tetrahydro-pyran-2-ylmethyl ester (11) – A flask was charged with **10** (1.63 g, 3.60 mmol) and anhydrous dichloromethane (60 ml). Sodium borohydride (0.15 g, 3.96 mmol) was added in portions at 0 ^{o}C and the reaction was stirred for 45 min. The solvent was removed under reduced pressure to leave a yellow solid. Solids were dissolved in dichloromethane (20 ml), washed with brine (50 ml) and water (50 ml). The organic layer was collected and dried over sodium sulfate. The solvent was removed under reduced pressure and further purified using silica column chromatography (10%-50% ethyl acetate:hexane gradient). The product was dried in vacuo to give a light yellow solid. Yield = 1.07 g (60.2%). ^{1}H NMR (500 MHz, $CDCl_3$/TMS): δ = 2.15 (12H, m), 4.17 (3H, m), 4.68 (1H, s), 5.09 (3H, m), 5.48 (2H, m), 6.97 (2H, d), 7.30 (2H, d). ^{13}C NMR (125 MHz, $CDCl_3$/TMS): δ = 170.35, 170.23, 170.12, 169.98, 156.44, 128.60, 117.08, 99.84, 71.19, 71.00, 68.81,

67.05, 66.62, 64.04, 61.56, 21.07, 20.99, 20.92. ESI-MS *m/z* $(M+Na)^+$ 477.2. Anal. Calcd for $C_{22}H_{28}O_{10}$: C 55.50, H 5.77, N 0. Found: C 55.48, H 5.97, N 0.06.

Imidazole-1-carboxylic acid 4-(3,4,5-triacetoxy-6-acetoxymethyl-tetrahydro-pyran-2-yloxy)-benzyl ester (12) – A flask was charged with **11** (2.8 g, 6.17 mmol), DMAP (0.75 g, 6.17 mmol), carbonyldiimidozale (2.0 g, 12.53 mmol), and anhydrous dichloromethane (40ml) and stirred for 9 h. The reaction mixture was washed with saturated sodium bicarbonate solution, and organic layer was dried in sodium sulfate. The solvent was removed under reduced pressure and purified silica gel column chromatography (20%-66% ethyl acetate:hexane gradient). The solvent was removed to leave a white solid. Yield = 3.13 g (92.4%). ^{1}H NMR (500 MHz, $CDCl_3$/TMS): δ = 2.08 (12H, m), 4.16 (3H, m), 5.10 (2H, m), 5.38 (2H, s), 5.49 (2H, m), 7.14 (3H, m), 7.40 (3H, m), 8.13 (1H, s). ^{13}C NMR (125 MHz, $CDCl_3$/TMS): δ = 170.31, 170.25, 170.17, 169.89, 157.95, 148.41, 137.87, 131.34, 131.22, 129.19, 117.09, 99.74, 71.04, 70.98, 68.79, 67.00, 66.23, 63.98, 61.45, 21.06, 20.91, 20.79, 20.69 Anal. Calcd for $C_{26}H_{30}N_2O_{11}$: C 54.74, H 5.15, N 5.11. Found: C 55.37, H 5.62, N 4.86.

Acetic acid 4,5-diacetoxy-2-acetoxymethyl-6-[4-(2-bromo-ethylcarbamoyloxymethyl)-phenoxy]-tetrahydro-pyran-3-yl ester (13) – The flask was charged with **12** (2.0 g, 3.65 mmol), anhydrous dichloromethane (20 ml), and methyl triflate (0.42 ml, 3.65 mmol) and stirred at 0 ^{o}C for 15 min. Triethylamine (0.51 ml, 3.65 mmol), 2-amino-ethylbromide (0.75 g, 3.65 mmol) and DMAP (10 mg, 0.081 mmol) were added to the reaction mixture. The solution was allowed to warm to RT and stirred overnight. The reaction was washed with saturated sodium carbonate (50 ml) and water (50 ml). The organic layer was collected and dried over sodium sulfate. The solution was

filtered, and the solvent was removed under reduced pressure. The remaining residue was dried in vacuo to give an oil. Yield = 1.05 g (48%). ^{1}H NMR (500 MHz, $CDCl_3$/TMS): δ = 2.08 (12H, m), 3.44 (2H, t), 3.59 (2H, t), 4.14 (2H, m), 5.03 (3H, m), 5.22 (2H, m), 5.42 (2H, m), 6.94 (2H, d), 7.31 (2H, d). ^{13}C NMR (125 MHz, $CDCl_3$/TMS): δ = 170.29, 170.23, 170.18, 169.43, 156.90, 132.42, 129.95, 117.00, 99.62, 71.15, 70.89, 68.70, 67.12, 66.98, 66.54, 61.49, 42.87, 32.64, 20.93, 20.86, 20.79, 20.12. Anal. Calcd for $C_{25}H_{32}BrNO_{11}$: C 47.68, H 5.00, N 2.32. Found: C 48.04, H 5.17, N 2.41.

[4,7-Bis-ethoxycarbonylmethyl-10-(2-{3-[4-(3,4,5-triacetoxy-6-acetoxymethyl-tetrahydro-pyran-2-yloxy)-phenyl]-propionylamino}-ethyl)-1,4,7,10tetraaza-cyclododec-1-yl]-acetic acid ethyl ester (14) – A solution of **13** (0.55 g, 0.91 mmol), cyclen (0.63 g, 3.65 mmol), and anhydrous dichloromethane (100 ml) was refluxed for 24 h. The solution was filtered and the solvent was removed under reduced pressure to a solid. The solid was redissolved with dichloromethane (15 ml), and the solution was washed with water (20 ml) and brine (20 ml). The organic layer was collected and dried over sodium sulfate. The solvent was removed to leave a beige solid. Anhydrous acetonitrile (40 ml), potassium carbonate (0.48 g, 3.45 mmol), and methyl bromoacetate (246 μl, 2.52 mmol) was added, and the reaction was stirred overnight. The solvent was removed, and the residue was purified using silica gel column chromatography (0%-8% methanol:dichloromethane gradient). The product was collected, and the solvent was removed. The product was dried in vacuo to give a light yellow solid. Yield = 0.40 g (48%) ^{1}H NMR (500 MHz, $CDCl_3$/TMS): δ = 1.83 (2H, b), 2.10 (12H, m), 2.34-3.65 (24H, b), 3.74 (9H, m), 4.18 (3H, m), 5.19 (4H, m), 5.49 (2H, m), 6.18 (1H, b), 6.97 (2H,

d), 7.32 (2H, d). Anal. Calcd for $C_{42}H_{63}N_5O_{17}\cdot 0.75HBr\cdot H_2O$: C 49.64, H 6.62, N 7.22, O 30.97, Br 6.35. Found: C 49.71, H 6.49, N 7.07, O 30.69, Br 6.05.

Gadolinium-[4,7-Bis-carboxymethyl-10-(2-{3-[4-(3,4,5-trihydroxy-6-hydroxymethyl-tetrahydro-pyran-2-yloxy)-phenyl]-propionylamino}-ethyl)-1,4,7,10tetraaza-cyclododec-1-yl]-acetic acid (15) – Compound **14** (0.1 g, 0.110 mmol) was dissolved in tetrahydrofuran (0.2 ml). A solution of 0.25 M NaOH solution (6.4 ml, 1.60 mmol) was added to the reaction and stirred for 3 hours at RT. A solution of gadolinium chloride (0.035 g, 0.133 mmol) in water (1 ml) was added to the reaction mixture. The pH was adjusted to 5.0, and the solution was stirred for 3 d. A solution of 1 M NaOH (1 ml) was added to adjust the pH to ~10. The resulting solution was filtered through a 0.25 μm syringe filter. Further purification was performed using HPLC. The product was lyophilized to give a fluffy white powder. Yield = 22 mg (25.7%) ESI-MS *m/z* $(M)^+$ 855.2 with gadolinium isotope pattern. Anal. Calcd for $C_{31}H_{46}GdN_5O_{13}\cdot Na$: C 41.00, H 5.05, N 9.79. Found: C 40.79, H 5.20, N 7.81.

Europium-[4,7-Bis-carboxymethyl-10-(2-{3-[4-(3,4,5-trihydroxy-6-hydroxymethyl-tetrahydro-pyran-2-yloxy)-phenyl]-propionylamino}-ethyl)-1,4,7,10tetraaza-cyclododec-1-yl]-acetic acid (16) – The flask was charged with **14** (0.1 g, 0.110 mmol) and 0.25 M NaOH solution (6.4 ml, 1.60 mmol), and the solution was stirred for 3 h at RT. A solution of europium chloride hexahydrate (0.030 g, 0.0819 mmol) and water (1 ml) was added to the reaction mixture. The pH was adjusted to 5.0, and the solution was stirred for 3 days. The pH was adjusted to ~10, by adding 1 M NaOH solution (1 ml). The cloudy solution was filtered through a 0.25 μm syringe filter. The resulting mixture was purified by HPLC. The product was lyophilized to leave a

fluffy white powder. Yield = 21 mg (24.7%). ^{1}H NMR (125 MHz, D_2O, at 75^{o}C): δ = 19.6 (b), 8.2 – 1.3 (m), -3.4 (b), -12.5 (b) ESI-MS *m/z* $(M)^{+}$ 849.6 with europium isotope pattern. Anal found for $C_{31}H_{46}EuN_5O_{13}\cdot 6H_2O$: C 37.58, H 5.89, N 7.30. Found: C 37.10, H 5.52, N 7.27.

Relaxivity and pH studies: The T_1 of each sample was obtained on a Bruker mq60 Minispec using an inversion recovery pulse sequence with appropriate recycle delays. This instrument has a proton Larmor frequency of 60 MHz and operates at 37 ^{o}C. Five relaxivity samples were prepared by serial dilutions with concentrations ranging between 0.1 mM and 2.0 mM of the paramagnetic complexes. The concentrations of Gd(III) complex solutions were determined from ICP-MS measurements were performed in triplicate.

For the relaxivity versus pH studies, the T_1 was determined for each pH point in intervals of 0.4 pH units. The concentrations for the two paramagnetic complex solutions were determined to be 0.839 mM for **5** and 0.789 mM for **15** by ICP-MS.

^{17}O NMR – Variable temperature ^{17}O NMR spectroscopy was used to determine the water exchange rate (τ_m) for the gadolinium complexes **5** and **15**. The paramagnetic complexes were dissolved in 1% ^{17}O enriched solution of water with a D_2O external lock. The solution of **5** was determined to have a concentration of 23.85 mM by ICP-MS. The solution for **15** was determined to be 23.35 mM by ICP-MS. The observed transverse relaxation rates were calculated from the signal width at half-height. The experiments were fit to a Swift-Connick equation on Origin 7.0.[30]

Enzyme Kinetics – Bovine liver β-galactosidase (Grade III – Sigma G 1875, Lot 104K7) was tested for efficacy using the Promega control assay using ONPG. A standard

curve was prepared using 1.33 mg/ml ONPG in phosphate buffer. The enzyme buffer (PBS) consisted of 137.0 mM NaCl, 2.7mM KCl, 8.1 mM Na_2HPO_4, and 1.47 mM KH_2PO_4. The varying enzyme-substrate mixtures were incubated for 30 m at 37 ^oC. The enzyme was stable for more than 6 h at 37^oC at its native pH in 7.4 in the PBS buffer, but activity decreased when it was incubated overnight.

The enzyme β-gal hydrolyzed the galactopyranose sugar of **5**, resulting in the decomposition of the linker to generate 4-hydroxy-3-nitrobenzyl alcohol, which was determined to have a molar absorptivity of $\varepsilon = 2641 \pm 50\ M^{-1}\ cm^{-1}$ at 420 nm. This value of ε obtained was used in calculations of enzyme kinetic values. The stock solution of **5** was determined by ICP-MS to be 2.18 mM. The stock enzyme solution was prepared by dissolving 1.55 mg of the β-gal enzyme in 1 ml of PBS buffer. 10 μl of the concentrated enzyme solution was diluted with 990 μl of the PBS solution to make a dilute enzyme solution of 15.5 μg β-gal/ml of PBS. The molecular weight for β-gal was determined to be 116,248 g/mol from the amino sequence of the protein and this value was used in enzyme kinetic experiments.[31] The background for the substrate solution of **5** at 420 nm was subtracted from the experiment prior to the evaluation enzyme kinetics for β-gal. The enzyme kinetic experiments were sampled in 30 s increments at 37 ^oC for 1 h. The initial velocity of the enzyme cleavage of the substrate assumed a direct correlation with product formation.

This turnover velocity was determined in pmol/sec of the processed 4-hydroxy-3-nitrobenzyl alcohol, which was charted versus substrate concentration between the range of 0.04 mM – 1.4 mM concentration of **5**. The measurements were performed in triplicate. A control experiment with no enzyme present was performed to rule out auto-

hydrolysis of **5**. The resulting Michaelis-Menten plot was fit using the hyperbola non-linear fit function on Origin 7.0 to determine the K_m and V_{max} of the substrate.[32,33] The enzyme hydrolysis of **5** was confirmed by LC-MS in a stop point experiment. The eluent gradient of 0% – 5% acetonitrile/water over 50 min was used to separate the reaction products on a ThermoElectron 4.6 * 150 mm 5 μm Aquasil C18 column. The starting material **5** and the hydrolysis products (galactopyranose, 4-hydroxy-3-nitrobenzyl alcohol, and **9**) were assigned using UV-visible signatures and mass spectrometry.

The colormetric enzyme kinetics of cleavage of **5** was confirmed with a relaxometric method. A 100 μl solution of enzyme at 15 μg/ml in PBS buffer was added to the 400 μl of solution of **5** at 0.798 mM in phosphate buffer. The T_1 change was observed over 1 h using a saturation recovery sequence in 3 m increments

Determination of q using europium fluorescence – Five samples were prepared, and the fluorescence lifetime decays for complexes **6** and **16** were measured between molar ratios of 0 to 0.8 H_2O:D_2O. Eighty scans were averaged for each molar ratio sample and fit to a monoexponential decay equation in Origin 7.0. The inverse of the decay lifetimes was plotted versus the molar ratio of H_2O:D_2O to yield a line with R^2 values >0.985. This line was used to extrapolate the τ^{-1} for complexes **6** and **16** in pure water. The Horrocks equation was used to calculate q from the observed $\tau^{-1}(D_2O)$ and the determined $\tau^{-1}(H_2O)$.[34]

Cell Culture and Labeling - NIH/3T3 cells were cultured in Dulbecco's modified Eagle medium with 2 mM L-glutamine and 10% calf bovine serum. Hep G2 cells were cultured in Eagle's minimal essential medium with 2 mM L-glutamine, 1.5 g/L sodium

bicarbonate, 1.0 mM sodium pyruvate, 0.1 mM non-essential amino acids and 10% fetal bovine serum.

Cells were plated in triplicate in 24-well plates in 1 mL of growth medium at a density of 1 X 10^5 cells/well for NIH/3T3 cells and at a density of 3 X 10^5 cells/well for Hep G2 cells. Cells were incubated at 37 °C and 5% CO_2 overnight. Europium analogs **6** and **16** were substituted for the gadolinium complexes **5** and **15** for the cell studies, and it was assumed that the identity of the lanthanide does not cause differences in either cellular uptake or toxicity. The agents **6** and **16** were dissolved in growth medium at a concentration of 5 mM for 0.5 mM studies and sterilized using a 0.2 μm syringe filter. For a final concentration of 0.5 mM 100 μL of 5 mM contrast agent-containing media was added to 900 μL of media per well. Cells were incubated for 0, 2, 4, 8, or 24 hours. Cells were washed three times with 1 mL of 1X PBS and trypsinized with 1000 μL of 0.25% trypsin-EDTA per well for 10 minutes. Cells were resuspended in an additional 300 μL of growth medium and transferred to 1.5 mL tubes. Cell viability was then determined using the Guava Technologies ViaCount system where cells were diluted 10 fold with the ViaCount reagent and counted by flow cytometry. The europium concentrations were determined by ICP-MS. The cell samples were digested with 350 μl of neat nitric acid for 4 hours at 70°C and cooled to room temperature. The sample was diluted into a total of 2 mL with water and 5 ppb In internal standard.

Synthesis – The routes used to synthesize complexes **5**, **6**, **15**, and **16** are outlined in **Schemes 2-1** to **Scheme 2-3**. While the synthesis of **15** is similar to that reported by Dumistra et al for a similar complex,[26] the synthesis of **5** was altered to improve yields. 4-hydroxy-3-nitrobenzaldehyde was coupled to a β-D-galactopyranose to give **1**.(**Scheme**

2-1) The aldehyde was reduced to an alcohol using sodium borohydride to give **2**. Initial attempts to synthesize the self-immolative arm **3** using carbonyldiimidazole (CDI) gave poor yields, thus was abandoned for a more direct route.(**Scheme 2-2**) Compound **2** was conjugated to 1-bromo-2-isocyanato-ethane. Alkylation of DO3A(*tris*-ethyl ester) with **3** gave the protected ligand **4**. Sodium hydroxide was used deprotect the carboxylate arms of **4** to give the free ligand which was metallated with either $GdCl_3$ or $EuCl_3$ in aqueous conditions. HPLC purification of **5** and **6** yielded compounds that gave satisfactory elemental analyses.

The synthesis of **15** generally follows that described by Duimstra et al.[26] 4-hydroxy-benzaldehyde was coupled to a β-D-galactopyranose to give **10** and the aldehyde was subsequently reduced to an alcohol using sodium borohydride to give **11**.(**Scheme 2-1**) This species was reacted with CDI to give the monoimidazolyl intermediate **12**.(**Scheme 2-2**) In one pot, **12** was methylated using methyl triflate and then immediately reacted with 2-amino-ethylbromide to give the self-immolative carbamate linker **13**. Cyclen was monoalkylated with the self-immolative arm, followed by alkylation with 3 equiv. of methyl bromoacetate to give **14**. Deprotection, metallation, and purification procedures to yield complexes **5** and **6** were similar to the procedures described for **15**.

Results and Discussion:

The relaxivity, r_{1P}, is defined as the efficiency of contrast agents to shorten the longitudinal relaxation time, T_1, of the protons of the surrounding water molecules. For small molecular weight contrast agents <1000 MW, the inner sphere water contribution, defined as q, constitutes approximately 50% of the overall relaxivity.[14] The r_{1P} values for

5 and **15** were determined to be 6.54 and 6.48 $s^{-1}mM^{-1}$, respectively, in pure water at 60 MHz at 37 ^{o}C.(**Figure 2-2**) These relaxivity measurements are considered high values when compared to other low-molecular weight, monomeric paramagnetic complexes such the reference complexes Gd(III)-DOTA (r_{1P} = 3.13 $s^{-1}mM^{-1}$) and Gd(III)-2hydroxypropyl-DO3A (r_{1P} = 2.99 $s^{-1}mM^{-1}$).[14,28] The r_{1P} magnitudes for complexes **5** and **15** imply that the q values are greater than 1 for both complexes.

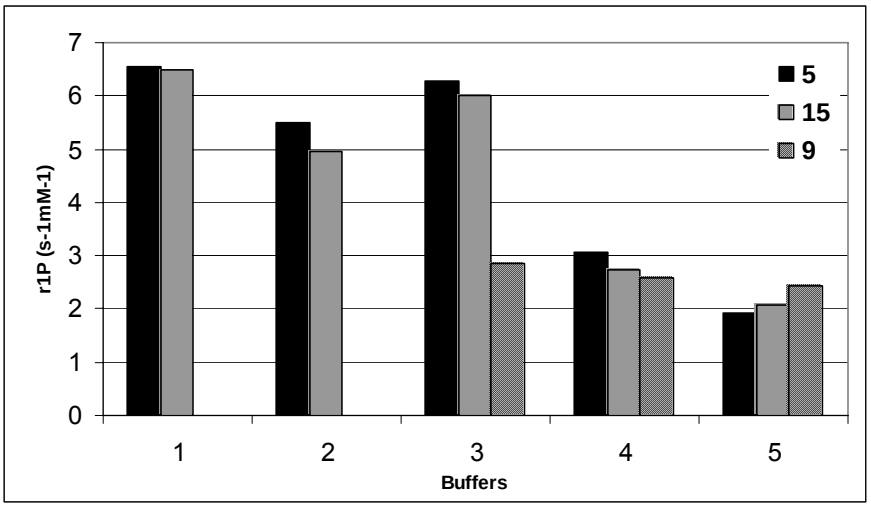

Figure 2-2. The r_{1P} values (at 37 ^{o}C, 60 MHz) in different buffer conditions conditions: [1] H_2O pH = 6.52; [2] Phosphate buffer (200 mM sodium phosphate, 2 mM $MgCl_2$, 100 mM mercaptoethanol) pH = 7.40; [3] MOPS buffer (10 mM MOPS, 100 mM NaCl) pH = 5.28; [4] MOPS/carbonate buffer (10 mM MOPS, 24 mM $NaHCO_3$) pH = 7.55; [5] Anion mimic buffer (100 mM NaCl, 0.9 mM $NaHPO_4$, 30 mM $NaHCO_3$, 0.13 sodium citrate, 2.3mM sodium lactate) pH = 8.53.

Relaxivity measurements of **5** and **15** in buffered solutions demonstrate that anions affect the water-lanthanide interaction.(**Table 2-1**) The r_{1P} for **5** was determined to be

5.51 $s^{-1}mM^{-1}$ in phosphate buffer, which is a decrease of 16% compared to the value obtained in for **5** neat water (**Figure 2-2**). Similar results are observed for **15**; the relaxivity is 23% lower in phosphate buffer than in water. The phosphate ion has been shown to exhibit monodentate binding to DO3A derivatives.[35] Phosphate anions compete with water for coordination sites, thereby lowering the inner-sphere water contribution of the overall relaxivity. MOPS buffer was chosen as a non-coordinating comparison. In MOPS, the r_{1P} values for **5** and **15** were measured to be 6.28 $s^{-1}mM^{-1}$ and 6.01 $s^{-1}mM^{-1}$ respectively. Not surprisingly, these relaxivity values are similar to the values observed for the complexes in neat water.[36]

	Water	PBS	MOPS	MOPS/carbonate	Anion mimic
5	6.54	5.51	6.28	3.07	1.92
15	6.48	4.96	6.01	2.74	2.07
9*	-	3.90	2.85	2.58	2.42
5 + β-gal	-	4.14	-	-	-
15 + β-gal	-	3.90	-	-	-

Table 2-1: Relaxivity values ($s^{-1}mM^{-1}$) of **5**, **15**, and **9** in varying buffers corresponding to Figure 2, including values after β-gal enzyme cleavage. *Values for **9** were taken from reference 28.

Physiological levels of anions like carbonate, citrate, and lactate have been shown to correspond to low relaxivity values, implying the lanthanide complex is coordinatively saturated.[37] Carbonate is known to strongly bind to heptacoordinate cyclen-based complexes such as Ln(DO3A).[38,39] The r_{1P} for **5** in MOPS with a 24 mM carbonate anion concentration was determined to be 3.07 $s^{-1}mM^{-1}$, which is a 47% decrease in relaxivity compared to **5** in pure water (**Figure 2-2**). Furthermore, the r_{1P} for **5** in the anion mimic buffer with a carbonate concentration of 30 mM was measured to be 1.92 $s^{-1}mM^{-1}$, which represents a remarkable 71% decrease compared to **5** in pure water. Similarly, the r_{1P} for **15** was found to be 2.74 $s^{-1}mM^{-1}$ in MOPS/carbonate buffer and 2.07 $s^{-1}mM^{-1}$ in the anion mimic buffer.

Cleavage of **5** and **15** by β-gal is expected to result in the formation of **9**. Upon introduction of β-gal to **5** in PBS, the relaxivity is observed to decrease by 25% in 1h. Upon a 13 h incubation of **15** with β-gal in PBS, the r_{1P} decreases from 4.96 $s^{-1}mM^{-1}$ to 3.90 $s^{-1}mM^{-1}$, a difference of 21%.(**Table 2-1**) These values compare well with the independently measured value for **9** in PBS buffer. Compound **9** was previously studied and the values are included in Table 2-1 for comparison.[28] The r_{1P} values for **5** and **15** in the buffer mimicking the in vivo anion concentrations, were both found to be lower than that of **9**.

The relaxivities of complexes **5** and **15** were found to have a similar dependence on pH. (**Figure 2-3**) Both **5** and **15** demonstrate stable relaxivity in the relevant physiological pH range of 4 to 8. At pH values < 4.0, the coordinated acetate arms and macrocyclic nitrogens become protonated to release the lanthanide from the chelate, resulting in r_{1P} values corresponding to aqua Gd(III) ion (~10 $s^{-1}mM^{-1}$).[19] At pH values > 8.5, a gradual

decrease in r_{1P} was observed. As no steps were taken to deaerate the solutions, dissolved CO_2 leads to the formation of HCO_3^- and CO_3^{2-} under these basic conditions. These ions, along with the hydroxyl ion, can coordinatively saturate the complex resulting in the low relaxivity values. At pH 12, complexes **5** and **15** are observed to have r_{1P} of ~2 $s^{-1}mM^{-1}$ typically attributed to purely 'outer-sphere' contribution. Analogous heptacoordinate DO3A complexes have similar pH profiles attributed to the binding of hydroxide and carbonate.[41,42]

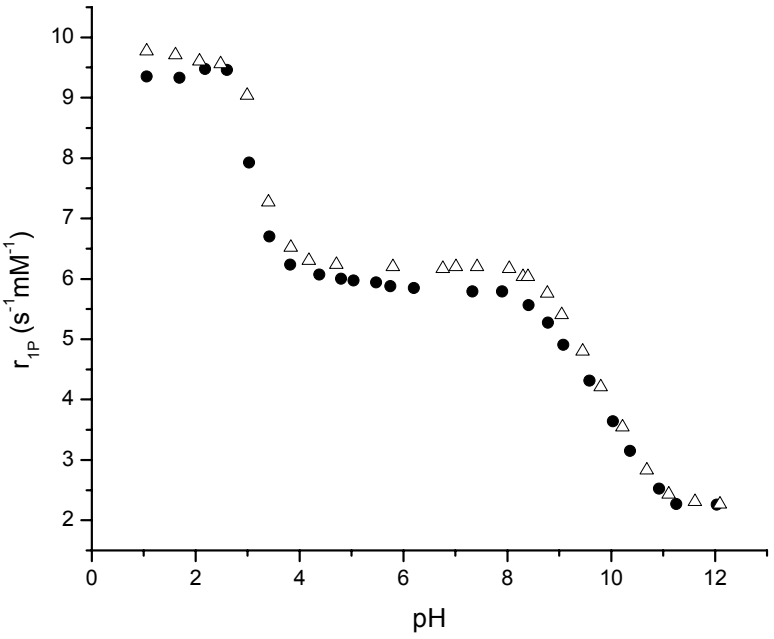

Figure 2-3. T_1-relaxivity vs pH for **5** (open triangles) and **15** (closed circles)

Fluorescence measurements for q corroborate the relaxivity data indicating q > 1. At neutral pH and at RT, **6** was found $\tau(D_2O)$ = 1.34 ms; $\tau(H_2O)$ = 0.42 ms. Using the Horrocks equation, the q for **6** is determined to be 1.5 (with correction factor for one amide = 1.4).[34] At the neutral pH and at RT, **16** was found to have $\tau(D_2O)$ = 1.81 ms;

$\tau(H_2O)$ = 0.49 ms. The q for **16** was determined to be 1.3 (with the correction factor for one amide q = 1.2). The luminescence studies of the europium-analog complexes, **6** and **16** gave non-integer values for q greater than 1 indicating that the donating ability of the carbamate carbonyl oxygen is minimal due to electron density delocalization and neutral charge of the complexes. Previous work by Dumistra et al observed a lower q and r_{1P} with a glucuronic sugar moiety.[28] The extra carboxylate on the glucuronic sugar can contribute to coordination back to the lanthanide. However, the β-D-galactopyranoside sugar moiety on **5** and **15** does not effectively donate electron density to the lanthanide, thereby leaving the complexes open for more than 1 inner sphere water to coordinate to the lanthanide center.

Variable temperature ^{17}O NMR determined that the water exchange rates (τ_M) for complexes **5** and **15** were 71 ns and 62 ns, respectively (**Figure 2-4**). These τ_M values are considered relatively fast rates of water exchange, which correspond to an associative exchange mechanism that is typical for lanthanide complexes with q = 2. When compared to other water exchange values for small (MW>1000) monomeric macrocyclic complexes like Gd(III)-DOTA = 108 ns and GdIII-DO3A = 77 ns,[14] τ_M values for **5** and **15** are closer to DO3A complexes with q of 2. A correlation of higher inner-sphere water and water exchange is attributed to the rigidity of the arms on the macrocycle what increases the energy necessary to reach the transition state in hydration equilibrium.[40] With two inner-sphere water molecules, the ^{17}O NMR data reaffirms the relaxivity and luminescence data, indicating little intramolecular interaction of carbamate carbonyl oxygen or the sugar moiety with the lanthanide on the macrocycle. Calculations of τ_M based on the Solomon-Bloembergen-Morgan theory of paramagnetic relaxation demonstrate that water

exchange rates for complexes **5** and **15** are within the optimal range for attaining maximum proton relaxivities for Gd(III)-based, macrocyclic MR imaging contrast agents.[14,42] Further experiments are needed to discern which mechanisms contribute to this increased rate of water exchange.

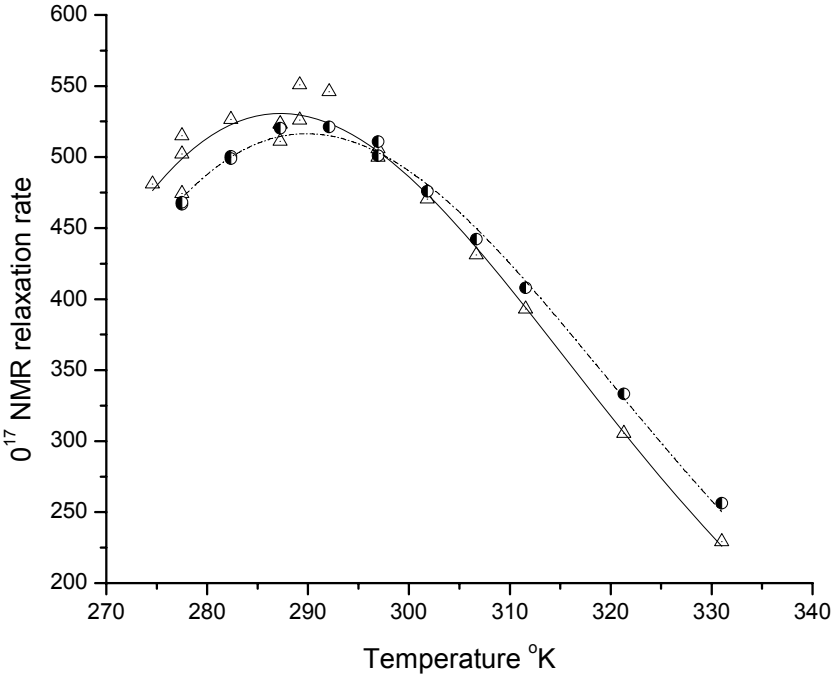

Figure 2-4. Variable temperature ^{17}O NMR transverse relaxation rate for **5** (half circles) and **15** (open triangles). The τ_M calculations with enthalpy parameters corresponding to O^{17} NMR for **5**: K_{ex}^{298} (x 10^9 s^{-1}) = 70.9 ± 5; ΔH_M (kJ/mol) = 42.0 ± 1; ΔH_V (kJ/mol) = 1 ΔH_R (kJ/mol) = 20.0. For **15**, K_{ex}^{298} (x 10^9 s^{-1}) = 61.9 ± 3; ΔH_M (kJ/mol) = 42.1 ± 2; ΔH_V (kJ/mol) = 1 ΔH_R (kJ/mol) = 19.4.

A color change from light yellow to dark orange was observed immediately upon introduction of β-gal to solutions of **5**. The color change is attributed to of the formation of hydroxy-3-nitrobenzyl alcohol. More than 80% of **5** was processed by β-gal within 1 h as determined by UV-visible spectroscopic measurements (monitoring at 420 nm). No color change is observed upon the introduction of β-gal to **15;** no new absorption peaks were observed.

Stop-point enzyme studies were performed on complexes **5** and **15** to confirm the hydrolysis products. **5** and **15** were incubated in a solution of β-gal and the reactions were monitored at discrete times by LCMS. An overnight incubation (13 h) for **15** yielded incomplete sugar hydrolysis (<50%). No colorimetric change is observed after the cleavage of the sugar moiety from **15**. Further enzyme studies were not pursued on **15**; the instability of β-gal at 37 ^{o}C for long periods of time precludes accurate measurement of the enzyme kinetic over the required reaction time. The β-gal enzyme processes **5** quickly but cleaves **15** slowly. The difference is presumably caused by the electron-withdrawing nitro group on the phenolic backbone of the pendant linker. Immediately after the hydrolysis of the galactopyranose sugar, the nitro adduct acts as a kinetic accelerator by lowering the phenolic pKa, enabling the alcohol to become deprotonated at physiological pH at 37 ^{o}C, inducing the dissolution of the linker.

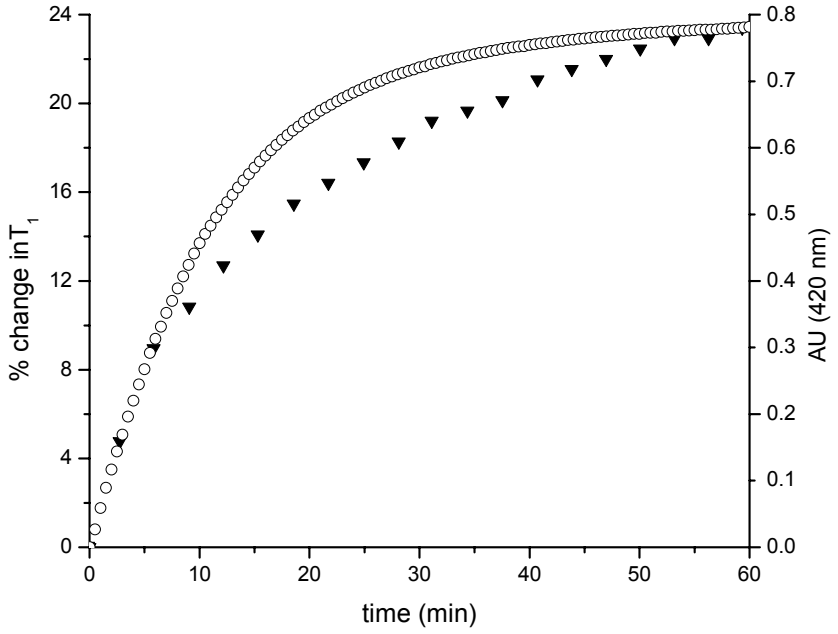

Figure 2-5. Kinetics of the hydrolysis of **5** catalyzed by β-galactosidase monitored by UV-vis at 420 nm (open circles, right y-axis.) and by bulk water T_1 relaxation (closed triangles, % change of T_1, left y-axis). The samples were prepared by combining 100 ml 15.5 μg β-gal/ml and 400 μl of 0.798 M **5** in PBS.

The kinetic parameters from a non-linear fit are tabulated in **Table 2-2**. A plot of the initial velocity (pmol/sec) versus substrate concentration (mM) was fit to a single-site Michaelis-Menten model. The k_{cat}/K_m was determined for ONPG and **5**. The data suggest that **5** is cleaved at a rate twofold faster than ONPG.[43] The release of carbon dioxide from the carbamate linker is presumed to provide the energetic sink resulting in the faster kinetics for **5** over ONPG. Futhermore, the enzyme reaction was monitored using magnetic resonance, an orthogonal method to UV-Visible spectroscopy (**Figure 2-5**). A change of 25% in T_1 over 1h was observed upon the introduction of β-gal to **5.** The UV-

vis and relaxometric data corroborate the hypothesis that β-gal processes **5** effectively and at a kinetic rate suitable for observing gene expression in whole animals in real-time.

Cell viability studies were performed to determine NIH/3T3 cells show greater than 95% viability for up to 24 hours when incubated with either the europium complexes of the agents **6** or **16**, indicating that these agents are not toxic to cells in culture.(**Figure 2-7**)

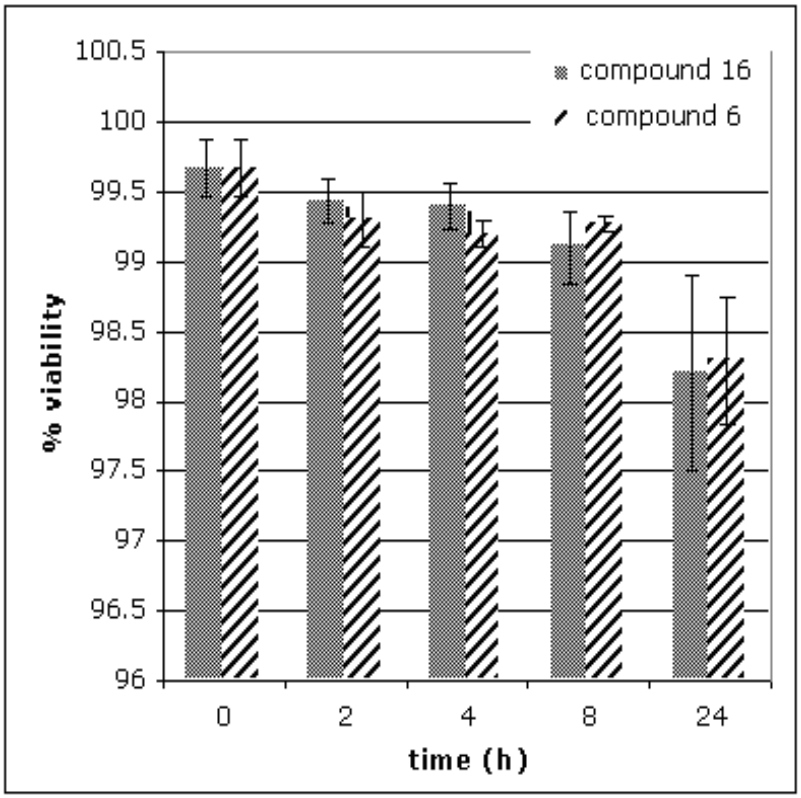

Figure 2-6. Cell viability studies for NIH/3T3 cells upon incubation of **6** and **16**.

Hep G2 cells express the asialoglycoprotein receptor on the cell surface and have been used to demonstrate that the β-galactosidase-responsive contrast agent β-EgadMe is taken into cells through a receptor-mediated mechanism.[45] Compared to NIH/3T3 cells, HepG2

cells preferentially take up both **6** and **16** by approximately 10 fold (**Figure 2-8**). This is an important observation, as receptor-mediated endocytosis is often one of the predominant pathways for cellular uptake of compounds from the interstitial space.[46] Agent **16** entered both cell lines more efficiently than **6**, which is attributed to the nitro adduct on the phenolic linker.

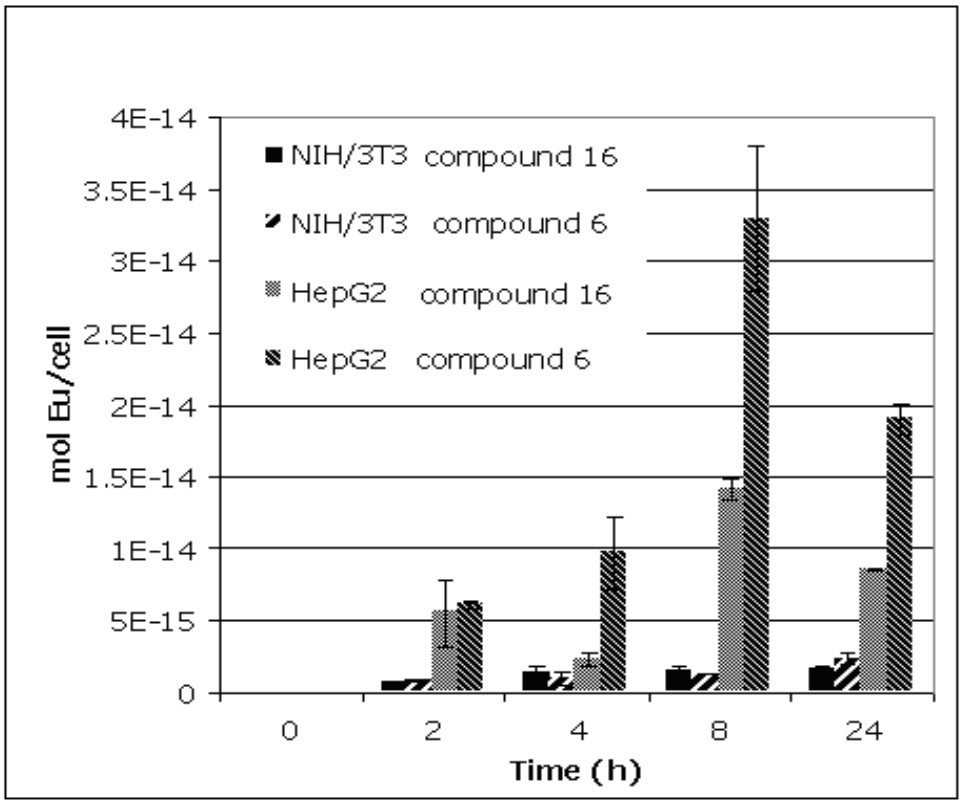

Figure 2-7. Cell uptake studies of the cell lines Hep G2 & NIH/3T3 for **6** and **16**.

	pH	K_M (mM)	*Vmax* (pmol s^{-1})	k_{cat}/K_M ($M^{-1}s^{-1}$)
Gd-5	7.4	1.3 ± 0.2	130.5 ± 10.2	118.2 ± 6.3
ONPG	7.4	2.3 ± 0.2	132.8 ± 4.9	67.1 ± 2.2

Table 2-2: The enzyme kinetic data comparing **5** vs ONPG. Data are averages of three runs ± 1 standard deviation. [a]At 37°C. [b]using PBS buffer of 200 mM sodium phosphate, 2 mM $MgCl_2$, 100 mM mercaptoethanol in pH 7.4 using 15.5 μg β-gal/ml PBS. [c]Bovine liver β-galactosidase.

Conclusion:

The synthesis and charactertization of MR contrast agents sensitive to the gene-tracking enzyme β-galactosidase is a step towards using MRI as a scientific tool to elucidate gene expression. The complexes **5** and **15** have a $q > 1$ and correspondingly high τ_m values. The pH, relaxivity and kinetic assays for **5** and **15** demonstrate these complexes have an affinity for anions such as carbonate and phosphate. These exogenous anions coordinate to the lanthanide in these complexes and can lower the hydration state prior to cleavage by β-gal. The nitro group on the phenol backbone linker is essential for desirable enzyme kinetics. The cell studies show that **6** and **16** are relatively non-toxic to cells and are taken up easily.

ACKNOWLEDGMENT: Dr. Luca Frullano for his help with ^{17}O NMR studies and Keith MacRenaris for his assistance with ICP-MS. Funding was provided by Grant NIH, CCNE.

SUPPORTING INFORMATION PARAGRAPH: The ratiometric q data, LC profile for stop point enzyme studies, and enzyme kinetic data is provided free of charge via the internet from http://pub.acs.org.

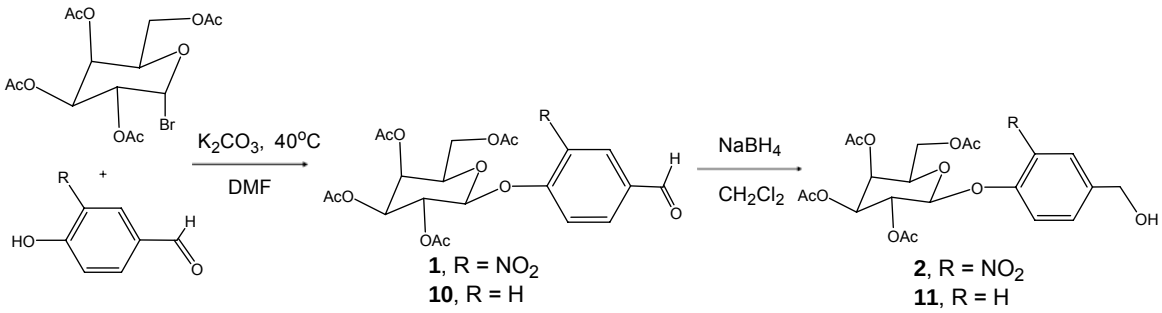

Scheme 2-1. Reactions showing the synthesis of the aldehyde protected-sugar compound **2** and **11**.

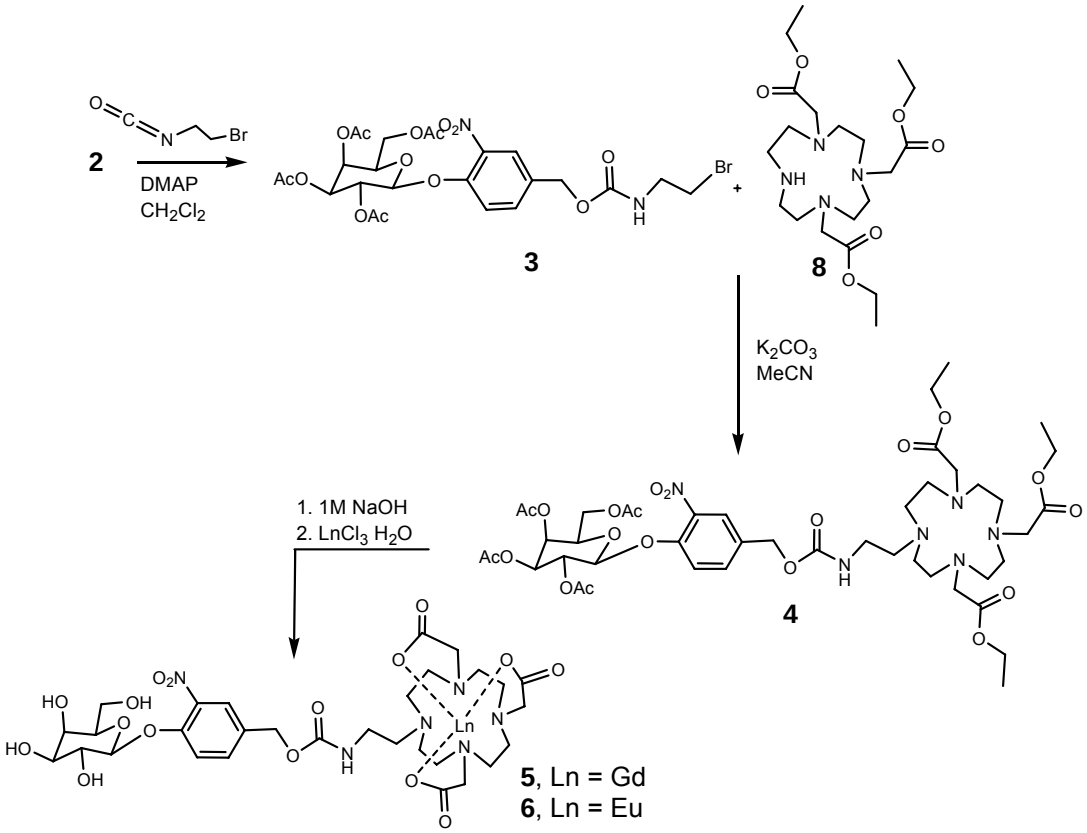

Scheme 2-2. The synthesis of the Eu and Gd analogs of the β-galactosidase sensitive MRI contrast agent uses a 3 + 1 addition of pendant arms onto cyclen.

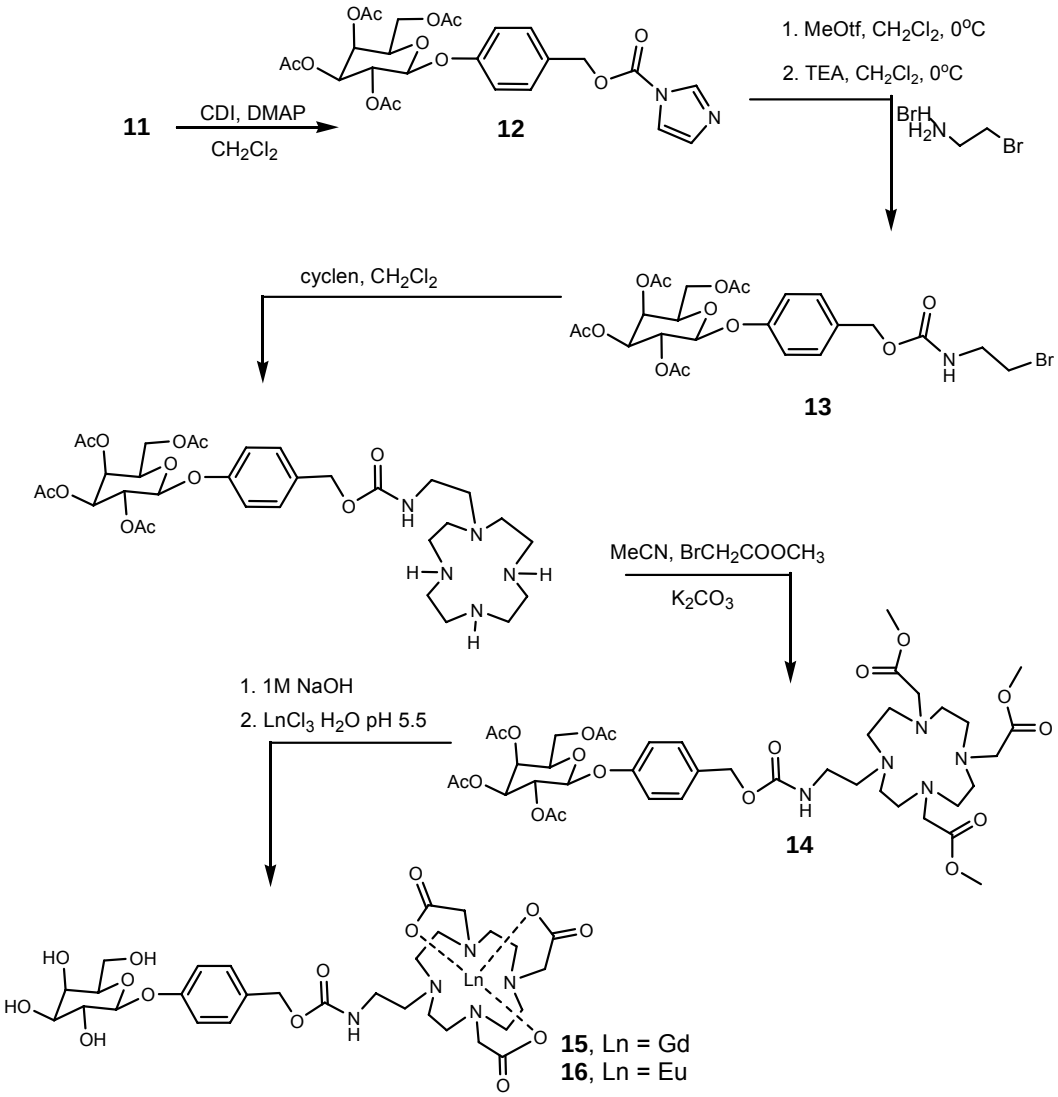

Scheme 2-3. The synthesis of the Eu and Gd analogs of the β-galactosidase responsive MR contrast agents **15** and **16** uses a 1 + 3 route for the addition of pendant arms onto cyclen.

Supporting Information:

Ratiometric q data

LC-MS trace of stop-point enzyme experiments

Michaelis-Menten Plots

Ratiometric q data

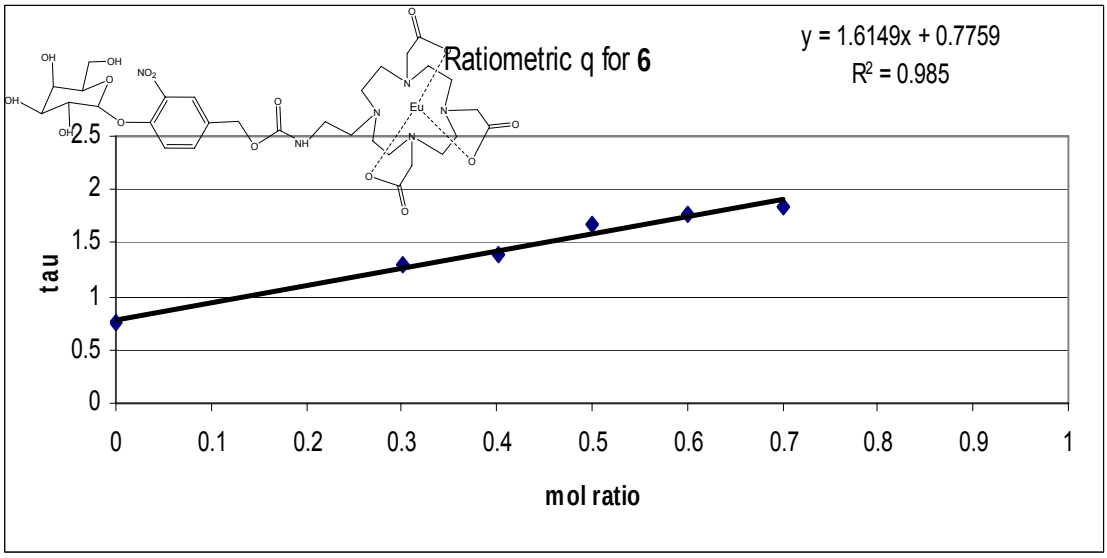

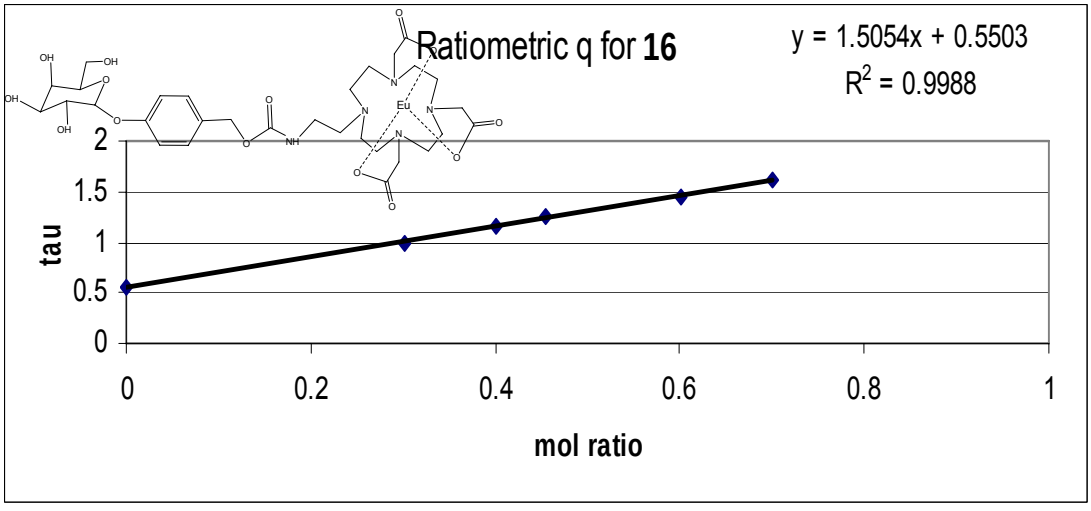

Figure 2-8: Each point represents an average of 50 scans to calculate τ, the inverse of the fluorescence decay lifetimes, from different molar concentrations of D_2O:H_2O between 0 and 0.8. The τ for the Eu(III) complexes **6** and **16** complexes in pure water was extrapolated from the ratiometric q curve and compared with τ values in pure D_2O. These values were entered into the Horrocks equations,[34] to determine q for these complexes.

LC-MS traces of stop-point enzyme experiments

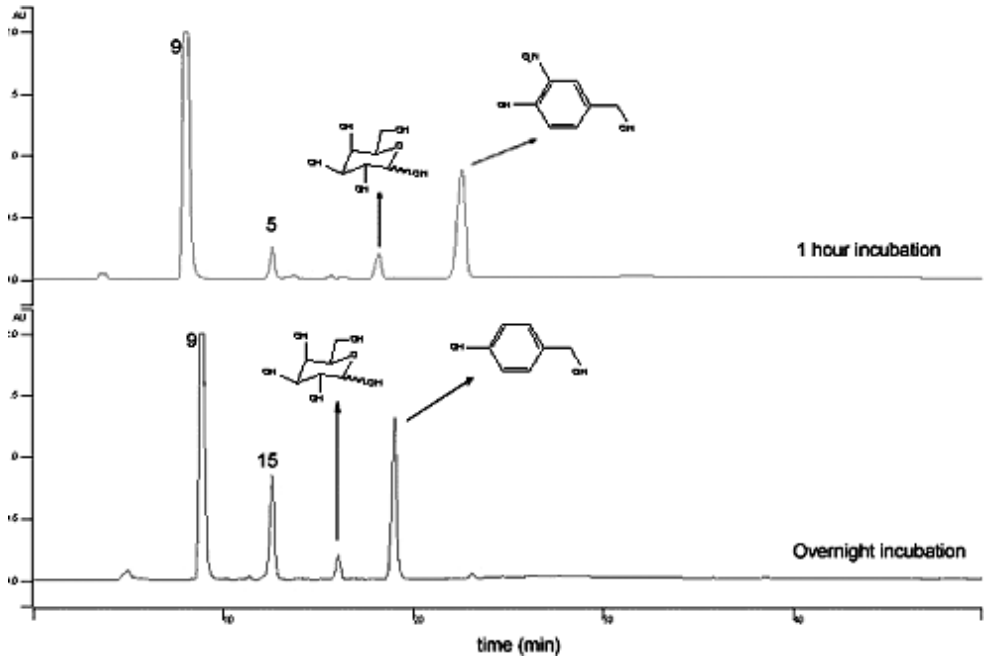

Figure 2-9: The enzyme stop-point study using LC-MS at 210 nm of the β-gal incubations of **5** and **15**. The peaks were assigned using UV-Vis signature and mass spectrometry.

Michaelis-Menten Plots

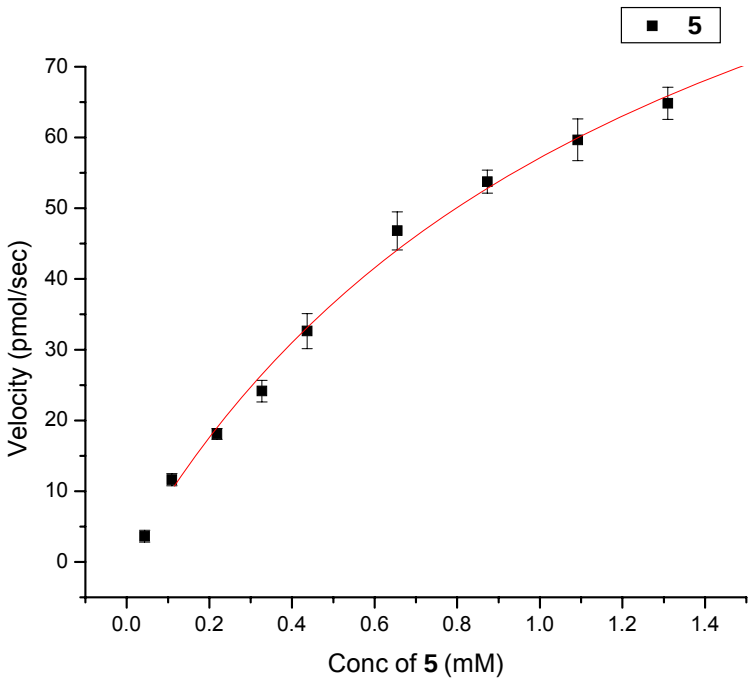

Figure 2-10: Kinetics of hydrolysis of **5** catalyzed by bovine liver β-galactosidase. Each point is the average of three runs (± 1 standard deviation). The line represents the best fit to Michaelis-Menten model. Conditions are PBS buffer of 200 mM sodium phosphate, 2 mM $MgCl_2$, 100 mM mercaptoethanol in pH 7.4 at 37°C using 15.5 μg β-gal/ml PBS.

Chapter 3:

Activatable Alkaline Phosphatase-responsive Magnetic Resonance Imaging Contrast Agent using the Self-Immolative Linker with a "Scorpion" blocking motif

ABSTRACT:

Two phosphatase-activatable gadolinium chelates **1** (gadolinium-{4,7-Bis-carboxymethyl-10-[2-(3-nitro-4-phosphonooxy-benzyloxycarbonylamino)-ethyl]-1,4,7,10 tetraaza-cyclododec-1-yl}-acetic acid), and **2** (gadolinium-3-(3-Nitro-4-phosphonooxy-phenyl)-3-ethylcarbamoyloxy]-propionic acid [2-(4,7,10-tris-carboxymethyl-1,4,7,10tetraaza-cyclododec-1-yl)) were synthesized and characterized. **1** and **2** exhibited inter- and intra-molecular anion binding respectively, to coordinatively saturate the hepta-dentate Ln-DO3A chelates with reversible oxy-anion binding. The hydration states of zero inner sphere waters for complexes prior to enzyme cleavage were confirmed by relaxivity in a variety of buffers and luminescent decay lifetime measurements of their Eu analogs. Preliminary enzyme studies were carried out and are reported in this chapter.

KEYWORDS: Alkaline phosphatase, magnetic resonance imaging, activatable contrast agent, enzyme responsive contrast agent, smart contrast agent, scorpion blocking, self-immolative linker, chromogenic probe, relaxometric, DOTA, DO3A, DTPA.

BRIEFS: Dual chromogenic and relaxometric contrast agent sensitive to alkaline phosphatase demonstrate fast enzyme kinetics and ability to blocking inner sphere water with an intramolecular acetate group.

Introduction:

Phosphorylation is a common regulatory mechanism in many biological signaling pathways. Protein kinases and phosphatases work in tandem to control a host of cellular functions such as proliferation, adhesion, cytoskeleton structure, and migration.[1-3] Perturbations in this delicate relationship have been correlated with oncogenic results.[4] Elevated levels of alkaline phosphatase are used clinically as diagnostic markers for a variety of squamous carcinomas.[5,6] We believe that magnetic resonance (MR) imaging with the aid of activatable paramagnetic agents, can image cancerous tissues that locally, over-express phosphatases. To our knowledge, the only Gd-based MR contrast agent responsive to phosphatase is described in a patent.[7] Once the phosphate group is cleaved, the unmasked biaryl, hydrophobic moiety on a Gd-DTPA based agent displays a higher affinity to human serum albumin. This slows the rotational correlation time (τ_R) and ultimately increases the overall r_1 of the agent.[7,8] Our approach modulates the hydration number (q) of the Gd(III)-complexes.

Our strategy for activating MR contrast agents uses anion binding to block inner-sphere water from accessing the lanthanide center. The modulation of the hydration state exploits the complexes ability to reversibly bind anions both inter-molecularly and intra-molecularly for **1** and **2**, respectively (**Figure 3-1**). The phosphate moiety is enzymatically hydrolyzed by phosphatases to induce an electron cascade along the *o*-nitro-phenyl carbamate linker to ultimately release the anion from the coordination site. **1** utilizes exogenous carbonate concentrations to bind to the hepta-coordinated Gd-DO3A derivative. **2** employs the intra-molecular acetate on the pendant sugar arm to coordinate back to the Gd-DO3A complex to saturate the complex.

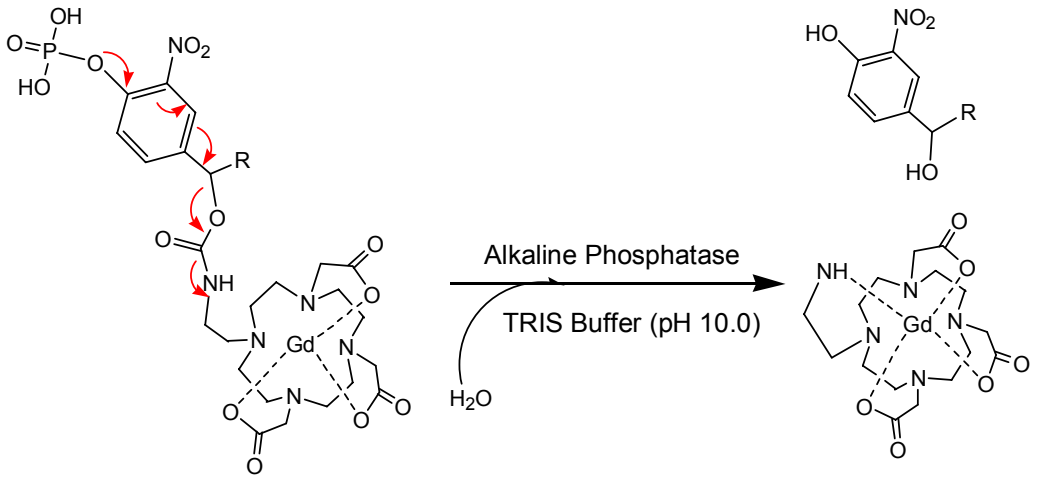

PNBCE-Gd-DO3A; R = H
PNPPCE-Gd-DO3A; R = CH_2COOH

Figure 3-1: Self-immolative mechanism for activation of phosphatase sensitive MR agents.

Agents **1** and **2** are new members of a self-immolative MR contrast agent family, which originated with the β-glucuronidase responsive complex.[9] Furthermore, q-modulation with using intra-molecular blocking moiety has been previously demonstrated to effectively impede inner-sphere water access in metabolic calcium and pH responsive agents.[10-13]

Experimental Section:

General Methods: All the reactions were performed under an atmosphere of dry N_2 unless otherwise indicated. All the solvents used were of the highest grade from a solvent system from GlassContours. All the compounds used in the reactions were of the highest grade available from Sigma-Aldrich (Milwaukee, WI) and Fisher (Hanover

Park, IL). 1,4,7,10-Tetrazacyclododecane (cyclen) was purchased from Strem. The di-tert-butyl phosphite was purchased from Lancaster Chemicals. The alkaline phosphatase enzyme, isolated from human placenta, was purchased from Sigma-Aldrich (Milwaukee, WI). The enzyme substrate *p*-nitrophenyl-phosphate (pNPP) was purchased as an Assay kit from BioAssay Systems. Water was purified using a Millipore Mili-Q Synthesis purifier. The NMR spectra were obtained on a Varian Mercury 400-MHz, Varian INOVA 500-MHz NMR spectrometer. The ^{17}O NMR was solely performed on the Varian INOVA-400 using a 1% ^{17}O enriched solution with an D_2O external lock. All the ^{13}C NMR spectra were performed on the Varian INOVA 400 MHz NMR using a 10mm broadband carbon probe. All the deuterated solvents were obtained from Sigma-Aldrich (Milwaukee, WI). The spectra obtained in $CDCl_3$ were referenced to 0.01% TMS internal standard, otherwise all other deuterated solvents were referenced to the residual solvent peak. Mass spectrometry (MS) was performed on a Varian 1200L quadrapole MS using electrospray ionization (ESI) using a direct methanol injection at 20 μl/min. The elemental analyses were performed at Desert Analytics (Tucson, AZ). The UV-Visible spectroscopy was performed on the HP5452 diode array spectrometer thermostated at 37^{o}C. The fluorescence measurements were obtained on a Hitachi F4500 fluorometer operating in the phosphorescence lifetime (short) mode. Inductively coupled plasma mass spectrometry (ICP-MS) measurements were performed on a VG Elemental PQ Excell spectrometer standardized with eight concentrations from 0-50 ppb Gd(III). An internal standard of 1 ppb In(III) was used in all of the ICP samples.

LCMS and Preparative HPLC – The analytic LC-MS was performed on a Varian Prostar model 210 with a 410 autosampler using a 100 μL sample loop. Two 210 pump heads were with a 5 ml/min leads split to a 363 fluorescence detector and a 330 photodiode array (PDA) detector, then connected to a 1200L quadrupole ESI-MS. A 3:1 split valve was used to direct the column-separated sample to 3 parts series connected light detectors and 1 part MS. All the runs used a 1 mL/min flow rate on a ThermoElectron 4.6 * 150 mm 5 μm Aquasil C18 column. The mobile phase used was millipore purified water and HPLC grade acetonitrile. The sample concentrations were run at a range of 0.2 – 3 mg/ml after it was filtered through a 0.25 μm Nylon Millipore Millex-GN syringe filter to remove all precipitates.

The preparative HPLC was the Varian Prostar model 210 consisting of two 210 pumps with a 25 ml/min heads with a 5 ml manual injection sample loop. The Prostar system has a 2 channel UV-Visible detector tandem to a HP-1046A fluorescence detector. The mobile phases were the same conditions used on the analytical LC-MS. The preparative concentrations ranging from 25 mg – 150 mg dissolved in 3 ml of water after they were filtered through a 0.25 μm Nylon Millipore Millex-GN filter. The preparative runs used a 15 ml/min on Atlantis Prep T3 10 μm 19 x 10 mm guard column.

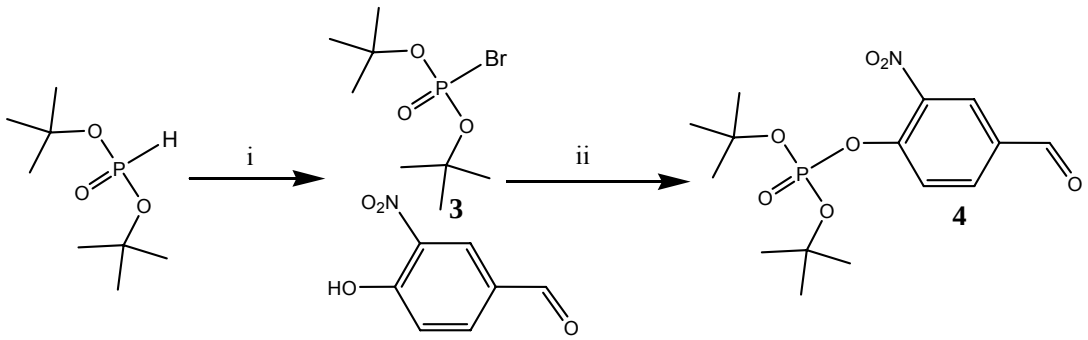

Scheme 3-1: i) CH_2Cl_2, 20% NaOH, CBr_4, $[(CH_3CH_2)_3(CH_2C_5H_5)N]Cl$, $[(CH_3\text{-}CH_2\text{-}CH_2\text{-}CH_2\text{-})_4N]OH$, 95.5%; ii) THF, DBU, DMF, 95.3%.

Phosphorobromidic acid di-tert-butyl ester (3) – The flask was charged with di-tert-butyl phosphite (13.0 g, 64 mmol), dichloromethane (50 ml), 20% NaOH (w/v) solution (40 ml), tetrabromomethane (10.0 g, 30.2 mmol), triethylbenzylammonium chloride (0.8 g, 3.51 mmol), and 2 drops of tetrabutylammonium hydroxide. The reaction was stired in ambient atmosphere at RT overnight. Another equivalent of dichloromethane (50ml) was added to the reaction mixture, and the resulting solution was washed with water. The organic layer was collected, dried over sodium sulfate, and the solvent was removed under reduced pressure to leave a light yellow oil. Yield = 17.77g (95.5%). ^{1}H NMR (400 MHz, $CHCl_3$): δ = 1.60 (18H, s). ^{13}P NMR (162 MHz, $CHCl_3$) from H_3PO_4: δ = -20.76.

Phosphoric acid di-tert-butyl ester 4-formyl-2-nitro-phenyl ester (4) – The flask was charged with **3** (17.7 g, 64.8 mmol) and anhydrous tetrahydrofuran (10 ml). A solution of 4-hydroxy-3-nitro-benzaldehyde (7.0 g, 41.9 mmol), DBU (6.0 ml, 40.1 mmol), DMAP (0.75 g, 6.13 mmol), anhydrous tetrahydrofuran (100 ml), and anhydrous dimethylformamide (75 ml) at 0^{o}C was added dropwise to the reaction over a period of 2 h. The solution was warmed to RT and stirred overnight. The solvent was removed under reduced pressure. The resulting residue was dissolved in dichloromethane and

washed with brine (50 ml) and water (50 ml). The organic layer was collected and dried over sodium sulfate. The solvent was removed under reduced pressure and dried in vacuo overnight to leave an orange oil. Yield = 14.43 g (95.3%) ^{1}H NMR (500 MHz, $CHCl_3$): δ = 1.53 (18H, s), 7.89 (1H, d), 8.08 (1H, d), 8.35 (1H, s), 10.01 (1H, s). ^{13}C NMR (125 MHz, $CHCl_3$): δ = 188.94, 148.64, 134.28, 132.29, 126.68, 122.82, 86.34, 29.98. ^{13}P NMR (162 MHz, $CHCl_3$) from H_3PO_4: δ = -16.61.

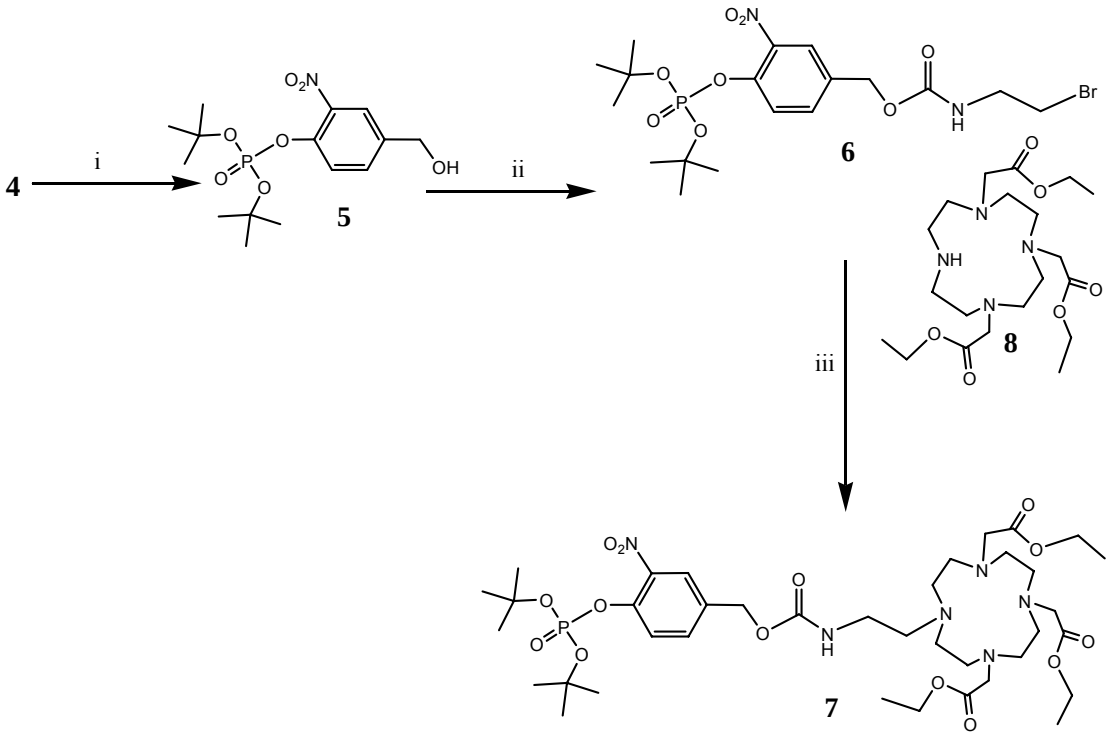

Scheme 3-2: i) $NaBH_4$, MeOH, CH_2Cl_2, 75.0%; ii) CH_2Cl_2, DMAP, BrC_2H_4NCO, 76%; iii) K_2CO_3, MeCN, $[(CH_3CH_2CH_2)_4N]OH$, 62.9%.

Phosphoric acid di-tert-butyl ester 4-hydroxymethyl-2-nitro-phenyl ester (5) – A flask was charged with **4** (5.25 g, 14.6 mmol), methanol (20 ml), and dichloromethane (5 ml) at –78 ^{o}C using a dry ice/acetone bath. Sodium borohydride (1.1 g, 29.1 mmol) was added to the mixture in portions. The solution was stirred at –78 ^{o}C for 4 h. The yellow solution was quenched with water (5 ml). The solution was allowed to warm to RT. Additional water (10 ml) and dichloromethane (10 ml) was added to the solution. After the extraction, the organic layer was collected, dried over sodium sulfate, and the organic layer was removed under reduced pressure. Further purification was performed on a triethylamine (TEA) deactivated silica gel column using a 50% ethyl acetate/49% hexane with 1% TEA as eluent. The appropriate fractions were collected and concentrated. The resulting residue was dried in vacuo for 48 h to leave a yellow solid. Yield = 3.90 g (75.0%) ^{1}H NMR (500 MHz, $CHCl_3$): δ = 1.57 (18H, s), 4.69 (2H, s), 7.52 (2H, m), 7.83 (1H, s). ^{13}C NMR (125 MHz, $CHCl_3$): δ = 142.68, 141.67, 138.84, 131.74, 123.19, 122.12, 85.71, 63.10, 29.89. ^{13}P NMR (162 MHz, $CHCl_3$) from H_3PO_4: δ = -16.07 ESI-MS: *m/z* found: 304.0, 360.1 calcd: $[M^{-}$-tertbutyl$]^{-}$ 304.2, [M] 361.3

(2-Bromo-ethyl)-carbamic acid 4-(di-tert-butoxy-phosphoryloxy)-3-nitro-benzyl ester (6) - A flask was charged with **5** (1.04 g, 28.8 mmol), anhydrous dichloromethane (10 ml), DMAP (0.387g, 31.7 mmol), and bromoethyl-isocyanate (2.6 ml, 28.8 mmol). The solution was stirred overnight to change the color of the solution to a reddish color. The solvent was removed under reduced pressure. The residue was further purified on a TEA-deactivated silica gel column using 50% ethyl acetate/49%hexane/1% TEA eluent. The appropriate fractions were collected and concentrated under reduce pressure. The

resulting compound was dried in vacuo for 24 h to leave yellow oil. Yield = 1.94 g (76.0%) ^{1}H NMR (500 MHz, $CHCl_3$): δ = 1.52 (18H, s), 3.44 (2H, t), 3.60 (2H, t), 5.12 (2H, s), 5.43 (1H, b), 7.51 (1H, d), 7.62 (1H, d), 7.82 (1H, s). ^{13}C NMR (125 MHz, $CHCl_3$): δ = 170.82, 157.85, 155.76, 143.08, 141.37, 133.52, 132.73, 124.14, 121.98, 85.18, 64.39, 60.08, 42.57, 41.71, 29.87. ^{13}P NMR (162 MHz, $CHCl_3$) from H_3PO_4: δ = -15.97. ESI-MS: *m/z* found: 454.9 calcd with Br isotope pattern: $[M^-$-tertbutyl$]^-$ 454.2.

(4,7-Bis-ethoxycarbonylmethyl-1,4,7,10tetraaza-cyclododec-1-yl)-acetic acid ethyl ester (8) – A flask was charged with cyclen (4.0 g, 23.2 mmol), sodium bicarbonate (6 g, 71.4 mmol), and anhydrous acetonitrile (200 ml). While stirring vigorously, ethylbromoacetate (5.8 ml, 52.3 mmol) was added dropwise over a 6 h period at RT. The reaction mixture was stirred for additional 48 h. The solution turns from a clear to an orange color. The solvent was removed under reduced pressue and the resulting residue was extracted in dichloromethane (200 ml) and water (100 ml)). The organic layer was collected, washed with brine (50 ml), and washed with water (100 ml, 2x). The organic layer was concentrated and further purification was made on the silica column using a 4% methanol:dichloromethane. The corresponding fractions were collected and concentrated. The product was then triterated twice in diethyl ether, and refrigerated for 3 d at –20 ^{o}C to result in white solids. The product filtered and dried in vacuo to leave a fine off-white powder. 3.618 g (36.2%) ^{1}H NMR (500 MHz, $CHCl_3$): δ = 1.27 (9H, t), 2.82 – 3.51 (24H, b), 4.16 (6H, q), 10.01 (1H, b). ^{13}C NMR (125 MHz, $CHCl_3$): δ = 171.32, 170.49, 94.94, 60.96, 57.44, 54.58, 49.47, 47.57, 14.41. ESI: *m/z* found 430.6 [M], calcd 430.5.

(4-{2-[4-(Di-tert-butoxy-phosphoryloxy)-3-nitro-benzyloxycarbonylamino]-ethyl}-7,10-bis-ethoxycarbonylmethyl-1,4,7,10tetraaza-cyclododec-1-yl)-acetic acid ethyl ester (7) – A flask was charged with **6** (1.948 g, 3.81 mmol), **8** (1.64 g, 3.81 mmol), potassium carbonate (0.65 g, 47.0 mmol), anhydrous acetonitrile (20 ml), and one drop of tetrabutylammonium hydroxide to act as a phase transfer catalyst. The solution was stirred at RT for 3 d. The solvent was removed under reduced pressure. The residue was extracted with dichloromethane (50 ml) and water (20 ml). The organic layer was collected, dried over sodium sulfate, and the solvent was removed under reduced pressure. Further purification was performed using a TEA-deactivated silica gel column using a gradient of 0%-5% methanol:dichloromethane with 1% TEA as eluent. The appropriate fractions were collected and concentrated. The product was dried in vacuo overnight to obtain of a yellow oil. 2.07 g (62.9%) ^{1}H NMR (500 MHz, $CHCl_3$): δ = 1.09 (3H, t), 1.25 (6H, t), 1.52 (18H, s), 2.05-3.83 (26H, b), 4.11 (6H, m), 5.10 (2H, s), 7.29 (1H, b), 7.53 (1H, d), 7.62 (1H, d), 7.82 (1H, s) ^{13}C NMR (125 MHz, $CHCl_3$): δ = 170.90, 170.72, 170.67, 155.73, 155.57, 142.84, 142.78, 141.170, 141.13, 141.09, 141.06, 133.76, 133.42, 132.68, 132.49, 124.04, 123.83, 121.73, 84.67, 67.35, 64.05, 63.86, 60.08, 59.63, 59.53, 55.75, 54.47, 52.18, 52.03, 51.61, 51.40, 51.30, 42.34, 39.22, 31.04, 29.81, 29.26, 29.23, 25.12, 13.81. ^{13}P NMR (162 MHz, $CHCl_3$) from H_3PO_4: δ = -15.94. ESI-MS: *m/z* found: 861.3 calcd: $[M]^+$ 860.9

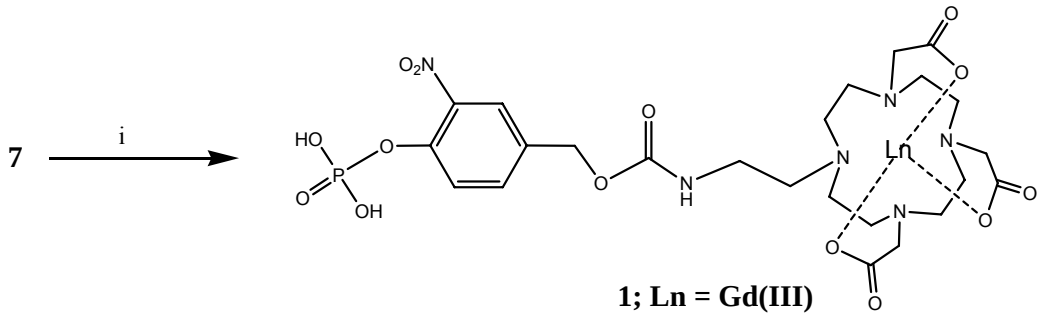

1; Ln = Gd(III)
9; Ln = Eu(III)

Scheme 3-3: i) 1) THF, TFA 2) H_2O, $Ln(X)_3$, pH 5.5

Gadolinium-{4,7-Bis-carboxymethyl-10-[2-(3-nitro-4-phosphonooxy-benzyloxycarbonylamino)-ethyl]-1,4,7,10tetraaza-cyclododec-1-yl}-acetic acid (1) - A flask was charged with **7** (0.212 g, 0.246 mmol) and tetrahydrofuran (10 ml). Trifluoroacetic acid (10 ml) was added in portions at 0 ^{o}C. The solution was stirred for 1 h. The TFA was removed and 1M NaOH solution (30 ml) was added. The solution was stirred for 3 h at RT, then the pH was adjusted 5.5 using 1M HCl solution. A solution of $Gd(OTF)_3$ (0.149 g, 0.246 mmol) in water (1 ml) was added to the reaction. The pH was readjusted to 5.5. The reaction was stirred for 2 d. The pH was raised ~10 by addition of a 1M NaOH solution (2 ml) to precipitate out the excess gadolinium. The solution was filtered through a 0.25 μm syringe filter. The sample was concentrated under reduced pressure and further purification was ran on the HPLC. The product fraction was collected and lypholized to obtain of a yellow fluffy powder. Yield = 40 mg (19.8%) ESI-MS: *m/z* found: 818.3, 840.2 calcd: $[M]^+$ 818.8, $[M+Na^+]^+$ 841.8. Anal. - %C 33.36 %H 4.29 %N 9.83 calc + $3H_2O$: C% 33.03 %H 4.62 %N 8.63.

Europium-{4,7-Bis-carboxymethyl-10-[2-(3-nitro-4-phosphonooxy-benzyloxycarbonylamino)-ethyl]-1,4,7,10tetraaza-cyclododec-1-yl}-acetic acid (9) - A flask was charged with **7** (0.200 g, 0.232 mmol) and tetrahydrofuran (3 ml). TFA (3 ml) was added in portions at 0^{o}C. The solution was stirred for 1 h. The TFA was removed and a 0.25M NaOH (30 ml) solution was added to the reaction mixture and stirred for 3 h at RT. The pH was adjusted pH to 5.5 using a 1M HCl solution. A solution of $EuCl_3$ (0.072, 0.279 mmol) in water (1 ml) was added to the reaction. The pH was readjusted back to 5.5. The reaction stirred for additional for 3 d. The pH was raised to ~10 by addition of 1M NaOH (2 ml) to precipitate out excess gadolinium and the solution was filtered through a 0.25 μm syringe filter. The sample was concentrated under reduced pressure and purified using HPLC. The product was collected and lypholized to obtain of a yellow fluffy powder. Yield = 28 mg (14.8%) ESI-MS: *m/z* found: 813.2 calcd: $[M]^{+}$ 813.5. Anal - %C 32.69 %H4.04 %N 9.49 calc + $2H_2O$ + Na: C% 33.04 %H 4.93 %N 9.63.

{4,7-Bis-carboxymethyl-10-[2-(3-nitro-4-phosphonooxy-benzyloxycarbonylamino)-ethyl]-1,4,7,10tetraaza-cyclododec-1-yl}-acetic acid (10) – A flask was charged with **7** (0.424 g, 0.492 mmol) and tetrahydrofuran (2 ml). A 1M NaOH solution (10 ml) was added and the reaction mixture was stirred overnight at RT. The solvent was removed under reduced pressure and added TFA to the flask at 0 ^{o}C. The reaction was stirred for 2 h. The TFA/solvent was removed under reduced pressure. The residue was triturated in water (4 ml) and filtered through a 0.25 μm filter. The

filtrate was further purified using HPLC. The product fraction was collected and lyophilized to a fluffy yellow powder. Yield = 0.0803 g (24.6%). ^{1}H NMR (500 MHz, $CHCl_3$): δ = 2.94 – 4.20 (34H, bm), 5.38 (2H, s), 7.80 (1H. b), 7.92 (1H, b), 8.19 (1H, s). ^{13}C NMR (125 MHz, $CHCl_3$): δ = 172.196, 158.23, 145.87, 142.12, 134.70, 133.37, 125.16, 123.85, 66.06, 57.17, 52.57, 51.80, 51.23, 49.94, 49.29, 41.74, 37.19, 28.59. ^{13}P NMR (162 MHz, $CHCl_3$) from H_3PO_4: δ = -3.60. ESI MS: *m/z* found: 663.2 calcd: $[M]^-$ 664.6.

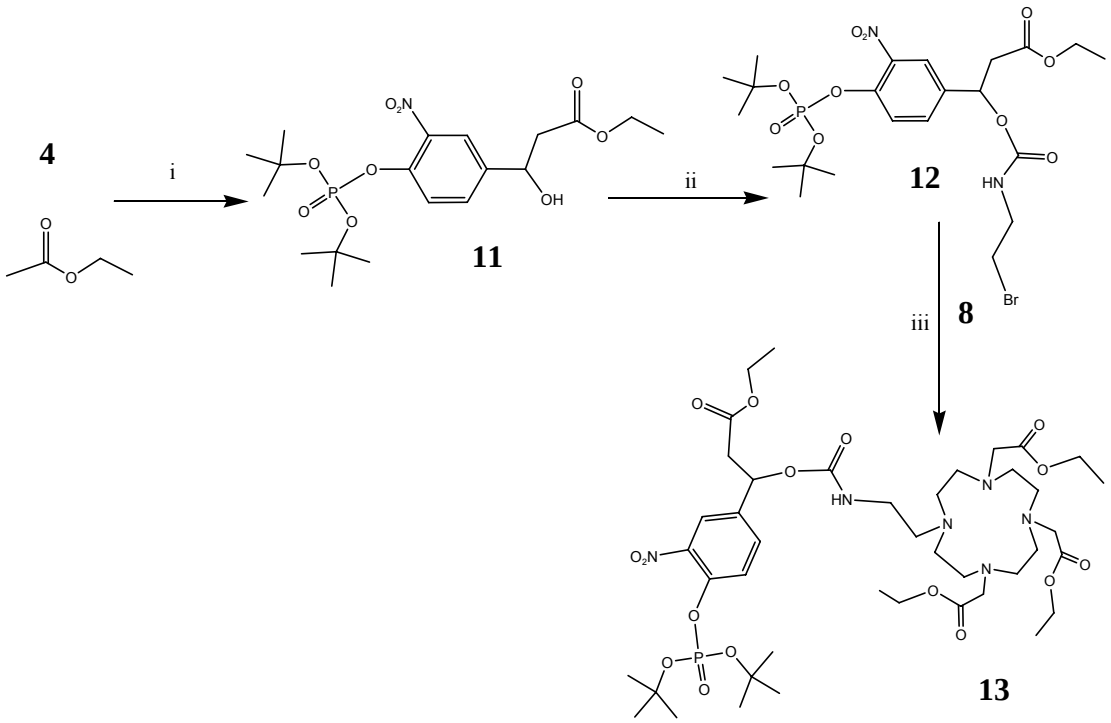

Scheme 3-4: i) THF, LDA, 4.9%; ii) DMAP, CH_2Cl_2, BrC_2H_4NCO, 79.7%; iii) K_2CO_3, MeCN, $[(CH_3CH_2CH_2)_4N]OH$, 17.1%

3-[4-(Di-tert-butoxy-phosphoryloxy)-3-nitro-phenyl]-3-hydroxy-propionic acid ethyl ester (11) – A flask was charged with anhydrous tetrahydrofuran (150 ml) and redistilled diispropylamine (20 ml, 142.7 mmol). The reaction temperature was lowered to –78 ^{o}C using a dry ice/acetone bath. 1.6 M *n*-butyl lithium (53 ml, 84.8 mmol) was added to the reaction mixture and stirred for 1 h. Redistilled ethyl acetate (11.4 ml, 116.7 mmol) was added to the reaction mixture and the reaction stirred for additional 1 h. A solution of **4** (14.43 g, 40.2 mmol) and anhydrous tetrahydrofuran (150 ml) was added dropwise over 4 h to the reaction mixture turning the solution a bright yellow color. The reaction was stirred at –78^{o}C for 7 h and afterwards quenched with water (50 ml). The solvent was removed under reduced pressure, and the resulting residue was extracted using dichloromethane (100 ml) and water (100 ml). The organic layer was collected, dried over sodium sulfate, and concentrated to an oil. Further purification was performed using a TEA-deactivated silica column using a 40% ethyl acetate:59%hexanes:1% TEA as eluent. The product fractions were collected and dried in vacuo to leave a yellow solid. Yield = 1.893 g (4.9%) ^{1}H NMR (500 MHz, $CHCl_3$): δ = 1.25 (3H, t), 1.49 (18H, s), 2.68 (2H, d), 4.02 (1H, b), 4.16 (2H, q), 5.13 (1H, t), 7.54 (2H, m), 7.86 (1H, s) ^{13}C NMR (125 MHz, $CHCl_3$): δ = 171.95, 143.21, 141.74, 139.92, 131.06, 122.66, 122.31, 85.45, 68.93, 61.24, 43.28, 29.88, 14.29. ^{13}P NMR (162 MHz, $CHCl_3$) from H_3PO_4: δ = -15.99. ESI-MS: *m/z* found: neg 444.2, 390.1; pos. 469.9 calcd: $[M]^-$ 447.4 [M-*t*-butyl]$^-$ 391.3 $[M+Na]^+$ 470.4.

3-(2-Bromo-ethylcarbamoyloxy)-3-[4-(di-tert-butoxy-phosphoryloxy)-3-nitro-phenyl]-propionic acid ethyl ester (12) - A flask was charged flask with **11** (1.893 g,

4.23 mmol), anhydrous dichloromethane (20 ml), bromoethyl isocyanate (0.456 ml, 50.5 mmol), and DMAP (0.62 g, 50.8 mmol). The solution was stirred and allowed to react for 2 d. The solution was concentrated under reduced pressure, and the reaction was purified on a TEA-deactivated silica gel column using 40% ethyl acetate:59%hexanes:1% as eluent. The removal of all volatiles under reduced pressure yielded an oil. Yield = 2.014 g (79.7%) ^{1}H NMR (500MHz, $CHCl_3$): δ = 1.25 (3H, m), 1.53 (18H, s), 3.40 (2H, t), 3.57 (2H, t), 3.64 (2H, m), 4.12 (3H, m), 6.09 (1H, t), 7.52 (2H, m), 7.80 (1H, s) ^{13}C NMR (125 MHz, $CHCl_3$): δ = 190.87, 169.19, 154.86, 143.79, 141.54, 136.47, 131.91, 123.77, 122.72, 105.32, 85.39, 71.42, 61.12, 47.51, 42.56, 31.38, 14.22. ^{13}P NMR (162 MHz, $CHCl_3$) from H_3PO_4: δ = -15.96.

3-[4-(Di-tert-butoxy-phosphoryloxy)-3-nitro-phenyl]-3-[2-(4,7,10-tris-ethoxycarbonylmethyl-1,4,7,10tetraaza-cyclododec-1-yl)-ethylcarbamoyloxy]-propionic acid ethyl ester (13) – A flask was charged with **12** (1.89 g, 3.16 mmol), **8** (1.36 g, 3.16 mmol), potassium carbonate (0.52 g, 3.76 mmol), anhydrous acetonitrile (20 ml), and 1 drop of tetrabutylammonium hydroxide to act as a phase transfer catalyst. The reaction was stirred at RT for 3 d. The solvent was removed and partitioned with dichloromethane (50 ml) and water (50 ml). The organic layer was collected, dried over sodium sulfate, and concentrated to an oil. The resulting residue was purified using a TEA-deactivated silica gel column 50% ethyl acetate:49%hexane:1%TEA as eluent to purify unreacted starting material **11**, then 2% methanol:dichloromethane 1% TEA to collect the product. The desired product was collected and dried in vacuo to afford a yellow solid. Yield = 0.513 g (17.1%) ^{1}H NMR (500 MHz, $CHCl_3$): δ = 1.04 (3H, t),

1.22 (9H, t), 1.45 (18H, s), 2.51 (8H, b), 2.68 (8H, b), 2.71 (8H, s), 3.53 (4H, m), 4.10 (8H, q), 4.39 (2H, d), 6.04 (1H, t), 7.58 (1H, s), 7.87 (1H, d), 7.99 (1H, d) ^{13}C NMR (125 MHz, $CHCl_3$): δ = 170.88, 170.37, 168.56, 166.93, 154.55, 142.78, 140.96, 136.70, 131.76, 131.49, 130.40, 128.14, 122.81, 121.49, 184.46, 70.15, 67.27, 60.68, 50.42, 54.03, 51.79, 51.65, 51.49, 51.32, 40.52, 38.05, 29.70, 29.08, 28.26, 23.09, 22.30, 13.67, 10.35, 7.44. ^{13}P NMR (162 MHz, $CHCl_3$) from H_3PO_4: δ = -16.01. ESI-MS: *m/z* found: pos. 947.6 neg. 889.52 calcd: $[M]^+$ 947.0 $[M\text{-tertbutyl}]^-$ 890.9.

3-(3-Nitro-4-phosphonooxy-phenyl)-3-[2-(4,7,10-tris-carboxymethyl-1,4,7,10tetraaza-cyclododec-1-yl)-ethylcarbamoyloxy]-propionic acid (14) – A flask was charged with **13** (0.262 g, 0.277 mmol), tetrahydrofuran (4 mL), and 1M NaOH solution (4 ml). The reaction was stirred overnight. The solvent was removed and TFA was added at 0^{o}C and stirred for 3 h. The TFA was removed under reduced pressure and the residue was reconstituted in water (4 ml). The reaction mixture was filtered through a 0.25 μm syringe filter. The resulting filtrate was purified using HPLC. The product fractions wer collected and lypholized to leave the product as a light yellow powder. Yield = 49.9 mg (24.9%) ^{1}H NMR (500 MHz, $CHCl_3$): δ = 2.85 – 3.78 (28H., bm), 6.39 (1H, t), 7.29 (1H, s), 7.48 (1H, s), 7.68 (1H, s). ^{13}P NMR (162 MHz, $CHCl_3$) from H_3PO_4: δ = -4.11 ESI MS: *m/z* found: 722.0 calcd: $[M]^+$ 722.6.

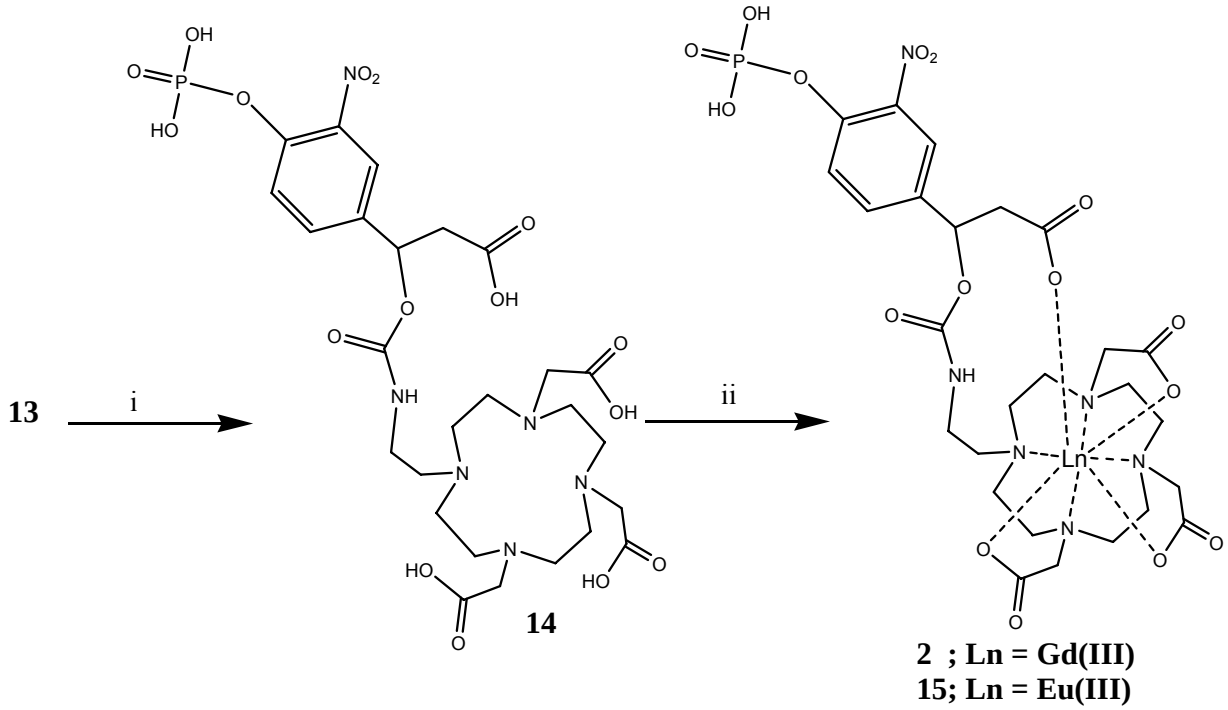

Scheme 3-5: i) 1) NaOH 2) TFA ii) H_2O, $Ln(X)_3$, pH 5.5.

Gadolinium-3-(3-Nitro-4-phosphonooxy-phenyl)-3-[2-(4,7,10-tris-carboxymethyl-1,4,7,10tetraaza-cyclododec-1-yl)-ethylcarbamoyloxy]-propionic acid (2) – A flask was charged with **14** (20 mg, 0.0276 mmol), water (5 ml), Gd(III)Cl_3·6 H_2O (9 mg, 0.0242 mmol) and adjusted pH to 5.0. The solution was stirred for 2 d. The pH was adjusted to ~10 with the addition of 1 M NaOH (1 ml). The solution was filtered thorough 0.25 μm syringe filter to rid of excess gadolinium. The solution was further purified using HPLC to collect product. The product was lyophilized to a red solid. Yield = 6.5 mg (26.8%) ESI MS: *m/z* found: neg. 876.06, 796.26 calcd: $[M]^-$ 876.81. $[M\text{-}PO_3^-]$ 796.84.

Europium-3-(3-Nitro-4-phosphonooxy-phenyl)-3-[2-(4,7,10-tris-carboxymethyl-1,4,7,10tetraaza-cyclododec-1-yl)-ethylcarbamoyloxy]-propionic acid (15) – A flask was charged with **14** (15 mg, 0.0208 mmol), water (5 ml), Eu(III)$Cl_3 \cdot 6\ H_2O$ (9 mg, 0.0245 mmol). The pH was adjusted to 5.0, and the solution was stirred for 2 d. The pH was adjusted to ~10 with the addition of 1M NaOH (1 ml). The reaction mixture was filtered thorough 0.25 μm syringe filter to remove excess europium. Further purification was performed using HPLC and the product fractions were collected. The fractions were concentrated and lypholized to yield a red solid. Yield = 4.6 mg (25.4%) *m/z* found: 871.37 calcd: $[M]^-$ 871.11

Relaxivity and pH studies: The T_1 of each sample was obtained on a Bruker mq60 Minispec using an inversion recovery pulse sequence with appropriate recycle delays. This instrument has a proton Larmor frequency of 60 MHz and operates at 37 ^oC. Five relaxivity samples were prepared in serial dilutions with concentrations ranging between 0.1 mM to 2.0 mM of the paramagnetic complexes. The concentration of gadolinium complex solutions **1** and **2** were determined from ICP-MS and performed in triplicate. The ICP samples were prepared by digesting 100 μl of the sample with 100 μl of concentrated nitric acid for 5 h. 20 μl of the nitric acid/sample solution was added to 290 μl nitric acid, 10 μl of indium standard, and 9680 μl of water. All the relaxivity slopes were fit to a line with $R^2 > 0.998$.

For the relaxivity versus pH studies, the T_1 was determined for each pH point in intervals of 0.4 pH units. The concentrations for the two paramagnetic complex solutions

were determined to be 0.895 mM for **1** and 0.337 mM for **2** by ICP-MS. The T_1 values were converted to relaxivity values and plotted versus their corresponding pH values.

^{17}O NMR – Variable temperature ^{17}O NMR was used to determine the water exchange rate (τ_m) for the gadolinium complex **1**. The paramagnetic complex was dissolved in 1% ^{17}O enriched solution of water with a D_2O external standard. The solution of **1** was determined to have a concentration of 17.82 mM by ICP-MS. The observed transverse ^{17}O relaxation rate of the sample is measured as a function of variable temperature by determining the line width of the ^{17}O NMR signal at half the peak height. The enriched ^{17}O water solution was subtracted from the observed rates of the paramagnetic solution. This normalized ^{17}O rate was plotted as function of temperature. The shape of the profiles is indicative of water exchange rates (τ_m) for the gadolinium (III) complex solutions. The parameters were fit to the Swift-Connick equation.[20]

Enzyme Kinetics – Alkaline phosphatase was tested for efficacy using the BioAssay Systems control assay using pNPP. A standard curve was prepared using mg/ml pNPP in TRIS buffer, and enzyme concentration . The varying enzyme-substrate mixtures were incubated for 30 min at 37 ^{o}C. The enzyme was stable for more than 24 h at 37 ^{o}C at its native pH in 10.0 in the TRIS buffer, and did not demonstrate decrease in enzyme activity after 24 h.

The enzyme phosphatase hydrolyzes the phosphate moiety of **1** and results in the decomposition of the linker to generate 4-hydroxy-3-nitrobenzyl alcohol, which has a molar absorptivity $\varepsilon = 2641 \pm 50$ M^{-1} cm^{-1} at 420 nm. The background for substrate

solution for **1** at 420 nm was subtracted from the experiment prior to the evaluation enzyme kinetics for alkaline phosphatase. The enzyme kinetic experiment was sampled in 30 s increments at 37 ^{o}C for 1 h. This turnover velocity was determined in μmol/min of the processed 4-hydroxy-3-nitrobenzyl alcohol which was charted versus substrate concentration. The measurements were performed in triplicates.

The colormetric enzyme kinetics of **1** was confirmed with an orthogonal, relaxometric method. A 100 μl solution of enzyme at 15 μg/ml in TRIS buffer was added to the 400 μl of solution of **1** at 0.798 mM in TRIS buffer. The change in T_1 observed over 1 h was determined to be due to the change in relaxivity of the contrast agent **1**. The T_1 change was observed over an hour period using a saturation recovery sequence in 3 min increment.

Determination of q using ratiometric fluorescence – The shortest lifetime measurable on the Hitachi F4500 fluorometer operating in the phosphorescence mode is 0.3 ms, which was near the detection limit for measuring decay lifetimes (τ) of europium complexes in H_2O. At neutral pH and at RT, **7** was found to have a $\tau(D_2O)$ = 1.745 ms; $\tau(H_2O)$ = 0.4949 ms. Using the Horrocks equation[16], $q = A(\tau^{-1}H_2O - \tau^{-1}D_2O - 0.31 - k)$, the q for **9** is determined to be 1.26 ± 0.1. At pH 4.05 and at RT, **15** was found to have $\tau(D_2O)$ = 0.85772 ms; $\tau(H_2O)$ = 0.38892 ms. At pH 10.12 and at RT, **15** was found to have $\tau(D_2O)$ = 0.76287 ms; $\tau(H_2O)$ = 0.43745 ms. Using the Horrocks equation, the q for **15** was determined to be 1.22 ± 0.1 at pH 4.05 and **15** was determined to be 0.58 ± 0.1 at pH 10.12.

Results and Discussion:

The relaxivity (r_{1P}), defined as the efficiency of contrast agents to relax the longitudinal relaxation rates of the surrounding water protons, of **1** in neat water is 5.26 $mM^{-1}s^{-1}$ and does not change significantly in MOPS, a non-coordinating buffer.[14] However, in the presence of carbonate, the r_{1P} of **1** decreases by 23% in the MOPS/carbonate buffer and decreases further to 51% in the anion mimic buffer with higher carbonate concentrations (Table 1). These buffers are within physiological range of carbonate and are designed to mimic the anion concentrations in the extracellular matrix.[15] Such low r_{1P} values for **1** indicate the overall relaxivity is predominately derived from the outer sphere water contribution in carbonate-rich environments. **2** exhibited constantly low r_{1P} values across all experimented buffers. The observed r_{1p} for **2** was ~3 $mM^{-1}s^{-1}$ for all buffers regardless of the presence of carbonate (**Table 3-1**). The low relaxivity values are attributed to the intra-molecular acetate back-binding to the lanthanide macrocycle to effectively block water access to the lanthanide. This new class of agent has an effective inner hydration number of zero and the blocking of inner sphere water function independently of exogenous anions in solution. Potentiometer studies are needed to determine if the intra-molecular acetate binding is thermodynamically favored to the inter-molecular carbonate binding.

Relaxivity Values:

Contrast Agent	Neat H_2O	MOPS	MOPS/Carbonate	Anion Mimic	TRIS
1	5.26	5.88	4.06	2.49	4.11
2	2.52	3.18	2.77	2.39	2.99

Table 3-1: Relaxivity, r_{1P}, (mM^{-1} s^{-1}) of **1** and **2** (at 37^0C, 60 MHz) under different buffering conditions. a) Neat H_2O, pH = 6.52; b) MOPS pH=5.28 (10 mM MOPS, 100 mM NaCl); c) MOPS/Carbonate pH=7.55 (10 mM MOPS, 24 mM $NaHCO_3$); d) Anion Mimic pH=8.53 (100 mM NaCl, 0.9 mM Na_2HPO_4, 30mM $NaHCO_3$, 0.13 mM sodium citrate, 2.3 mM sodium lactate); e) TRIS pH=10.0 (100mM TRIS, 10mM $MgCl_2$)

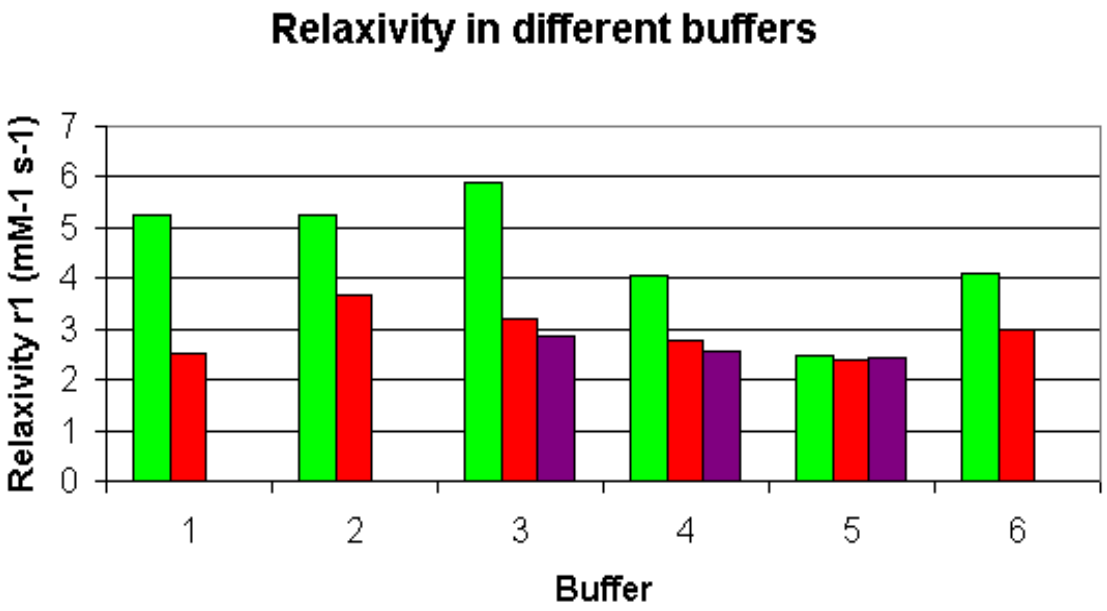

Figure 3-4: A graphical representation of the relaxivity data of **1** (green), **2** (red), and 2-aminoethyl-Gd^{3+}-DO3A (purple). 1) Neat H_2O, pH = 6.52; 2) Phosphate buffer (200 mM sodium phosphate, 2 mM $MgCl_2$, 100 mM mercaptoethanol) pH = 7.40; 3) MOPS pH=5.28 (10 mM MOPS, 100 mM NaCl); 4) MOPS/Carbonate pH=7.55 (10 mM MOPS, 24 mM $NaHCO_3$); 5) Anion Mimic pH=8.53 (100 mM NaCl, 0.9 mM Na_2HPO_4, 30mM $NaHCO_3$, 0.13 mM sodium citrate, 2.3 mM sodium lactate); 6) TRIS pH=10.0 (100mM TRIS, 10mM $MgCl_2$)

Luminescence decay studies were performed on the europium analogs of both complexes. Using the Horrocks equation[16], **1-Eu** has demonstrated a q value of 1.3 ± 0.1 at pH = 6.85. This q value is greater than 1 indicating the carbamate carbonyl oxygen on pendant phosphate containing arm is weakly coordinating to the lanthanide. The neutral charge of the **1-Eu** and the delocalized electron density around the carbamate are responsible for the weak interaction between the linker and the lanthanide. **2-Eu** was

determined to have a q = 1.2 ± 0.1 and q = 0.6 ± 0.1 at pH 4.05 and 10.12 respectively. These varying q values in different pH conditions are a result of the dangling acetate arm becoming protonated and ligating off the lanthanide center at lower pH values, but remaining coordinated at higher pH values. Acetate groups do not exhibit strong binding affinity and demonstrate bidentate ternary complexation with lanthanides.[17] The bis-coordinating acetate group on **2-Eu** is bound to the lanthanide when deprotonated to coordinately saturate the lanthanide-DO3A complex to form an eleven-membered ring, but at lower pH values, the acetate group becomes protonated and displaced from the lanthanide to accommodate a higher hydration state.

The pH profile for **2** demonstrates a remarkably different curve than **1** (**Figure 3-2**). The relaxivity for **1** is stable between pH ranges 4 and 8.5. At low pH values, **1** increases in relaxivity to (~11 $mM^{-1}s^{-1}$) which is characteristic of T_1-relaxivity of Gd(III) aqua ion.[18] At low pH values, the acetate arms and macrocycle nitrogens become protonated thereby releasing the lanthanide to the solution. Increasing pH values to 12.0 decreases the r_{1P} of **1** to ~2 $mM^{-1}s^{-1}$ which is the indicative of a q = 0 complex. In alkaline conditions, dissolved carbon dioxide and high concentration of hydroxyl anions form hydrogencarbonate which along with hydroxyl anions binds to hepta-coordinated Ln-DO3A derivatives.[19] **2** exhibited similar low relaxivity at ~2 $mM^{-1}s^{-1}$ from pH 6.0 to 12.0, which is attributed to the "scorpion" coordinated acetate group coordinately saturating the lanthanide. Between pH values 4.0 and 6.0, the r_{1P} for **2** increases at a different rate than between the pH range 1.0 to 4.0. The increase in T_1-relaxivity between the pH from 4.0 to 6.0 is attributed to the intramolecular acetate arm becoming protonated and discharging from the 8^{th} and 9^{th} coordination site of Gd(III) center,

thereby creating a q = 2 complex. In the pH range lower than 4.0, the lanthanide is released from the chelate to release the naked Gd(III) into solution.

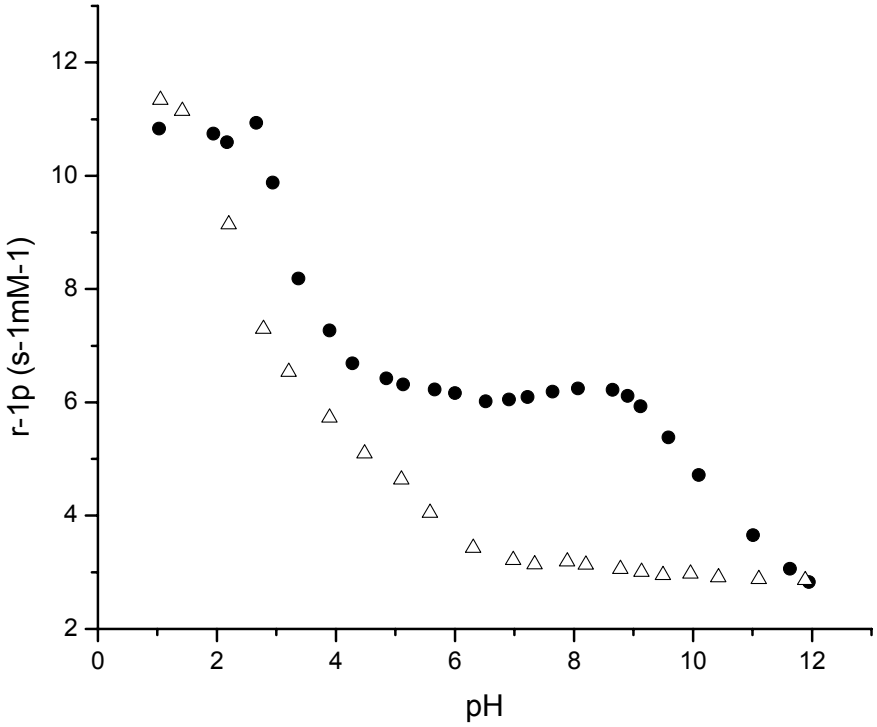

Figure 3-2: The r_{1p} vs pH profile for **1** (closed circles) and **2** (open triangles).

The mean residence lifetime (τ_M) of coordinated water was obtained for **1** and **2** from the temperature effect on the ^{17}O NMR transverse relaxation rate. The experimental data was fit using the Swift-Connick formula.[20] The water exchange rate for **1** was determined to be τ_M = 18 ns when q was fixed at 2 and τ_M = 27 ns when q was fixed at 1. The water exchange curve for **1** was characteristic of complexes with fast τ_M similar to complexes like Gd(III)DO3A = 77 ns.[18] However, the water exchange curve for **2**

demonstrated little correlation between temperature and ^{17}O NMR transverse rate, highly suggestive that **2** has zero waters that are in exchange with the bulk (q = 0) at physiological pH.

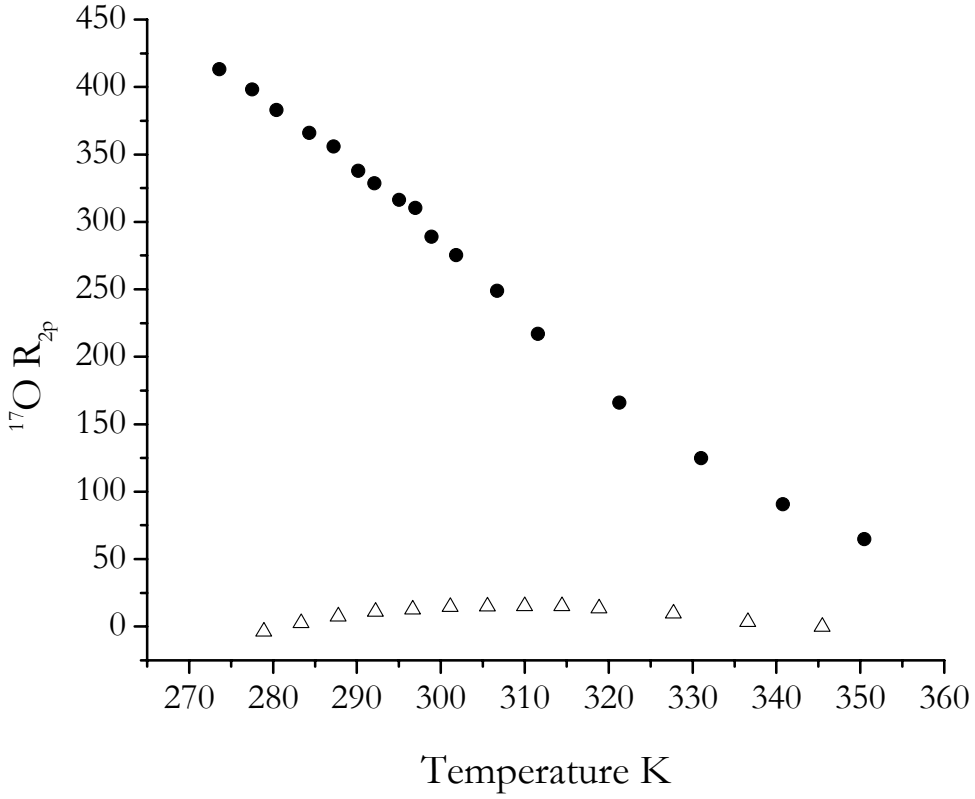

Figure 3-3: The variable temperature ^{17}O NMR transverse relaxation rate for for **1** (closed circles) and **2** (open triangles). Fitting parameters for **1**: K_{ex}^{298} (x 10^9 s^{-1}) = 70.9 ± 5; ΔH_M (kJ/mol) = 42.0 ± 1; ΔH_V (kJ/mol) = 1; ΔH_R (kJ/mol) = 20.0.

Enzyme studies were performed on **1** using alkaline phosphatase from human placenta. The phosphatase enzyme hydrolyzes the phosphate moiety to leave the 2-nitro-phenol, which is deprotonated at physiological pH. This induces a cascade of electrons to create

a semi-quinone intermediate and releasing carbon dioxide from the carbamate linker (**Figure 3-1**). **1** was tested against a known chromogenic substrate, *p*-nitrophenyl phosphate (pNPP). The enzyme-turnover maximum for **1** was discovered to be 30.36 μmol/min while the pNPP was found to be 29.00 μmol/min in TRIS buffer. Preliminary enzyme studies indicate that alkaline phosphatase was found to process **1** at a slightly faster rate than pNPP. A colormetric assay was confirmed by a relaxometric enzyme assay as the T_1 of **1** was found to display a decrease of 29.8% over 30 min. Unfortunately, the enzyme studies for **2** were unremarkable.

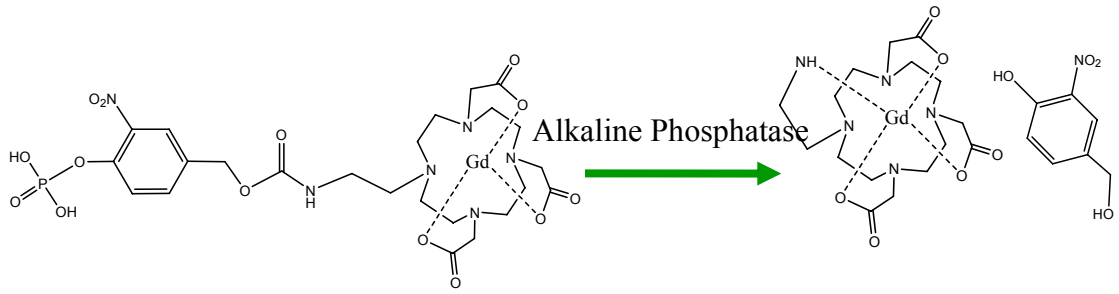

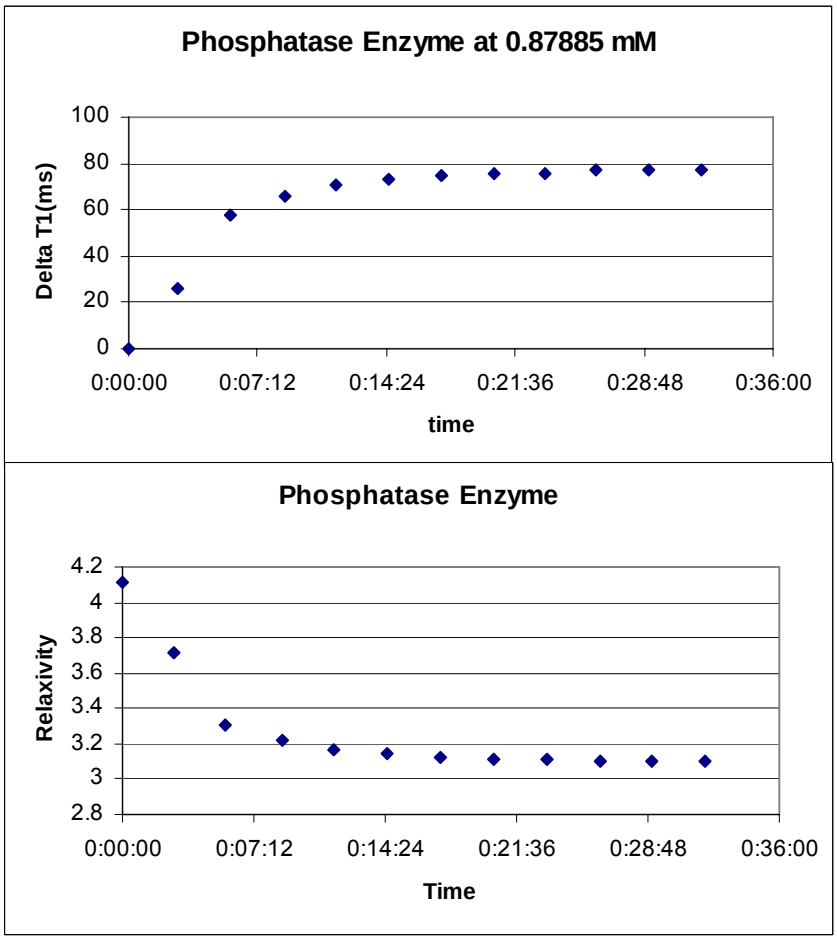

Figure 3-6: Relaxometric enzyme studies for **1** a) Top graph is the T_1 difference over time and b) is the representation of the change in relaxivity vs time.

In summary, inorganic phosphate responsive MR contrast agents have been synthesized. **1** demonstrated an affinity for oxy-anions like carbonate. A new "scorpion" blocking strategy to restrict inner sphere water access has been demonstrated for efficacy in **2** prior to enzyme cleavage.

ACKNOWLEDGMENT: Dr. Luca Frullano for his help ^{17}O NMR studies and Keith MacRenaris for his assistance with ICP-MS, Dr. Amanda Eckermann for her assistance in editing this manuscript.

Chapter 4:

Toward the Design and Synthesis of a Bridged Enzyme-Activated Contrast Agent

Abstract:

A new activatable magnetic resonance imaging (MRI) contrast agent has been designed with an alkyl linker that bridges over a macrocycle coordinating Gd^{3+}. This alkyl bridge incorporates two functionalities. It prevents water from coordinating to the paramagnetic Gd^{3+} ion and can be cleaved by β-galactosidase. Following the hydrolysis of galactopyranose sugar, a cascade reaction will release the alkyl bridge from the contrast agent to leave a coordination site for water to interact directly with Gd^{3+}, resulting in an increase of the MR signal. This novel method of activating contrast agents can serve as a template for a host of second-generation enzyme responsive contrast agents.

Introduction:

Lanthanide-based contrast agents have become a mainstay in the field of MRI.[1] The signal intensity in MRI results from the longitudinal relaxation time (T_1) and transverse relaxation time (T_2) of water protons.[2] MRI contrast agents decrease the T_1 (spin-lattice) and T_2 (spin-spin) of the nearby water protons thereby enhancing the signal contrast, which is proportional to 1/T. The lanthanide of choice for T_1 MRI contrast agents is Gd^{3+} because it is the most paramagnetic stable ion, with the slowest electron relaxation time (T_{1e}) of all the lanthanides.[3] One drawback of Gd^{3+} is that it is toxic when not chelated. Macrocyclic ligands like 1,4,7,10-tetraazacyclododecane-1,4,7,10-tetraacetic acid (DOTA) are efficient chelators for lanthanide^{3+} ions. The $[Gd\text{-}DOTA]^-$ complex is kinetically and thermodynamically stable under physiological conditions, thus mediating the toxicity of the free lanthanide ion.[4] When chelated, Gd^{3+} based contrast agents are powerful tools for MR imaging.

Activatable contrast agents alter the signal enhancing ability in response to biological phenomena including enzyme activity and the presence of specific ions.[5,6] The first contrast agent sensitive to enzymatic activity was Egad, which showed an increase in signal enhancement upon exposure to β-galactosidase.[7] The relaxivity of MRI contrast agents change linearly with the hydration number, *q*, which is the number of water molecules that are directly bound to the complex per Gd^{3+} center. The target contrast agent is designed to modulate *q* with a novel cascade mechanism in which the MRI signal intensity increase from low to high upon introduction of β-galactosidase (**Figure 4-1**).

The target contrast agent **1** is a macrocycle with a hydrophobic alkyl-bridge that sterically shields water from coordinating to the Gd^{3+} ion. The state of the contrast agent before introduction of the enzyme is labeled as the low enhancement state. In the low enhancement state, water will not be able to coordinate to Gd^{3+}; therefore the T_1 of surrounding water protons will not be shortened via inner sphere relaxation, which requires direct contact between water and the lanthanide ion. The absence of inner sphere effect should result in a 60% decrease of the contrast agent relaxivity.[8] The alkyl bridge serves to cover the coordination site, eliminating direct water interaction with Gd^{3+}.

The alkyl-bridge is designed to be removed in the presence of β-galactosidase. Two galactopyranose sugars are presented at opposite ends of the alkyl-bridge (**Figure 4-1**). β-galactosidase should enzymatically cleave the galactopyranose sugars, inducing a cascade reaction along the phenyl backbone to leave $[Gd\text{-}DOTA]^-$, a known contrast agent. In the cleaved form, water can coordinate to Gd^{3+} and the agent is considered to

be in the high enhancement state. The hydrolysis-induced cascade mechanism has been tested as a drug delivery mechanism for fluorouracil.[9] The target contrast agent **1** uses a similar cascade reaction, which leaves the contrast agent in the high enhancement state when water is able to directly interaction with the Gd^{3+} center. This research project has explored the feasibility of using a bridged alkyl-chain on the macrocycle as a new family of activatable contrast agents.

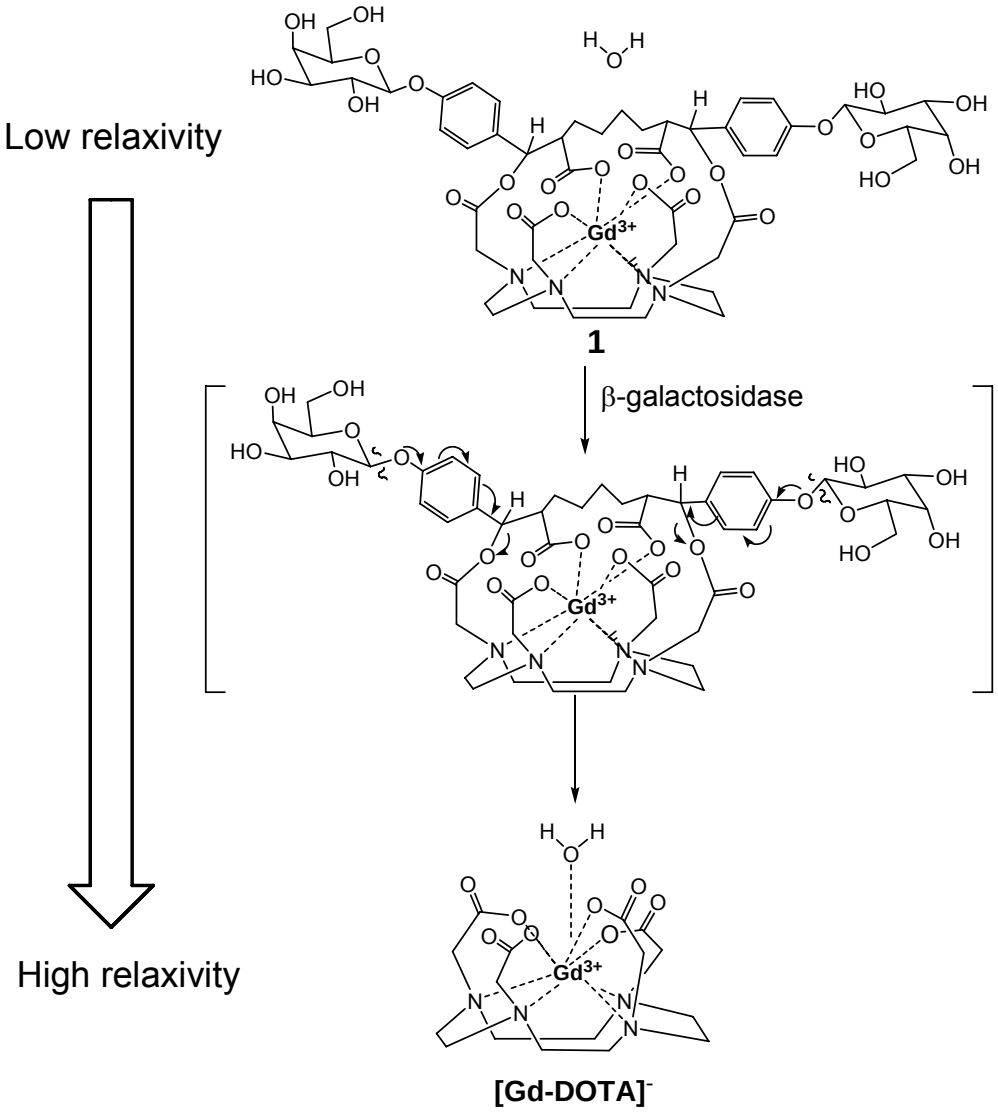

Figure 4-1: Schematic of the activation of target complex **1**. β-galactosidase induces a cascade reaction releasing the alkyl bridge leaving $[Gd\text{-}DOTA]^-$.

Objective:

The goal of the project is to make *q*-modulated contrast agents with an enzyme-responsive alkyl-bridge which serves to increase in relaxivity upon activation. With the modification of the cleavable moieties, the target contrast agent can be sensitive to a variety of physiological activities, such as matrix metalloproteases (MMP), β-galactosidase, and β-glucuronidase.

Experimental:

All reactions were carried out under dry N_2 atmosphere. All the solvent used in the reactions were of the highest grade purchased from Aldrich (Milwaukee, WI) and Fisher (Hanover Park, IL). The 1,4,7,10-tetraazacyclododecane 1,7-bis(acetic acid tert-butyl ester was purchased from Macrocyclics (Dallas, TX). NMR spectra were obtained on Varian Mercury 400-MHz, Varian INOVA 500-MHz, or Varian Gemini 2000 300-Mhz NMR spectrometer. Mass spectrometry was performed on Varian 1200L quadrapole MS using electrospray ionization (ESI) and fast atomic bombardment (FAB).

Octanedioic acid dimethyl ester (3) Suberic acid (2.76 g, 15.84 mmol) and *p*-toluenesulfonic acid monohydrate (0.62 g, 3.26 mmol) was dissolved in MeOH (200 ml). The solution was refluxed overnight. The solvent was removed under reduced pressure and the residue was washed with CH_2Cl_2 (150 ml) and H_2O (150 ml). The organic layer was collected, and the solvent removed under reduced pressure to give an oil. The oil was purified using silica gel chromatography using 5% ethyl acetate:hexane. The fractions collected and solvent was removed in vacuo. The clear yellow oil was collected

to yield 2.61 g (82%). ^{1}H NMR (300 MHz, $CHCl_3$): δ = 1.25 (4H, m), 1.58 (4H, m), 2.27 (4H, t), 3.59 (6H, s). ^{13}C NMR (125 MHz, $CHCl_3$): δ = 112.62, 51.19, 34.56, 29.08, 25.63. ESI-MS: *m/z* found 225.0 $(M+Na^+)^+$, calcd 225.12.

2,7-Bis-(hydroxy-phenyl-methyl)-octanedioic acid dimethyl ester (4) Lithium diisipropylamine (LDA) was first prepared by dissolving diisopropylamine (4.5 ml, 31.84 mmol) and 1.6M *n*-butyl lithium (11.8 ml, 18.89 mmol) in THF at -78^{o}C. The LDA solution was allowed to stir for 15 min at -78^{o}C. The product **3** (1.10 g, 5.43 mmol) was added to the mixture and allowed to stir for 10 min. Benzaldehyde (3.34 ml, 33.05 mmol) was added to the mixture which turned the solution cloudy. After 1 hour, the solution was quenched with water (~100 ml). The mixture was washed with CH_2Cl_2 and H_2O and the organic layer was collected. The CH_2Cl_2 layer was washed with H_2O (~100 ml), $NaHCO_3$ solution (~100 ml), and H_2O (~100 ml). The organic layer was collected, and the solvent was removed under reduced pressure, and dried in vacuo. Silica gel chromatography was used with a gradient eluent of 5%, 10%, 20%, 30% ethyl acetate/hexane solutions to purify the mixture. The desired compound was collected, the solvent removed, and dried in vacuo to leave a yellow oil to yield 0.357 g (16%). ^{1}H NMR (400 MHz, $CHCl_3$): δ = 1.10 (4H, bs), 1.65 (4H, bs), 2.71 (2H, q), 2.79 (2H, s), 3.59 (6H, s), 4.91 (2H, d), 7.19 (10H, m). ^{13}C NMR (125 MHz, $CHCl_3$): δ = 175.60, 141.72, 128.52, 127.92, 126.27, 74.32, 53.02, 51.85, 27.45, 26.97. ESI-MS: *m/z* found 437.0 $(M+Na^+)^+$, calcd 437.14

2,7-Bis-[(2-bromo-acetoxy)-phenyl-methyl]-octanedioic acid dimethyl ester (5) To a solution of bromoacetyl bromide (0.25 ml, 2.83 mmol) in CH_2Cl_2 (10 ml) at -78^oC, a mixture of **4** (0.2932 g, 0.707 mmol), dimethylaminopyridine (DMAP) (0.0043 g, $3.54x10^{-2}$ mmol), and pyridine (0.171 ml, 2.12 mmol) was added dropwise over a period of 2 hours. The solution was an orange color because some of the bromoacetyl bromide decomposed after exposure to ambient atmosphere. After the solution was warmed to RT and stirred overnight, the solution turned a cloudy beige color. The solution was washed with H_2O (~50ml), and the organic layer was collected and the solvent was removed under reduced pressure. The residual oil was purified using silica gel chromatography with 30% ethyl acetate/hexane. The product was collected and dried in vacuo to yield 0.590g (89%). ^1H NMR (500 MHz, $CHCl_3$): δ = 1.19 (4H, bs), 1.72 (4H, bs), 2.98 (2H, q), 3.54 (6H, s), 3.86 (4H, s), 5.92 (2H, d), 7.32 (10H, m). ^{13}C NMR (125 MHz, $CHCl_3$): δ = 173.19, 166.62, 137.29, 128.78, 128.59, 126.91, 77.78, 52.116, 51.97, 51.93, 27.03, 25.48. ESI-MS: *m/z* found 679.1 $(M+Na^+)^+$, calcd 679.36

19,24-Bis-methoxycarbonylmethyl-3,14-dioxo-5,12-diphenyl-4,13-dioxa-1,16,19,24-tetraaza-bicyclo[14.5.5]hexacosane-6,11-dicarboxylic acid dimethyl ester (6) A flask was charged with 1,4,7,10-tetraazacyclododecane 1,7-bis(acetic acid tert-butyl ester): DOTA (0.1835 g, 0.459 mmol) and triethylamine (0.165 ml, 2.29 mmol) dissolved in acetonitrile (20 ml) and stirred at 0^oC. A solution of **5** (0.301 g, 0.458 mmol) in acetonitrile (15 ml) was added dropwise over 5 hours. The solution was stirred vigorously for 5 days. The solution was extracted with CH_2Cl_2 (~50 ml) and H_2O (~50 ml). The organic layer was collected and removed with reduced pressure to leave a

yellow oil. The oil was run on a silica column with an eluent gradient of 2%, 5%, 10% methanol/CH_2Cl_2. The yellow oil gave a yield 0.0154 g (37%). ^{1}H NMR (500MHz, $CHCl_3$): δ = 1.12 (4H, bs), 1.48 (4H, bs), 2.65 (8H, bs), 2.81 (8H, bs), 3.08 (8H, bs), 3.20 (6H, s), 3.48 (4H, s), 3.84 (2H, m), 4.61 (6H, s), 5.93 (2H, m), 7.23 (10H, m). ^{13}C NMR (125 MHz, $CHCl_3$): δ = 170.45, 169.52, 1284, 128.61, 126.89, 81.74, 64.878, 56.01, 55.36, 51.87. 49.58, 49.18, 44.82, 28.28, 8.44. ESI-MS: *m/z* found 917.7 $(M+Na^+)^+$, calcd 918.09.

Octanedioic acid bis-(2-trimethylsilanyl-ethyl) ester (8) Suberic acid (0.49 g, 2.81 mmol), *p*-toulenesulfonic acid monohydrate (0.088 g, 0.46 mmol), and 2-trimethylsilylethanol (2.0 ml, 13.95 mmol) was dissolved in CH_2Cl_2 (20 ml). The solution was refluxed 15 h. The solvent was removed under reduced pressure and the residual oil was washed with CH_2Cl_2 (50 ml) and H_2O (50 ml). The organic layer collected and removed under reduced pressure to clear oil. The oil was purified using silica gel chromatography with 5% ethyl acetate:hexane. The fractions were collected and solvent was removed in vacuo. Clear oil was collected to yield 1.01 g (95%) ^{1}H NMR (400 MHz, $CHCl_3$): δ = 0.02 (9H, s), 1.92 (4H, t), 1.23 (4H, bs), 1.49 (4H, bs), 2.18 (4H, t), 4.19 (4H, t). ^{13}C NMR (125 MHz, $CHCl_3$): δ = 174.01, 62.62, 34.65, 29.02, 25.02, 17.54, -1.28. ESI-MS: *m/z* found 391.4 $(M+Na^+)^+$, calcd 391.23

2,7-Bis-(hydroxy-phenyl-methyl)-octanedioic acid bis-(2-trimethylsilanyl-ethyl) ester (9) LDA was first prepared by dissolving diispropylamine (0.56 ml, 3.99 mmol) and

2.5M *n*-butyl-lithium (1.12 ml, 2.80 mmol) in THF (15 ml) at -78°C. The LDA solution was allowed to stir for 15 mins at -78°C. The product **8** (0.5 g, 1.33 mmol) was added to the mixture and allowed to stir for 10 min. Benzylaldehyde (0.40 ml, 3.99 mmol) was added to the mixture which turned the solution cloudy. After 1 h, the solution was quenched with water (~10 ml). The mixture was washed with CH_2Cl_2 (20 ml) and H_2O (20 ml) and the organic layer was collected. The CH_2Cl_2 layer was washed with H_2O (~10ml), $NaHCO_3$ solution (~10 ml), and with H_2O (~10 ml). The organic layer was collected, removed under reduced pressure, and dried in vacuo overnight. The oil was purified using a silica gel column with a gradient of 10%, 50% ethyl acetate/hexane solutions. A second silica gel column was used to purify with a 20% ethyl acetate:hexane solution. The desired compound was collected and the solvent removed to leave a yellow oil. The oil was dried in vacuo to yield 0.45 g (55%). ^{1}H NMR (500MHz, $CHCl_3$): δ = 0.08 (18H, s), 0.82 (2H, t), 0.96 (2H, t), 1.10 (4H, bs), 1.50 (4H, m), 2.63 (2H, q), 3.00 (2H, m -OH), 4.12 (2H, t), 4.19 (2H, t), 4.78 (2H, d), 4.91 (2H, d), 7.19 (10H, m). ^{13}C NMR (125 MHz, $CHCl_3$): δ = 175.25, 141.79, 128.41, 127.78, 126.32, 75.58, 63.10, 53.19, 29.37, 28.23, 17.40, -1.36. ESI-MS: *m/z* found 609.2 $(M+Na^+)^+$, calcd 609.9

2,7-Bis-[(2-bromo-acetoxy)-phenyl-methyl]-octanedioic acid bis-(2-trimethylsilanyl-ethyl) ester (10) To a solution of bromoacetyl bromide (0.03 ml, 0.34 mmol) in CH_2Cl_2 (12 ml) at -78°C, a mixture of product **9** (0.0869 g, 0.148 mmol), DMAP (0.05g, 4.10×10^{-2} mmol), and pyridine (0.02 ml, 0.029 mmol) was added dropwise over a period of 2 hours. After the solution was warmed to RT and stirred overnight, the solution became cloudy yellow. The solution was washed with CH_2Cl_2 (~50 ml) and H_2O (~50 ml), and

the organic layer was collected and the solvent removed under reduced pressure. The residual oil was purified on a silica gel column using a gradient of 0%, 5%, 15% ethyl acetate/hexane. The product was collected and dried in vacuo to leave yellow oil to give yield 0.0158g (13%). ^{1}H NMR (500MHz, $CHCl_3$): δ = 0.08 (18H, s), 0.74 (4H, t), 1.23 (4H, bs), 1.72 (4H, bs), 2.90 (2H, q), 3.84 (4H, s), 3.97 (4H, t), 5.93 (2H, d), 7.19 (10H, m). ^{13}C NMR (125 MHz, $CHCl_3$): δ = 172.38, 166.29, 137.73, 129.15, 128.64, 127.34, 78.11, 63.16, 52.26, 29.92, 27.27, 25.96, 17.36, -1.25. ESI-MS: *m/z* found 849.2 $(M+Na^{+})^{+}$, calcd 849.16

1,4,7,10tetraaza-Cyclododecane-1,7-dicarboxylic acid dibenzyl ester (11) A solution of 1,4,7,10-tetraazacyclododecane (2.513 g, 14.58 mmol), H_2O (18 ml), conc. HCl (5 ml), and dioxane (15 ml) was added to a flask and the pH was adjusted to 2-3 using a 2M NaOH solution. Benzyl chloroformate (5.33 ml, 37.93 mmol) in dioxane (15ml) was added to the solution over a period of 16 h. pH was constantly monitored and adjusted with the 2M NaOH solution, pH was between 2-3 for the duration of the addition. A white solid residue remained after the solvent was removed under reduced pressure. The residue was washed with Et_2O (~100ml) and H_2O (100 ml). The Et_2O layer was collected and the solvent was removed under reduced pressure. This fraction proved to be 1,4,7,10-tetra-kis(benzyloxycarbonyl)-1,4,7,10-tetraazacyclododecane. The remaining solute was mixed with 20% (w/v) NaOH solution and extracted with 3 portions of Et_2O. The organic layer was washed with 5% (w/v) NaOH solution (2x), and Et_2O was collected and the solvent was removed under reduced pressure to give a colorless oil. Yield: 1.0585 (60%). ^{1}H NMR (500 MHz, $CHCl_3$): δ = 7.35 (10H, m), 5.15 (4H, s), 3.42

(8H, bs), 2.85 (8H, bs). ^{13}C NMR (125 MHz, $CHCl_3$): δ = 156.59, 136.55, 128.31, 127.78, 127.67, 66.76, 50.94, 50.59, 50.53, 50.06, 49.42, 48.95, 48.34, 48.04. ESI-MS: *m/z* found 441.3 $(M+H)^+$, calcd 440.24

Bromo-acetic acid 2-trimethylsilanyl-ethyl ester (12) A solution of 2-trimethylsilylethanol (2 ml, 13.9 mmol), pyridine (1.35 ml, 16.69 mmol), and DMAP (0.16 g, 1.31 mmol) in CH_2Cl_2 (10 ml) was added dropwise over a 30 min period to a solution of bromoacetyl bromide in CH_2Cl_2 (10 ml) at -78°C. The solution was allowed to warm to room temperature and solution stirred for 10 h. The orange precipitates were filtered and the filtrate was dried under reduced pressure. The remaining solution was distilled under vacuum. A clear liquid, which boiled at 67°C under vacuum was collected to yield 1.587 g (48%). ^1H NMR (400 MHz, $CHCl_3$): δ = 0.15 (9H, s), 1.07 (2H, t), 3.84 (2H, s), 4.27 (2H, t). ^{13}C NMR (125 MHz, $CHCl_3$): δ = 167.50, 65.03, 26.35, 17.46, -1.25.

4,10-Bis-(2-trimethylsilanyl-ethoxycarbonylmethyl)-1,4,7,10tetraaza-cyclododecane-1,7-dicarboxylic acid dibenzyl ester (13) 11 (0.491 g, 1.12 mmol), **12** (0.556 g, 2.33 mmol), diisopropylethylamine (DIPEA) (0.41 ml, 2.35 mmol), and acetonitrile (12 ml) were loaded into a flask. The solution was stirred and heated at 40°C for 14 hours, then heated at 80°C for 8 hours. The solution was allowed to cool to RT and the solvent was removed under reduced pressure. The yellow oil was washed with Et_2O and H_2O. The organic layer was washed with H_2O (~50ml), 5% NaOH solution (~50ml), and H_2O (~50ml) consecutively. The organic layer was removed under reduce pressure. The

remaining oil was purified on a silica gel column with 40% ethyl acetate/hexane. The product was collected and dried under reduced pressure to leave dark, yellow oil. Yield 0.656g (77%). ^{1}H NMR (400 MHz, $CHCl_3$): δ = 0.05 (18H, s), 0.96 (4H, t), 2.87 (8H, bs), 3.30 (4H, bs), 3.45 (8H, bs), 4.16 (4H, t), 5.14 (4H, s), 7.26 (10H, m). ^{13}C NMR (125 MHz, $CHCl_3$): δ = 171.55, 156.67, 137.04, 128.12, 128.04, 67.17, 62.74, 55.25, 54.83, 46.52, 17.65, -1.32. ESI-MS: *m/z* found 757.5 $(M+H)^+$, calcd 757.08.

[7-(2-Trimethylsilanyl-ethoxycarbonylmethyl)-1,4,7,10tetraaza-cyclododec-1-yl]-acetic acid 2-trimethylsilanyl-ethyl ester (14) 13 (0.656 g, 0.866 mmol) was added to a solution of 10% Pd/C powder (0.179 g) in absolute ethanol (20 ml). The product was shaken under H_2 pressure for 48 hours. The black solution was filtered thorough celite and the ethanol was removed under reduced pressure. The white solids were extracted with Et_2O (~50 ml) and cold 20% NaOH solution (~50 ml). The organic layer was removed under reduce pressure to leave a yellow oil, which was dried in vacuo. Yield: 0.3371 (80%). ^{1}H NMR (400MHz, $CHCl_3$): δ = 0.08 (9H, s), 1.03 (4H, t), 2.10 (2H, bs), 2.61 (8H, bs), 2.84 (8H, bs), 3.44 (4H,s), 4.09 (4H, t). ^{13}C NMR (400MHz, $CHCl_3$): δ = 171.8, 88.10, 62.82, 56.48, 52.19, 45.84, 17.70, -1.25. ESI-MS: *m/z* found 489.4 (M+H), calcd 488.3.

3,14-Dioxo-5,12-diphenyl-19,24-bis-(2-trimethylsilanyl-ethoxycarbonylmethyl)-4,13-dioxa-1,16,19,24-tetraaza-bicyclo[14.5.5]hexacosane-6,11-dicarboxylic acid bis-(2-trimethylsilanyl-ethyl) ester (15) 14 (0.02 g, $1.90\text{x}10^{-2}$ mmol) and triethylamine (0.005 g, 0.0475 mmol) was dissolved in acetonitrile (1ml). A solution of acetonitrile (2ml) and

10 (0.0158 g, $1.90x10^{-2}$ mmol) was added dropwise over 24 hour at RT. The solution turned a darker brown color. The solvent was removed under reduced pressure, and the remaining oil was extracted with CH_2Cl_2 and dH_2O. The organic layer was collected and removed under reduced pressure to leave brown oil. The oil is purified on an activated silica column (slurry with 2% TEA) with gradient 0% - 5% methanol/CH_2Cl_2. The first band with UV activity, CAM stain, and Pt-stain was collected and further purified on a silica gel column using gradient 0% - 5% methanol/CH_2Cl_2 to yield: 0.015g (67%). ^{1}H NMR (600 MHz, $CHCl_3$): δ = 0.07 (18H, s), 0.09 (18H, s), 0.58 (4H, t), 1.04 (4H, t), 1.19 (4H, bs), 1.84 (4H, bs), 2.21 (8H, bs), 2.53 (8H, bs), 3.07 (2H, d), 3.50 (4H, s), 3.62 (4H, s), 3.82 (4H, t), 4.18 (4H, t), 5.99 (2H, d), 7.32 (10H, m). ^{13}C NMR (125 MHz, $CHCl_3$): δ = 174.23, 171.59, 139.23, 138.23, 128.64, 127.34, 125.46, 73.27, 63.59, 62.31, 55.43, 53.44, 52.74, 49.23, 29.53, 28.78, 25.89, 18.63, -0.05. ESI-MS: *m/z* found 1177.6 $(M+Na^+)^+$, calcd 1177.6

2,7-Bis-[(2-bromo-acetoxy)-p-tolyl-methyl]-octanedioic acid bis-(2-trimethylsilanyl-ethyl) ester (17) Reaction conditions and purification conditions similar to compound **9**, except *p*-toluene aldehyde in place of benzyl-aldehyde. The reaction was quenched in H_2O after 2 hours at -78^{o}C. The solvent was removed. The reaction was then subjected to the reaction conditions for **10** in situ. Yield (34%) ^{1}H NMR (500 MHz, $CHCl_3$): δ = 0.08 (18H, s), 0.72 (2H, t), 1.03 (2H, t), 1.27 (4H, bs), 1.72 (4H, bs), 2.31 (6H, s), 2.83 (2H, q), 2.94 (2H, q), 3.81 (4H, s), 3.93 (4H, t), 4.23 (2H, t), 5.84 (2H, d), 7.21 (8H, m). ^{13}C NMR (125 MHz, $CHCl_3$): δ = 172.33, 166.25, 139.01, 134.69, 129.30, 127.31, 79.03,

63.08, 52.12, 28.74, 27.29, 21.45, 17.66, -1.26. ESI-MS: *m/z* found 877.2 $(M+Na^+)^+$, calcd 877.2

3,14-Dioxo-5,12-di-p-tolyl-19,24-bis-(2-trimethylsilanyl-ethoxycarbonylmethyl)-4,13-dioxa-1,16,19,24-tetraaza-bicyclo[14.5.5]hexacosane-6,11-dicarboxylic acid bis-(2-trimethylsilanyl-ethyl) ester (18) **17** and **14** were subjected to reactions conditions and purification conditions similar to **15**. Yield (58%) ^{1}H NMR (500 MHz, $CHCl_3$): δ = -0.04 (18H, s), 0.07 (18H, s), 1.57 (4H, t), 1.10 (4H, t), 1.15 (4H, bs), 1.59 (4H, bs), 2.21 (8H, bs) 2.28 (6H, s), 2.53 (8H, bs), 3.07 (2H, m), 3.80 (4H, t), 4.36 (4H, t), 5.93 (2H, d), 7.19 (4H, d), 7.21 (4H, d). ^{13}C NMR (125 MHz, $CHCl_3$): δ = 174.74, 172.03, 138.86, 134.96, 129.24, 127.76, 125.67, 64.24, 62.64, 55.84, 54.25, 52.79, 52.60, 48.67, 29.87, 21.36, 17.31, 14.31, -1.01, -1.34. ESI-MS: *m/z* found 1205.4 $(M+Na^+)^+$, calcd 1205.7

19,24-Bis-carboxymethyl-3,14-dioxo-5,12-di-p-tolyl-4,13-dioxa-1,16,19,24-tetraaza-bicyclo[14.5.5]hexacosane-6,11-dicarboxylic acid europium (III) complex (20) A flask was charged with **18** (0.021 g, mmol), tetrabutylammonium fluoride in 75% H_2O (0.061g), and THF (4 ml). Solution was stirred for 2 hours. A molecular weight cutoff 500 dialysis membrane was used to remove excess salts. The aqueous solution was replaced every 2 hours with deionized water. After 2 days of dialysis, the solution was lyophilized. A solution of $EuCl_3$ (0.082 g, mmol) and deprotected ligand, and dH_2O (5 ml) was prepared and pH was adjusted to 6. The solution was stirred until the pH was constant for days. The solution was lyophilized to leave a white powder. ESI-MS: *m/z* found 922.6, 932.6 $(M+Na^+)^+$, calcd 931.26

Bis-2-(Hydroxy-{4-[3,4,5-tris-(tert-butyl-dimethyl-silanyloxy)-6-trimethylsilanyloxymethyl-tetrahydro-pyran-2-yloxy]-phenyl}-methyl)-octanedioic acid bis-(2-trimethylsilanyl-ethyl) ester (21) **8** and 4-[3,4,5-Tris-(tert-butyl-dimethyl-silanyloxy)-6-trimethylsilanyloxymethyl-tetrahydro-pyran-2-yloxy] were subjected to similar reaction and purification conditions as **9**. Two isomers were separated during purification. Yield: Isomer 1 - (22.9%) Isomer 2 - (18.3%) ^{1}H NMR (500 MHz, $CHCl_3$): δ = 0.08 (66H, s), 0.92 (72H, s), 1.22 (4H, bs), 1.67 (4H, bs), 2.60 (2H, m), 3.67 (6H, sugar H), 4.03 (10H, sugar H, t), 4.83 (2H, d), 6.94 (4H, bs), 6.20 (4H, d). ^{13}C NMR (125 MHz, $CHCl_3$): δ = 175.17, 157.08, 134.88, 127.35, 115.95, 75.23, 71.66, 62.98, 54.61, 29.97, 27.10, 26.30, 18.84, 17.56, -1.14. ESI-MS: *m/z* found 1878.4, 1946.6 $(M+Na^{+})^{+}$, calcd 1878.1

2-((2-Bromo-acetoxy)-{4-[3,4,5-tris-(tert-butyl-dimethyl-silanyloxy)-6-trimethylsilanyloxymethyl-tetrahydro-pyran-2-yloxy]-phenyl}-methyl)-octanedioic acid bis-(2-trimethylsilanyl-ethyl) ester isomer 1 and 2 (22) **21** was subjected to similar reaction conditions and purification conditions as **10**. Yield = (78%). ^{1}H NMR (500 MHz, $CHCl_3$): δ = 0.00 (18H, s), 0.08 (48H, s), 0.79 (4H, t), 0.96 (72H, s), 1.15 (4H, bs), 1.74 (4H, bs), 2.92 (2H, q), 3.62 (4H, sugar H), 4.78 (4H, s), 3.94 (4H, t), 4.12 (6H, sugar H), 4.82 (2H, sugar H), 5.93 (2H, d), 6.98 (4H, bs), 7.22 (4H, d). ^{13}C NMR (125 MHz, $CHCl_3$): δ = 172.43, 166.22, 157.74, 131.10, 130.72, 128.68, 116.08, 111.63, 101.11, 93.92, 77.88, 71.71, 63.03, 52.09, 38.92, 36.83, 32.15, 30.55, 29.58, 27.34, 26.24,

24.73. 18.76, 17.40, 14.35, 1.23, -1.28. FAB-MS: *m/z* found 2116.8 $(M+Na^+)^+$, calcd 2117.94

3,14-Dioxo-5,12-di-3,4,5-Tris-(tert-butyl-dimethyl-silanyloxy)-6-(tert-butyl-dimethyl-silanyloxymethyl)-tetrahydro-pyran-2-ol -19,24-bis-(2-trimethylsilanyl-ethoxycarbonylmethyl)-4,13-dioxa-1,16,19,24-tetraaza-bicyclo[14.5.5]hexacosane-6,11-dicarboxylic acid bis-(2-trimethylsilanyl-ethyl) ester (23) **22** was subjected to similar reaction conditions and purification conditions as **15**. Yield = 55% ^{1}H NMR (500 MHz, $CHCl_3$): δ = 0.03 (18H, s), 0.06 (18H, s), 0.12 (48H, s), 0.63 (4H, t), 0.94 (72H, s), 1.09 (4H, t), 1.28 (4H, bs), 1.63 (4H, bs), 2.43 (16H, macrocycle H, bs), 3.07 (2H, m), 3.37 (4H, s), 3.76 (8H, sugar H, bs), 4.13 (4H, s), 4.39 (8H, sugar H, bs), 4.83 (2H, sugar H, bs), 5.97 (2H, d), 6.91 (4H, bs), 7.21 (4H, d). ^{13}C NMR (125 MHz, $CHCl_3$): δ = 174.73, 174.59, 171.96, 158.90, 131.09, 128.95, 116.05, 76.42, 71.69, 64.25, 62.98, 62.71, 60.89, 56.19, 55.89, 54.33, 52.94, 52.79, 49.01, 29.91, 27.01, 26.51, 26.22, 26.04, 18.29, 17.37, 17.25, 1.23, -0.96, -1.35. FAB-MS: *m/z* found 2446.3 $(M+H)^+$, calcd 2446.4

Tetradecanedioic acid bis-(2-trimethylsilanyl-ethyl) ester (27) 1,12-dodecanedicarboxylic acid subjected to similar reaction conditions and purification conditions as suberic acid to form **8**. Yield = 60% ^{1}H NMR (500 MHz, $CHCl_3$): δ = 0.03 (18H, s), 0.93 (4H, t), 1.28(16H, bs), 1.57 (4H, m), 2.29 (4H, t), 4.16 (4H, t). ^{13}C NMR (125 MHz, $CHCl_3$): δ = 175.45, 62.58, 34.76, 29.77, 29.65, 29.48, 29.38, 25.21, 17.52, -1.27. ESI-MS: *m/z* found 481.2, 939.6 $(M+Na^+)^+$, calcd 481.3

Bis-2-(Hydroxy-{4-[3,4,5-tris-(tert-butyl-dimethyl-silanyloxy)-6-trimethylsilanyloxymethyl-tetrahydro-pyran-2-yloxy]-phenyl}-methyl)-tetradecanedioic acid bis-(2-trimethylsilanyl-ethyl) ester (28) **27** was subjected to similar reaction conditions and purification techniques used for **9**. Yield = 55% ^{1}H NMR (500 MHz, $CHCl_3$): δ = 0.08 (66H, s), 0.93 (72H, s), 1.01 (16H, bs), 1.51 (4H, m), 2.89 (2H, m), 3.67 (6H, sugar H, bs), 4.12 (4H, sugar H, bs), 4.16 (4H, t), 4.72 (2H, d), 4.91 (2H, bs), 7.01 (4H, bs), 7.21 (4H, d). ^{13}C NMR (125 MHz, $CHCl_3$): δ = 174.49, 158.33, 137.00, 129.42, 127.63, 116.58, 101.99, 76.12, 74.97, 73.46, 64.11, 63.12, 56.73, 31.23, 29.71, 29.21, 29.19, 29.11, 20.14, 19.18, -1.19. FAB-MS: *m/z* found 1962.3 $(M+Na^+)^+$, calcd 1962.2

2-((2-Bromo-acetoxy)-{4-[3,4,5-tris-(tert-butyl-dimethyl-silanyloxy)-6-trimethylsilanyloxymethyl-tetrahydro-pyran-2-yloxy]-phenyl}-methyl)-tetradecanedioic acid bis-(2-trimethylsilanyl-ethyl) ester (29) **28** was subjected to similar reaction conditions and purification techniques used for **10**. Yield = 83% ^{1}H NMR (500MHz, $CHCl_3$): δ = 0.10 (66H, s), 1.02 (72H, s), 1.48 (16H, bs), 1.56 (4H, m), 2.97(4H, m), 3.70 (6H, sugar H, bs), 3.76 (4H, s), 4.02 (4H, sugar H, bs), 4.21 (4H, t), 4.90 (2H, sugar H, bs), 5.81 (2H, d), 7.01 (4H, bs), 7.21 (4H, d).

3,14-Dioxo-5,12-di-3,4,5-Tris-(tert-butyl-dimethyl-silanyloxy)-6-(tert-butyl-dimethyl-silanyloxymethyl)-tetrahydro-pyran-2-ol

-19,24-bis-(2-trimethylsilanyl-ethoxycarbonylmethyl)-4,13-dioxa-1,16,19,24-tetraaza-bicyclo[14.5.5]dotriacontane-6,17-dicarboxylic acid (2-trimethylsilanyl-ethyl) ester (30) 29 was subjected to similar reaction and purification conditions as used for **15**. Yield = 35% ^{1}H NMR (500 MHz, $CHCl_3$): δ = 0.09 (84H, s), 1.00 (72H, s), 1.48 (16H, bs), 1.56 (4H, m), 1.79 (4H, m), 2.04 (4H, bs), 2.83 (16H, macrocycle H, bs), 3.49 (6H, sugar H, bs), 3.76 (4H, s), 4.14 (4H, t), 4.22 (4H, sugar H, bs), 4.97 (2H, sugar H, bs), 5.85 (2H, d), 7.01 (4H, bs), 7.24 (4H, d). FAB-MS: *m/z* found 2529.6 $(M+Na^+)^+$, calcd 2530.5

Results and Discussion:

Initial synthetic efforts were directed towards **2**, a model complex for the bis-galactopyranose complex **1**. The model complex **2** without the sugar complexities was designed to study the binding pocket and synthetic feasibility of the bridged complex.

The synthesis of **2** using acid-sensitive protecting groups proved to be unsuccessful (**Scheme 4-2**). In the presence of TFA, selective deprotection of the methyl esters and tert-butyl esters did not occur; instead, the alkyl bridge was cleaved first to leave DOTA. Although the acid-sensitive protecting group did not yield the desired model complex **2**, the ligand **6** demonstrated the feasibility of the ring closing of the alkyl bridge over the macrocycle.

The alkyl bridge was found to cleave under acid conditions, thus necessitating the use of an orthogonal protecting group to protect the acetate arms on the macrocycle and the alkyl-bridge. The use of a fluorine-sensitive protecting group provided that selectivity (**Scheme 4-3**). Ligand **15** was synthesized using TMS(ethyl) protecting groups. NMR experiments of **15** demonstrated the existence of a binding pocket between

macrocycle and the alkyl bridge. The deprotection and metallation of ligand **15** proved to be difficult. However, a mass spectrum of a toluene analog complex **20**, showed the ligand can bind to a metal.

The preliminary data of metal binding to the bridged ligand gave precedence to synthesize the bis-galactopyranose ligand **23 (Scheme 4-3)**. The in situ deprotection/metallation step of **23** to yield **1** was followed by fluorescence and UV-visible spectroscopy, which gave indication of metal-ligand interaction. The reaction mixture was separated using high performance liquid chromatography and the peaks corresponding to the fluorescence of Gd^{3+} were collected. However, the mass spectrum indicated the presence of the deprotected ligand **24** and not the metallated complex **1**. This result was further confirmed by NMR spectroscopy of the purified compound. Metallation under these initial conditions was unsuccessful for the ligand **24**.

A $-(CH_2)_{10}-$ alkyl bridge ligand **30** was synthesized and characterized (**Scheme 4-4**). The design of the longer alkyl chain over the macrocycle should allow the lanthanide to better access the ligand pocket. This new design with a longer change allows for the lanthanide coordinate and a series of different lengths can determine the optimal chain length for metallation and water blocking. However, the metalation step was unsuccessful and the Gd^{3+} does not coordinate for **30**. Another strategy that can be employed for coordination of the lanthanide to the bridged ligand is the addtition of the metal prior to bridging the ligand. A disulfide bridge synthesis is proposed as a possible solution to the issue of metallation for the bridged complexes (**Scheme 4-5**). This synthetic strategy has yet to be explored.

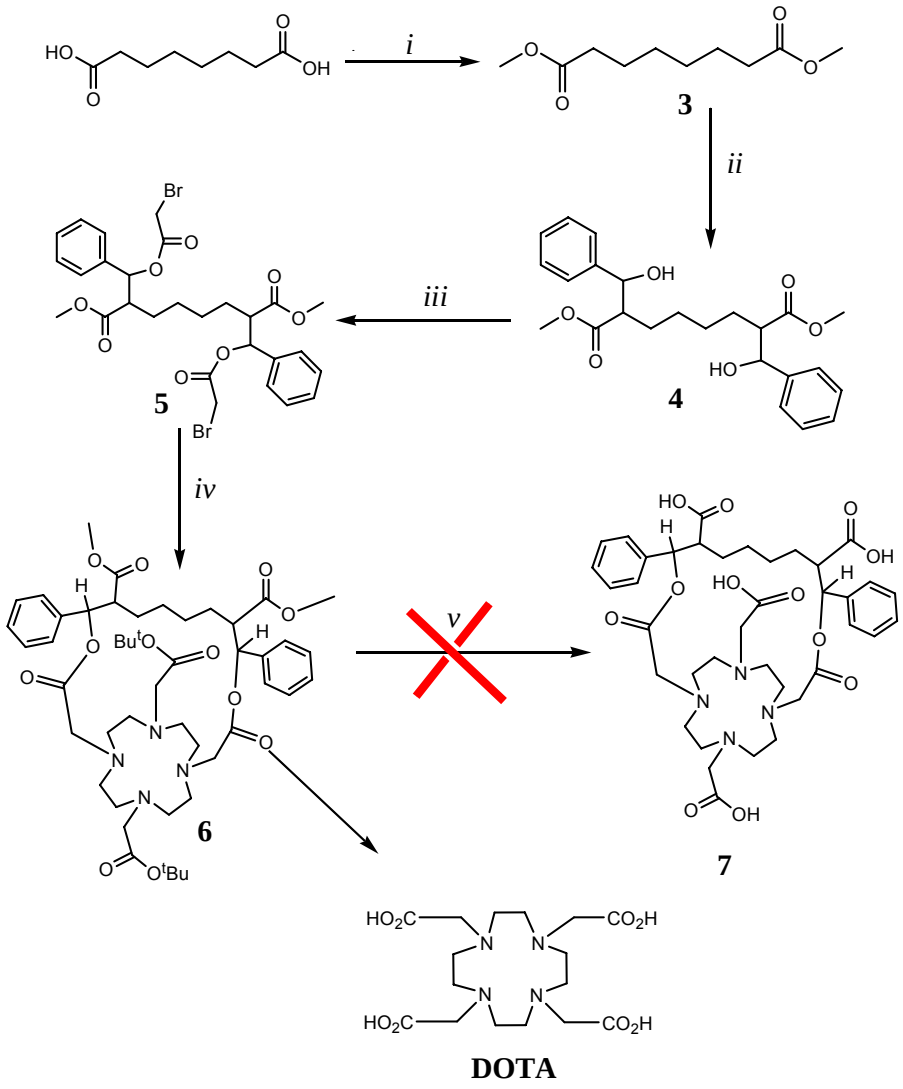

Scheme 4-1: The synthetic scheme for the methyl & tert-butyl protected model ligand. After exposure to TFA, DOTA was formed instead of the desired product **7**. *i*. *p*-toluenesulfonic acid, MeOH *ii.* lithium diispropylamine, THF. *iii*. pyridine, DMAP, CH_2Cl_2 *iv*. Bis 1,7 acetic acid tert-butyl ester DO2A, TEA, MeCN *v*. TFA, Et_2O

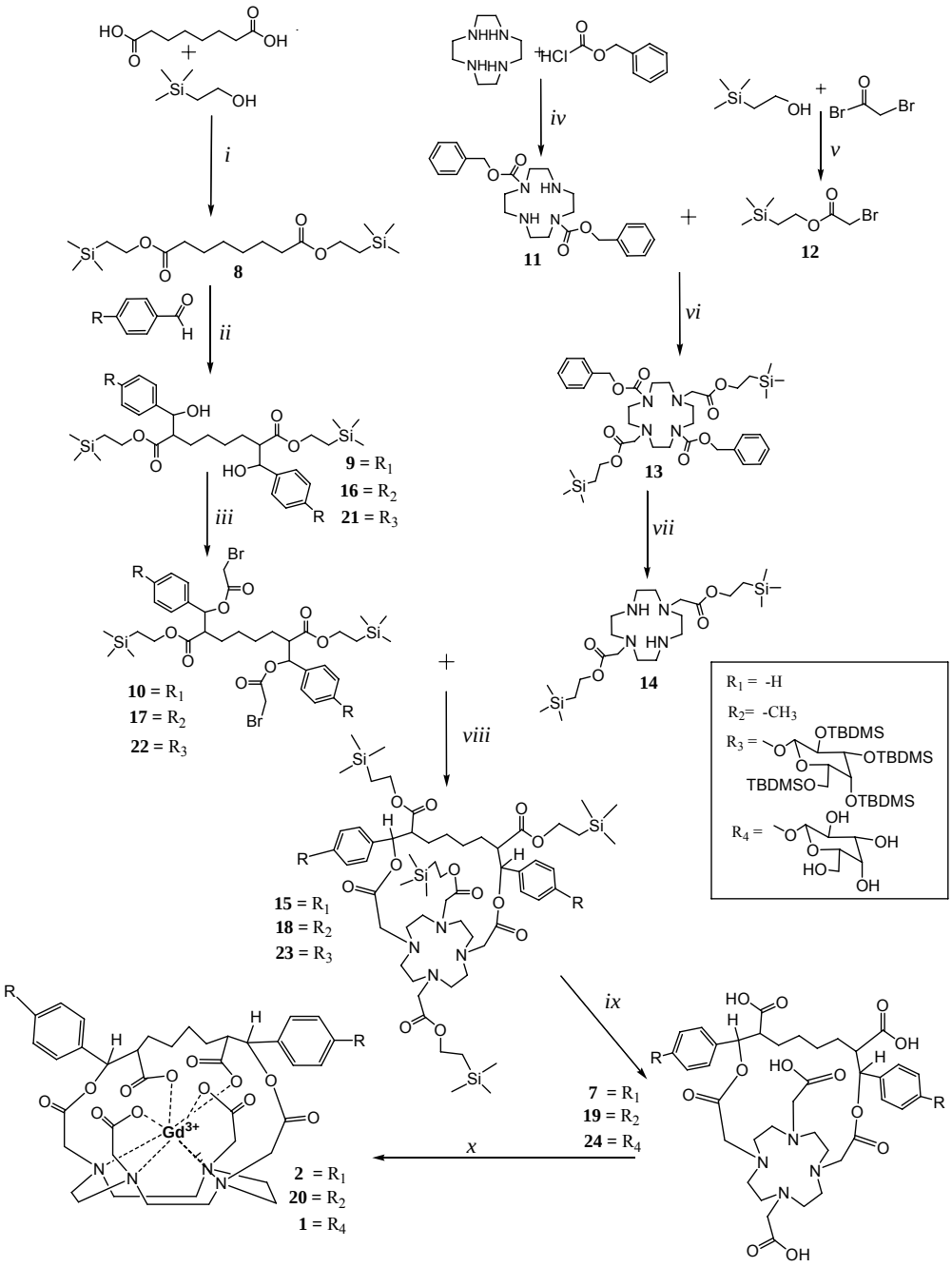

Scheme 4-2: The synthetic scheme for the synthesis of complexes that utilizes fluorine sensitive protecting groups. *i*. *p*-toluenesulfonic acid, CH_2Cl_2 *ii*. lithium diispropylamine, THF *iii.* pyridine, DMAP, bromoacetyl bromide, CH_2Cl_2 *iv.* HCl/NaOH, dioxane *v.* pyridine, DMAP, bromoacetyl bromide, CH_2Cl_2 *vi*. DIPEA, MeCN *vii*. 10%Pd/C, H_2 Et_2O *viii*. TEA, MeCN *ix*. TBAF, DMF *x*. MCl_3, H_2O

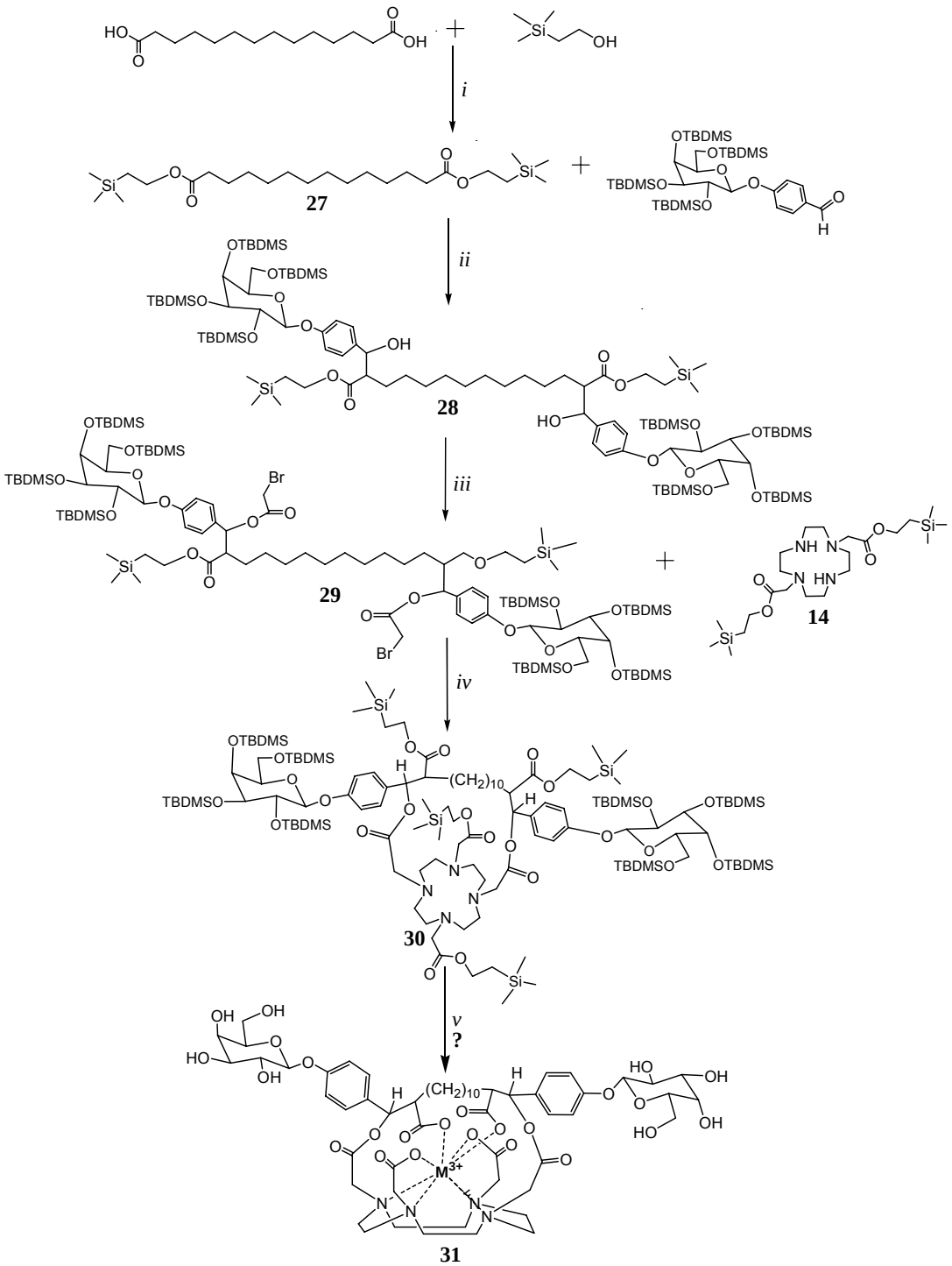

Scheme 4-3: Synthetic route of the $-(CH_2)_{10}-$ bridged ligand **30**. *i*. *p*-toluenesulfonic acid, CH_2Cl_2 *ii*. lithium diispropylamine, THF *iii*. pyridine, DMAP, bromoacetyl bromide, CH_2Cl_2 *iv*. TEA, MeCN *v*. 1. TASF, DMF 2. MCl_3, H_2O

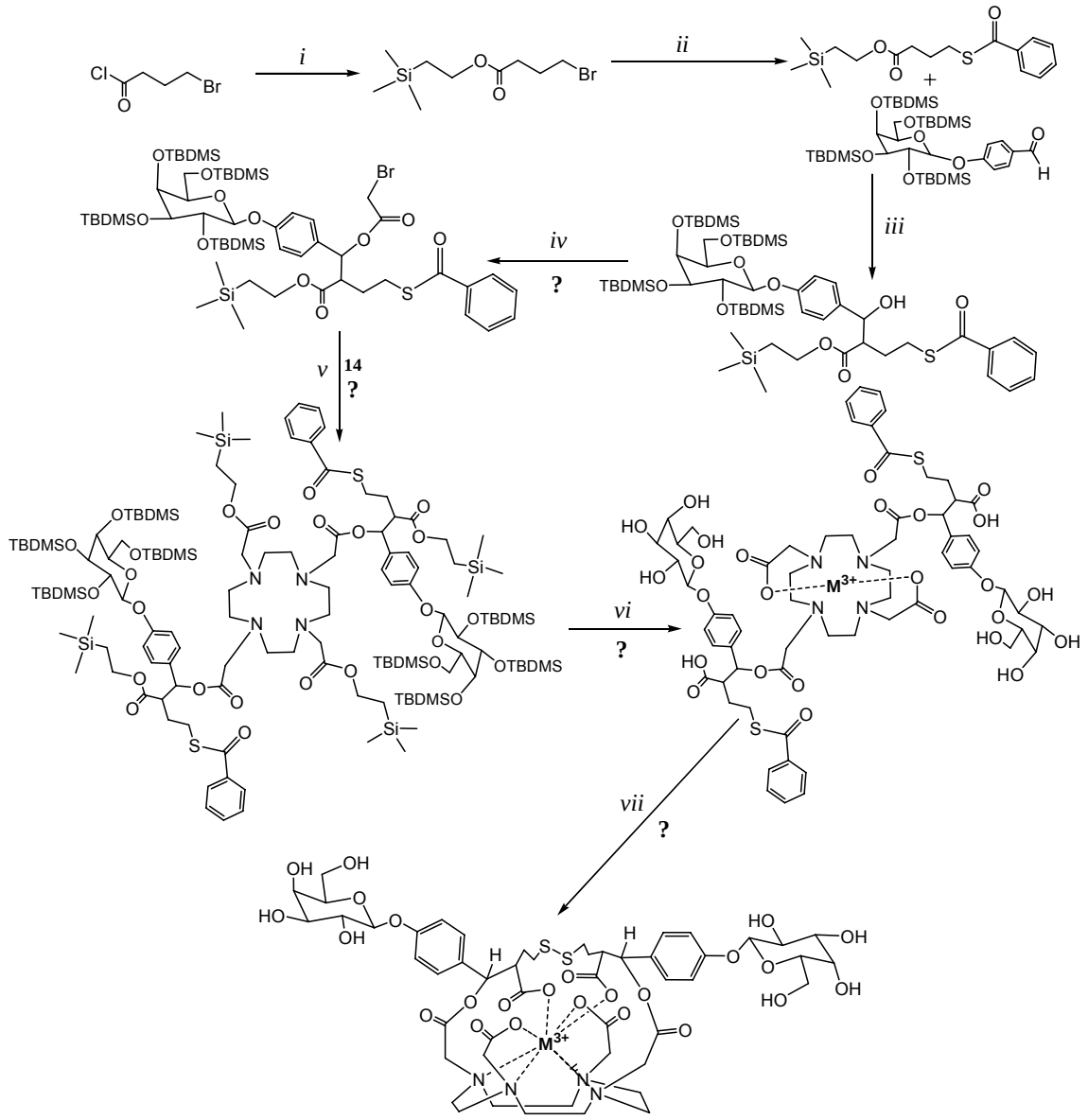

Scheme 4-4: Proposed synthetic scheme to metallate prior to bridging the complex using a disulfide linkage *i* pyridine, DMAP, bromoacetyl bromide. *ii*. thiobenzoic acid, K_2CO_3, EtOH *iii.* lithium diispropylamine, THF *iv.*. pyridine, DMAP, bromoacetyl bromide, CH_2Cl_2 *v*. TEA, MeCN *vi.* 1. TASF, DMF 2. MCl_3, H_2O *vii*. O_2, H_2O

Addendum:

Mustard DNA-Alkylating Magnetic Resonance Imaging Contrast Agents

ABSTRACT:

A magnetic resonance (MR) contrast agent based on Gd^{3+}-DOTA has been conjugated with a chemotherapeutic mustard DNA alkylating group. Upon activation with thionyl chloride, and the presence of DNA, the alkylating MR contrast agent was found to increase in r_{1p} by a 235%. This increase in r_{1p} is attributed to the slowing of the rotational correlation time (τ_R). An agarose gel electrophoresis was performed to determine that the supercoiled DNA was alkylated by the activated mustard MR contrast agent.

Introduction:

Cancer is the third leading cause of death in America, accounting for approximately 13% of all death this year.[1] In 2004, the prevalence of cancer was 10,326,000 in a total population of 293,655,404 in the United States. That is approximately 3.5% of Americans who are living with a cancer diagnosis.[2] 7.6 million people around the world died from cancer in 2000.[3]

Cancer progresses in stages. Although, the specific genesis of tumors has not been identified, scientists believe heterogeneous factors, i.e. genetic inheritance or environmental carcinogens, transform a single or population of somatic cells to become tumerogenic.[4] The primary neoplasm generally goes undetected until it has gone through a significant progressive growth. Vascularization follows with neoplastic secretion of angiogenetic factors like vascular permeability factor (VPF) and vascular endothelial growth factor (VEGF), which help recruit blood vessels to feed the cancer growth needs.[5] The tumor rapidly invades the surrounding tissue through the basal membrane in a process called intravasation.[6] In the invaded tissue, the tumor continues to grow during

the arrest stage. Eventually, the cancer acquires the ability to build metastases at distant sites via lymphatic system.

The nucleotide concentration in normal cells is relatively constant. Somatic cells tightly regulate nucleotide synthesis predominantly utilizing the purine salvage pathway for its nucleotide acid needs.[7] Conversely, tumors replicate rapidly, increasing its demand for nucleotides for its insatiable proliferation. Tumors uniquely use the de novo purine pathway, rather than the purine salvage pathway, to meet its genetic requirements. This is precisely why chemotherapeutic drugs can preferentially affect tumor cells over normal cells. Many drugs debilitate the cell's capacity to synthesis nucleotide via the de novo pathways.

In the classical definition of chemotherapy, the goal is to selectively kill malignant cell in vivo, while allowing enough normal cells of critical tissues to survive.[8] Chemotherapeutic agents target the primary neoplasm during the progressive growth stage, thus preventing the proliferation of the cancer and eventually promoting the elimination of the tumor. However, chemotherapeutics have the undesired side of effect of attacking normal organ cells with rapid dividing characteristics such as bone marrow, gastro-intestinal (GI) epithelium, hair follicle cells, and taste buds. Chemotherapy works well for lymphomas and leukemia, but falls short with common tumors like colon, rectal, lung, and breast cancer, which have a lower proportion of dividing cells.

Chemotherapeutics can be broken up into different categories: anti-metabolic agents, anti-folate agents, covalent DNA binding and non-covalent DNA binding agents, inhibitors of chromatin function, drugs that affect endocrine function, and drugs that target cell signaling. The scope of this manuscript is limited to the category of covalent

DNA cross-linkers, specifically DNA mustard agents. Note, that any of the other chemotherapeutics can be conjugated with an MR contrast agent to get the desired effect to selective imaging for tumors.

Alkylating agents are the drugs that covalently cross-link DNA. Sulfur mustard is a precursor of the nitrogen mustard, which are both members of mustard gas family.[9] The first sulfur mustard experiments were carried out in 1931 with the purpose as a chemical, nerve agent during war times. It was discovered that the respiratory tract and bone marrow were especially susceptible to the mustard agents. The sulfur mustards were changed to nitrogen mustards because the hyper-reactivity of the sulfur agents would only damage the distal respiratory epithelium.[10] The less reactive nitrogen agent was found to be more deadly because of its ability to reach the deep lung parenchyma. The 1st clinical trials for the mustard agent for use against cancer did not occur until 1942. Intravenous injections of the milder nitrogen mustard agent were discovered to be cytotoxic to dividing cells. The mustard agents were discovered to cross-link DNA adducts of neighboring guanine residues on DNA strands.[11] The nitrogen on the 15th position of guanine was found to be the most likely position on the nucleic acid to be alkylated due to the electron-rich ring of the purine (**Figure A-1**).[12]

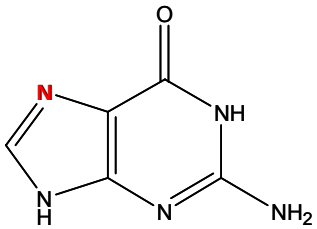

Figure A-1: The 15th nitrogen of guanine (red) most likely to be alkylated with the mustard agent.

The alkylating mustard agent is unique in its structure. It contains an amine, with two pendant ethyl halides (**Figure A-2**).[13] The lone pair of sp3 orbital electrons of the nitrogen performs an S_N2 attack on the chloride to form an aziridine that is positively charged. This reactive intermediate can react with water or with an electrophile like DNA. These azidine is short-lived; approximately 1 equivalent of the chloride is released from the nitrogen mustard within 15 mins under aqueous conditions.[14] The second halide is longer-lived and can endure in for two hours. The nitrogen mustard in effect is attacked by the guanine residue and served to cross link adjacent strands to deform and bend the DNA so that it is no longer functional.

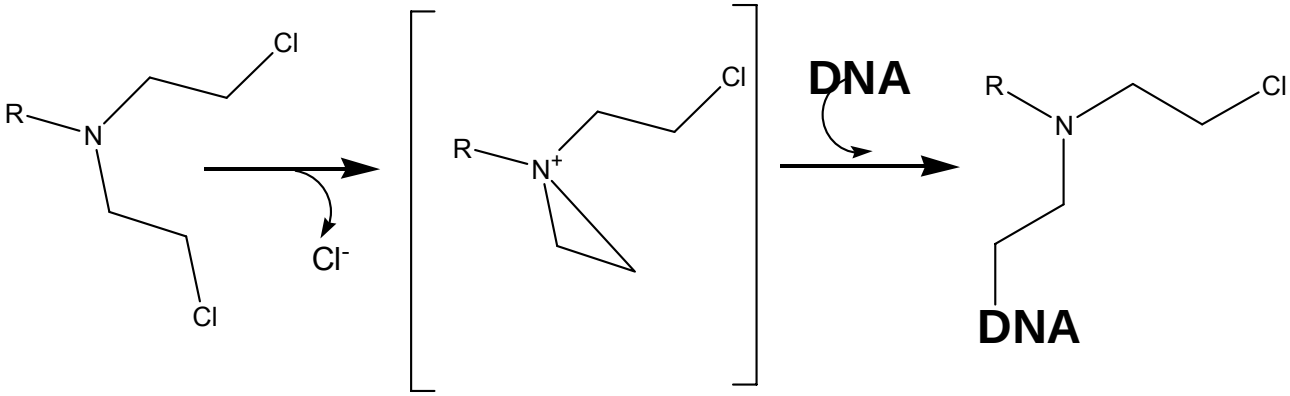

Figure A-2: Activated nitrogen mustard with its effect of crosslinking DNA. It can react again and link two strands of DNA.

The alkylating nature of the nitrogen mustard creates a variety of problems for the dividing cell. The mustard agent decreases the ability of DNA to act as a template for DNA polymerase to replicate the DNA strands. Although excision repair can repair alkylated DNA, too much alkylation does irreversible damage to the cell.[15] Proliferating cells are especially susceptible to the nitrogen mustards although all cell cycle stages can be adversely affected by the DNA damaging effects of the drug. Examples of nitrogen mustard compounds are Melphalan, Cyclophosphamide, and Idosfamide, all of which crosslink DNA strands.

These chemotherapeutic agents are intravenously injected and distributed systemically. However, there is no method to image the efficacy of these chemotherapeutics and their distribution. The only current method to determine which cells take up the drug is from gross clinical finding. The side-effects experienced from the patient are a clinical methodology used by doctors to determine the locations of non-desirable targeting of the drug. However, a contrast agent conjugated to any chemotherapeutics can track which cells preferentially take the drugs and which cells are being harmed most adversely. Scientist can gain the ability to image drug delivery and discover the ability to image the localizations of drug distribution

Magnetic Resonance imaging (MRI) makes it possible to image the drug delivery with paramagnetic contrast agents conjugated to DNA alkylating agents. Scientists can observe the localization of the chemotherapeutic due to the covalent bonding nature of the alkylating agent. MRI with the aid of Gd^{3+} chelated contrast agents in conjunction with alkylating agents may be able to image smaller tumors with aggressive proliferation.

This addendum presents an example of such an agent, its synthesis and possible other future directions for such a complex.[16]

Experimental Section:

General Methods - All the reactions were run under dry N_2 atmosphere unless otherwise indicated. All the anhydrous solvents used were from a solvent system from GlassContours. All the compounds used in the reactions were available from Aldrich (Milwaukee, WI) and Fisher (Hanover Park, IL). 1,4,7,10-Tetrazacyclododecane (cyclen) was purchased from Strem. Water was purified using a Millipore Milli-Q Synthesis purifier. The NMR spectra were obtained on Varian Mercury 400-MHz, Varian INOVA 500-MHz NMR spectrometer. Mass spectrometry was performed on Varian 1200L quadrapole MS using electrospray ionization (ESI). The elemental analyses were performed at Desert Analytics (Tucson, AZ). The UV-Visible spectroscopy was performed on the HP5452 diode array spectrometer thermostated at 37^{o}C. The fluorescence measurements were performed on the Hitachi F4500 fluorometer. ICP-MS measurements were performed on a VG Elemental PQ Excell spectrometer standardized with eight concentrations from 0-50 ppb Gd(III). An internal standard of 1 ppb In(III) was used in all of the ICP samples.

LC-MS and Preparative LC – The analytic LC-MS was performed on a Varian Prostar model 210 with a 410 autosampler on a 100 μl sample loop. Two 210 pump heads pumped the effluent at 5 ml/min to split to a 363 fluorescence detector and a 330

photodiode array (PDA) detector, then connected to a 1200L quadrupole ESI-MS. A 3:1 split valve was used to direct the column-separated sample to 3 parts series connected light detectors and 1 part MS. All the runs used a 1 ml/min flow rate on a ThermoElectron 4.6 * 150 mm 5 μm Aquasil C18 column. The mobile phase used was millipore purified water and HPLC grade acetonitrile.

The preparative LC was the Varian Prostar model 210 consisting of two 210 pumps with 25 ml/min heads with a 5 ml manual injection sample loop. The Prostar system has a 2 channel UV-Visible detector tandem to a HP-1046A fluorescence detector. The mobile phases were under the same conditions used on the analytical LC-MS. The preparative concentrations ranged between 25 mg – 150 mg dissolved in 3 ml of water. The preparative runs used a 15 ml/min on Atlantis Prep T3 10 μm 19 x
10 mm guard column.

DNA purification - The DNA used in the experiment was Vector Puck 18, which was chosen for being a nonspecific circular DNA. The Vector Puck 18 is supercoiled and a plasmid DNA that is 3505 base pairs long. A Qiagen PCR MegaPrep clean up kit was used to purify the DNA after yeast was cultured and the exo-nuclear components lysed. The kit provided a membrane that bound the DNA. Once the DNA was bound, the membrane was washed 4 times with ethanol, and the DNA was eluted with deionized water. The total purified DNA amount was 80 mg of DNA.

Relaxivity - T_1 values of each sample was obtained on a Bruker mq60 Minispec using an inversion recovery pulse sequence with appropriate recycle delays. This instrument has a

proton Larmor frequency of 60 MHz and operates at 37 ^{o}C. The concentrations of gadolinium complex solutions were determined from ICP-MS and performed in triplicate.

Synthesis -

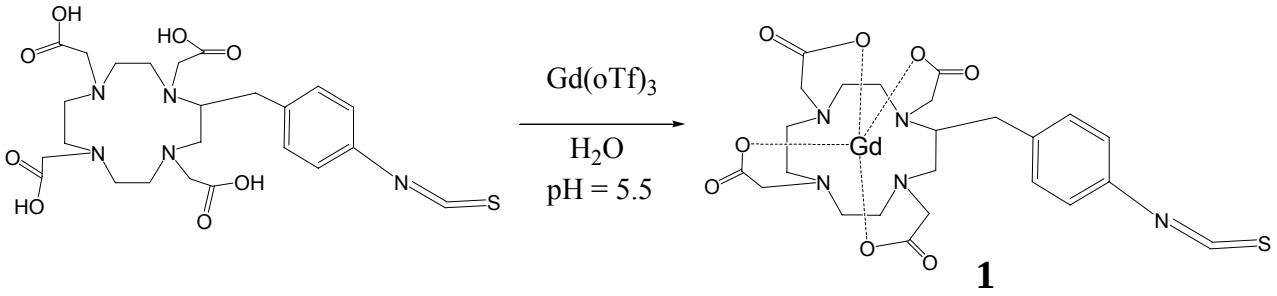

1

Gadolinium-[4,7,10-Tris-carboxymethyl-2-(4-isothiocyanato-benzyl)-1,4,7,10tetraaza-cyclododec-1-yl]-acetic acid (1) – A flask was charged with p-benzyl-DOTA (0.100 g, 1.81 x 10^{-4} mol) and deionized H_2O (2 ml). The pH of the solution was adjusted to 5.0 using 0.25 M HCl and 0.25 M NaOH solution. A solution of gadolinium triflate (0.05 g, 8.27 x 10^{-5} mol) and deionized H_2O (1ml) was added to the ligand mixture dropwise. The pH was adjusted back to 5.5 and stabilized over 3 hr period. The solution was allowed to stir overnight. The solution was purified using HPLC. The appropriate fractions were collected and lyophilized to a white powder. Yield = 0.085 g (66.5%). ESI: m/z found 704.3 [M^{+}], calcd 705.1

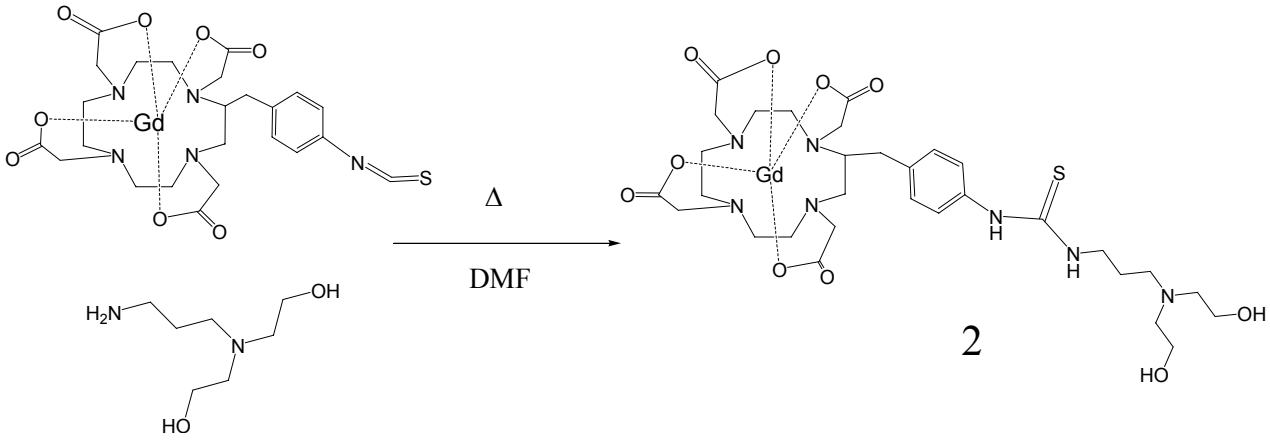

Gadolinium-{2-[4-(3-{3-[Bis-(2-hydroxy-ethyl)-amino]-propyl}-thioureido)-benzyl]-4,7,10-tris-carboxymethyl-1,4,7,10tetraaza-cyclododec-1-yl}-acetic acid (2) – A flask was charged with **1** (0.085 g, 1.21 x 10^{-4} mol), 2-[(3-Amino-propyl)-(2-hydroxy-ethyl)-amino]-ethanol (0.05 ml), and dimethyl-formamide (10 ml). The temperature was raised to 40^{o}C and allowed to stir overnight. The solvent was removed under reduced pressure. Deionized H_2O (3 ml) was added to the remaining oil to dissolve to compound. The solution was filtered through a 0.2 μm filter. The solution was purified on the HPLC. The appropriate fraction was collected and lyophilized. Yield = 0.0524 g (49.9%) ESI: m/z found 867.3 [M^+], calcd 867.2 Anal. - %C 43.23 %H 5.57 %N 10.68 %S 2.49 calc: C% 42.94 H% 5.46 N% 11.31 S% 3.70

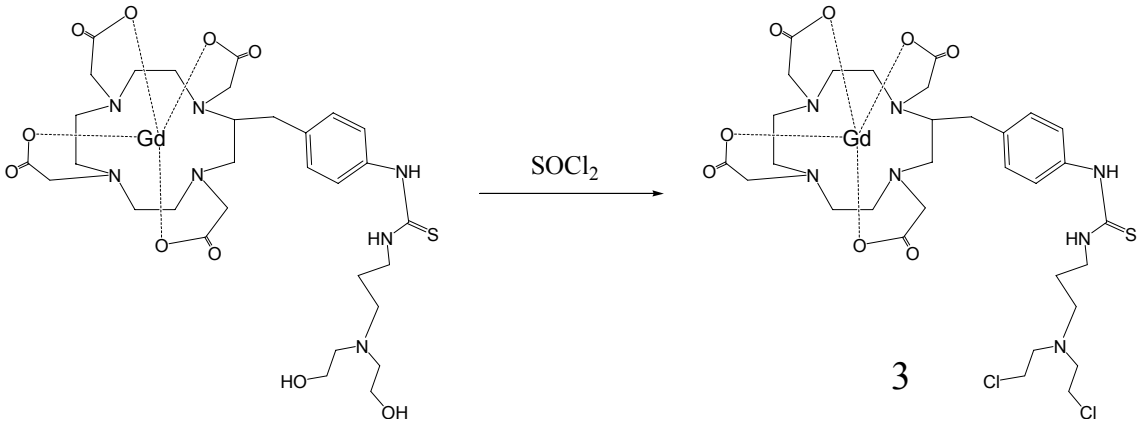

Gadolinium-{2-[4-(3-{3-[Bis-(2-chloro-ethyl)-amino]-propyl}-thioureido)-benzyl]-4,7,10-tris-carboxymethyl-1,4,7,10tetraaza-cyclododec-1-yl}-acetic acid (3) – A flask was charged with **2** (0.98 mg, 1.13 x 10^{-3} mmol) and the temperature was dropped to 0^{o}C using an ice bath. Thionyl chloride (1 ml) was added to the solid, and allowed to stir for 5 hr. The solution was warmed to R.T. and stirred for an additional 5 hrs. The thionyl chloride was removed and the solution was titerated with diethyl ether (3mL) twice. The solvent was removed under reduced pressure and dried in vacuo for 1 h.

DNA alkylation experiment - Four sample tubes were made. Sample tube 1 contained 0.5 ml of 1.15 x 10^{-3} M solution of **2**. Sample tube 2 contained 0.5 ml of 1.13 x 10^{-3} M solution of **3**. Sample tube 3 contained 0.25 ml of 1.15 x 10^{-3} M of **2** + 2.46 x 10^{-3} M solution of DNA base pairs (BP) in Tris/Borate/EDTA buffer (TBE). Sample tube 4 contained 0.25 ml of 1.13 x 10^{-3} M of **3** + 2.46 x 10^{-3} M solution of DNA BP in TBE buffer. The T_1's were taken for all 4 samples at multiple time points over the course of a day. The concentration of ICP-MS for each sample tube was taken in triplicate and fit to a standard curve of a known Gd^{3+} concentration solution. The concentration of BP in

solution is an estimate from the weight of the sample and the estimated MW of the ~3500 BP supercoiled DNA. The concentration of **2** and **3** was estimated to be half the concentration of the concentration of BP because it was rationalized that the nucleotide guanine and its base pair cytosine would constitute approximately half the DNA sequence.

Agarose gel electrophoresis – An agarose gel was made with three wells to separate the shorter versus longer pieces of DNA. The run time for the gel was 1.5 hr. The dye used to make the DNA band visible is ethidium bromide (EtBr), which fluoresces under UV when intercalated into DNA or RNA. The 2 samples were run with a ladder. The positive sample A was 1.13 x 10^{-3} M solution **3** in a solution of 2.46 x 10^{-3} M DNA BP in TBE buffer. The negative control sample B was the 1.15 x 10^{-3} M solution of **2** in 2.46 x 10-3 M of DNA BP in TBE buffer. Restriction enzymes were added to each well to splice the DNA into appropriate segments. Sample A and B were run along side a ladder with only the supercoiled DNA BP. The samples and DNA ladder was visualized by ethidium bromide staining on a 0.8% TAE agarose gel.

Results and Discussion:

The relaxivity, r_{1P}, is defined as the efficiency of contrast agents to shorten the longitudinal relaxation time, T_1, of the protons belonging to the surrounding water molecules.[17] The higher the relaxivity, the lower concentration of contrast agent is need to observe a contrast on the MRI. Small molecular weight contrast agents have

demonstrated to have low relaxivity, mainly restricted by its fast rotational correlation time (τ_R).[18]

The relaxivity for **2** was determined to be 5.4 $mM^{-1}s^{-1}$ in TBE buffer. This r_{1p} value is considered on the high for a q = 1 complex. Small molecular weight, monomeric Gd^{3+}-DOTA agents with a single inner sphere water at 60 MHz display relaxivities less than 4 $mM^{-1}s^{-1}$.[16] This is attributed to the fast rotational correlation time (τ_R) and it slow water exchange rate (τ_M). Four acetate arms on the tetrazamacrocycle are attached to the Gd^{3+} center, and fluctuate between two conformations.[19] However, unlike the Gd^{3+}-DOTA derivative does not allow for a variety of motion of the acetate arms on the complex. The DOTA acetate arms are essentially locked into a major or minor conformation. This attributes to the DOTA low water exchange rate, while DO3A has a more open structure.

The relaxivity of the activated mustard complex **3** was not taken. In water, the chloride mustard was effervescent to hydrolyze back to **2** in a matter of minutes. After activation of **2** with stannous chloride, **3** was formed. With the introduction of supercoiled DNA to the activated mustard Gd^{3+} complex, the relaxivity for **3** increased from 5.4 $mM^{-1}s^{-1}$ to 18.1 $mM^{-1}s^{-1}$ in TBE buffer. A time course relaxivity study demonstrated that the relaxivity did not change very much after 1 h, indicating that the DNA alkylation was immediate and rapid.

After 1 day incubation, an agrase gel electrophoresis study was performed to determine the efficacy of this MR mustard contrast agent. The samples and DNA ladder was visualized by ethidium bromide staining on a 0.8% TAE agarose gel. This result of the ethimidian bromide treated gel electrophoresis is shown in **Figure A-3**.

In **Figure A-3**, Lane 1 contained the native Puck supercoiled DNA. Lane 2 contained the DNA plus the hydroxyl contrast agent **2**. Lane 3 contained the DNA plus the activated mustard MR contrast agent **3**. A restriction enzyme trypsinogen was added to the gel to observe the fragment peaks to determine the overall size of the DNA. Lane 1 demonstrated patterns consist with the standard ladder. Lane 1 served as a control to determine that the signature DNA pattern created by the restriction enzyme. Lane 2 demonstrated the hydroxyl contrast agent **2** minimally associated with the DNA. Although some restriction activity of the restriction enzyme was inhibited, the majority of the function and cleavage pattern was conserved. Lane 3 demonstrated that the activated mustard agent added to the DNA sequence and prevented the restriction enzyme from recognizing and cleaving the specific sites. The majority of the DNA is does not move to the cathode because the DNA sequence is too large and has not been recognized or cleaved by the restriction enzyme. The activated mustard MR contrast agent **3** cross-linked DNA and increase in relaxivity in the process.

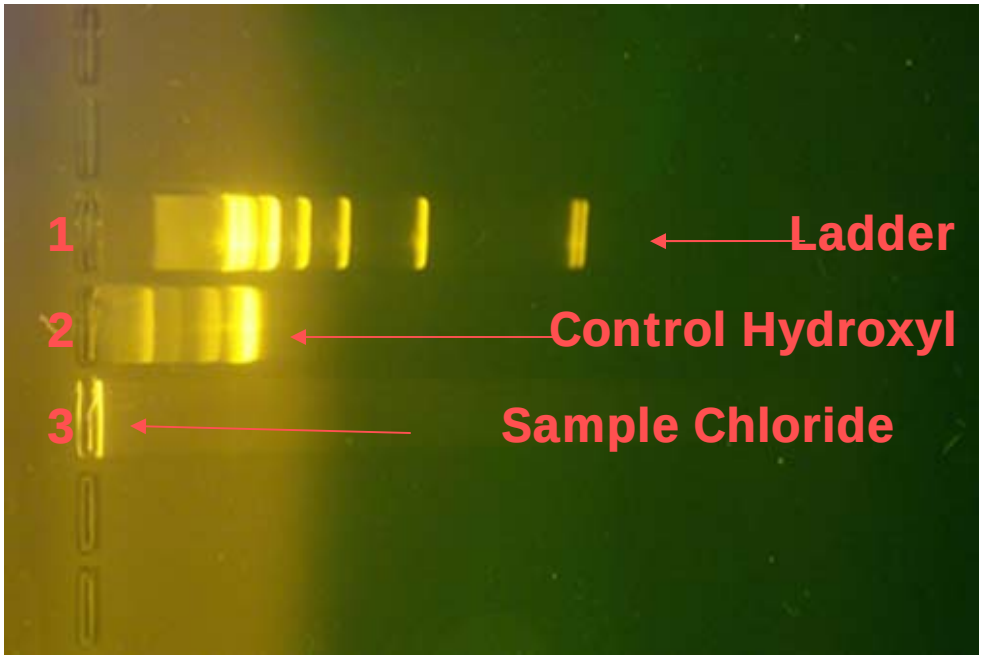

Figure A-3: The samples and DNA ladder was visualized by ethidium bromide staining on a 0.8% TAE agarose gel. Lane 1 is the ladder with the DNA after exposure to restriction enzymes. Lane 2 is DNA after exposure to 2 the unactivated hydroxyl MR contrast agent **2**. Lane 3 is the DNA after exposure to the activated mustard agent **3**.

REFERENCES

Chapter 1

(1) Gerlach, W.; Stern, O., Das magnetische Moment des Silberatoms. *Zeitschrift für Physik* **1922**, *9*, 353-355.

(2) Gorter, C. J. *Physica (The Hague)* **1936**, *3*, 503.

(3) Van der Waals, J. H., Ed. *Encyclopedia of Magnetic Resonance Imaging*; Wiley, 1996; Vol. 1., 677.

(4) Rabi, I. I.; Zacharias, J. R.; Millman, S.; Kusch, P., Milestones in magnetic resonance: 'a new method of measuring nuclear magnetic moment. *Journal of Magnetic Resonance Imaging* **1938**, *2*, 131-133.

(5) Bloch, F. *Nature* **1952**, *170*, 911-912.

(6) Purcell, E. M.; Torrey, H. C.; Pound, R. V., Resonance Absorption by Nuclear Magnetic Moments in a Solid *Physical Review* **1946**, *69*, 37.

(7) Zimmerman, H. E.; Lewis, R. G.; McCullough, J. J.; Padwa, A.; Staley, S.; Semmelhack, M. F., The Relation of Cyclohexenone to Cyclohexadienone Rearrangements. *Journal of the American Chemical Society* **1966**, *88*, 1965.

(8) Lauterbur, P. C., Image Formation by Induced Local Interactions: Examples Employing Nuclear Magnetic Resonance. *Nature* **1973**, *242*, 190-191.

(9) Kumar A; D., W.; R.R., E. NMR Fourier Zeugmatography. *Journal of Magnetic Resonance* **1975**, *18*, 69-83.

(10) Mansfield, P.; Maudsley, A. A., Planar spin imaging by NMR. *Journal of Physics C: Solid State Physics* **1976**, *9*, L409-411.

(11) Mansfield, P.; Maudsley, A. A., Line scan proton spin imaging in biological structures by NMR. *Physics in Medicine and Biology* **1976**, *21*, 847-852.

(12) Damadian, T. F. In *New York Times*: New York, Oct. 11, 2003.

(13) Merbach, A. E.; Toth, E., Eds. *The Chemistry of Contrast Agents in Medical Magnetic Resonance Imaging*; 1 ed.; John Wiley & Sons, LTD.: West Sussex, England, 2001.

(14) Caravan, P.; Ellison, J. J.; McMurry, T. J.; Lauffer, R. B., Gadolinium chelates as MRI contrast agents: Structure, Dynamics, and Applications. *Chemical Review* **1999**, *92*, 2293-2352.

(15) Duimstra, J. A. In *Chemistry*; California Institute of Technology: Pasadena, 2006, p 146.

(16) Ashcroft, N. W.; Mermin, N. D., Eds. *Solid State Physics*; Saunders College; Harcourt Brace: Orlando, 1976.

(17) Toth, E.; Helm, L.; Merbach, A. E., Relaxivity of MRI contrast agents. *Topics in Current Chemistry* **2002**, *221*, 62-98.

(18) Nolte, J. *The Human Brain: An Introduction to Its Functional Anatomy*; Fifth Edition ed.; Mobsy, Inc: St. Louis, Missouri, 2002.

(19) Zuo, C. S.; Metz, K. R.; Sun, Y.; Sherry, D. A., TmDOTA- A sensitive probe for MR thermometry in vivo. *Journal of Magnetic Resonance* **1998**, *133*, 53-60.

(20) Woods, M.; Kovacs, Z.; Zhang, S.; Sherry, D. A., Towards the rational design of magnetic resonance imaging contrast agents: Isolation of the two coordination isomers of lanthanide DOTA-type complexes. *Angewandte Chemie-International Edition in English* **2003**, *42*, 5889-5892.

(21) Bartolini, M. E.; Pekar, J.; Chettle, D. R.; McNeill, F.; Scott, A.; Sykes, J.; Prato, F. S.; Moran, G. R. An investigation of the toxicity of gadolinium based MRI contrast agents using neutron activation analysis. *Magnetic Resonance Imaging* **2003,** *21,* 541-544.

(22) Shellock, F. G.; Kanal, E., Safety of Magnetic Resonance Imaging Contrast Agents. *Journal of Magnetic Resonance Imaging* **1999**, *10*, 477-484.

(23) Raghunand, N.; Howison, C.; Sherry, D. A.; Zhang, S.; Gillies, R. J., Renal and systemic pH imaging by contrast-enhanced MRI. *Magnetic Resonance in Medicine* **2003**, *49*, 249-257.

(24) Ergün, I.; Keven, K.; Uruç, I.; Ekmekçi, Y.; Canbakan, B.; Erden, I.; Karatan, O., The safety of gadolinium in patients with stage 3 and 4 renal failure. *Nephrology Dialysis Transplantation* **2006**, *21*, 697-700.

(25) Ahrens, E. T.; Rothbacher, U.; Jacobs, R. E.; Fraser, S. E., A model for MRI contrast enhancement using T1 agents. *Proceeding of the National Academy of Sciences of the United States of America* **1998**, *95*, 8443-8448.

(26) Aime, S.; Botta, M.; Fasano, M.; Terreno, E., Lanthanide (III) chelates for NMR biomedical applications. *Chemical Society Review* **1998**, *27*, 19-29

(27) Supkowski, R. M.; Horrocks, W. D., On the determination of the number of water molecules, q, coordinated to europium(III) ions in solution from luminsecence decay lifetimes. *Inorganica Chemica Acta* **2002**, *340*, 44-48.

(28) Beeby, A.; Clarkson, I. M.; Dickins, R. S.; Faulkner, S.; Parker, D.; Royle, L.; de Sousa, A. S.; Williams, J. A. G.; Woods, M., Non-radiative deactivation of the excited states of europium, terbium and ytterbium complexes by proximate energy-matched OH, NH, and CH oscillators: an improved luminescence method for establishing solution hydration states. *Journal of the Chemical Society: Perkins Transactions* **1999**, *2*, 493-503.

(29) Horrocks, W. D.; Sudnick, D. R., Lanthanide ions probes of structure in biology. Laser-induced luminescence decay, constants provide a direct measure of the number of metal-coordinated water molecules. *Journal of the American Chemical Society* **1979**, *101*, 334-340.

(30) Alpoim, M. C.; Urbano, A. M.; C.F., G.; Peters, J. A., Determination of the number of inner-sphere water molecules in lanthanide(III) polyaminocarboxylate complexes. *Journal of the Chemical Society: Dalton Transactions* **1992**, 463 - 467.

(31) Toth, E.; Dhubhghaill, O. M.; Besson, G.; Helm, L.; Merbach, A. E., Coordination equilibrium - a clue for fast water exchange on potential magnetic resonance imaging contrast agents?. *Magnetic Resonance in Chemistry* **1999**, *37*, 701-708.

(32) Cossy, C.; Helm, L.; Merbach, A. E., Oxygen-17 Nuclear magnetic resonance kinetic study of water exchange on the lanthanide(III) aqua ions. *Inorganic Chemistry* **1998**, *27*, 1973-1979.

(33) Swift, T. J.; Connick, R. E. J., NMR-Relaxation Mechanisms of O^{17} in Aqueous Solutions of Paramagnetic Cations and the Lifetime of Water Molecules in the First Coordination Sphere. *Journal of Chemical Physics* **1962**, *37*, 307.

(34) Pisaniello, D. L.; Helm, L.; Meier, P.; Merbach, A. E., Variable pressure and temperature nuclear magnetic resonance and visible spectrophotometric studies of lanthanide ions in dimethylformamide: solvation and solvent exchange dynamics. *Journal of the American Chemical Society* **1983**, *105*, 4528-4536.

(35) Geralades, C. F.; Zhang, S.; Sherry, D. A., Comparison of crystal field dependent and indepedent methods to analyse lanthanide induced NMR shifts in axially symmetric complexes. Part I. Systems with C3 symmetry axis. *Inorganica Chemica Acta* **2004**, *357*, 381-395.

(36) Dunand, F. A.; Toth, E.; Hollister, R.; Merbach, A. E., Lipari-Szabo approach as a tool for the analysis of macromolecular gadolinium (III)-based MRI contrast agents illustrated by the [Gd(EGTA-BA-(CH2)12)nN+ polymer. *Journal of the Biological Inorganic Chemistry* **2001**, *6*, 247-255.

(37) Belorizky, E.; Fries, P. H. Simple analytical approximation of the longitundinal electronic relaxation rate of Gd(III) complexes in solutions. *Physical Chemistry Chemical Physics* **2004**, *6*, 2341-2351.

(38) Belorizky, E.; Fries, P. H. Simple analytical approximation of the longitundinal electronic relaxation rate of Gd(III) complexes in solutions. *Physical Chemistry Chemical Physics Phys. Chem. Chem. Phys.* **2004**, *6*, 2341-2351.

(39) Nicolle, G.; Yerly, F.; Imbert, D.; Bottger, U.; Bunzli, J.; Merbach, A. E., Towards binuclear polyaminocarboxylate MRI contrast agents? Spectroscopic and MD study of the peculiar aqueous behavior of the Ln(III) chelates of OHEC (Ln = Eu, Gd, and Tb): Implications for relaxivity. *Chemistry - A European Journal* **2003**, *9*, 5453-5467.

(40) Costes, J. P.; Dupuis, A.; Laurent, J. P., An original heteronuclear VO2+, Gd3+ complex with nonet ground state. *Dalton Transactions* **1998**, 735-736.

(41) Muller, R. N.; Elst, L. V.; Laurent, S., Spin transition molecular materials: intelligent contrast agent for magnetic resonance imaging. *Journal of the American Chemical Society* **2003**, *125*, 8405-8407.

(42) Caravan, P.; Astashkin, A. V.; Raitsimring, A. M., The gadolinium(III)-water hydrogen distance in MRI contrast agents. *Inorganic Chemistry* **2003**, *42*, 3972-3974.

(43) Peters, J.; Raber, D. J., Lanthanide induced shifts and relaxation rate enhancements. *Progress in Nuclear Magnetic Resonance Spectroscopy* **1996**, *28*, 283-350.

(44) Bogdanov, A. A.; Lewin, M.; Weissleder, R., Approaches and agents for imaging the vascular system. *Advanced Drug Reviews* **1999**, *37*, 279-293.

(45) Woods, M.; Kiefer, G. E.; Bott, S.; Castillo-Muzquiz, A.; Eshelbrenner, C.; Michaudet, L.; McMillan, K.; Mudiguda, S. D.; Orgin, D.; Tircso, G.; Zhang, S.; Zhao, P.; Sherry, D. A., Synthesis, relaxometric, and photophysical properties of a new pH-responsive MRI contrast agent: The effect of other ligating groups on dissociation of a p-nitrophenolic pendant arm. *Journal of the American Chemical Society* **2004**, *126*, 9248-9256.

(46) Aime, S.; Barge, A.; Botta, M.; Howard, J. A.; Kataky, R.; Lowe, M. P.; Moloney, J. M.; Parker, D.; de Sousa, A. S., Dependence of the relaxivity and luminescence of gadolinium and europium amino-acid complexes on hydrogencarbonate and pH. *Chemical Communication* **1999**, 1047-1048.

(47) Aime, S.; Barge, A.; Castelli, D. D.; Fedeli, F.; Mortillaro, A.; Nielson, F. U.; Terreno, E., Paramagnetic lanthanide (III) complexes as pH-sensitive chemical

exchange saturation transfer (CEST) contrast agents for MRI applications. *Magnetic Resonance in Medicine* **2002**, *47*, 639-648.

(48) Aime, S.; Botta, M.; Crich, S. G.; Giovenzana, G. B.; Pagliarin, R.; Sisti, M.; Terreno, E., NMR relaxation Studies of Gd(III) complexes with hetadentate macrocyclic ligands. *Magnetic Resonance in Chemistry* **1998**, *36*, 200-208.

(49) Lokling, K.; Fossheim, S. L.; Skurtveit, R.; Bjornerud, A.; Klaveness, J., pH-sensitive paramagnetic liposomes as MRI contrast agents in vitro feasibility studies. *Magnetic Resonance Imaging* **2001**, *19*, 731-738.

(50) Hanaoka, A.; Kikuchi, K.; Urano, Y.; Narazaki, M.; Yokawa, T.; Sakamoto, S.; Yamaguchi, K.; Nagano, T., Design and Synthesis of a Novel Magnetic Resonance Imaging Contrast agent for Selective sensing of Zinc Ion. *Chemistry and Biology* **2002**, *9*, 1027-1032.

(51) Hanaoka, A.; Kikuchi, K.; Urano, Y.; Nagano, T., Selective Sensing of Zinc ions with Novel Magnetic Renonance Imaging Contrast agent. *Journal of the Chemical Society: Perkins Transactions* **2001**, *2*, 1840-1843.

(52) Major, J. L.; Parigi, G.; Luchinat, C.; T.J., M., The synthesis and in vitro testing of a zinc-activated MRI contrast agent. *Proceeding of the National Academy of Sciences of the United States of America* **2007**, *104*, 13881-13886.

(53) Li, W. H.; Fraser, S. E.; Meade, T. J., A calcium-sensitive magnetic resonance imaging contrast agent. *Journal of the American Chemical Society* **1999**, *121*, 1413-1414.

(54) Li, W. H.; Parigi, G.; Fragai, M.; Luchinat, C.; Meade, T., Mechanistic studies of a calcium-dependent MRI contrast agent. *Inorganic Chemistry* **2002**, *41*, 4018-4024.

(55) Voet, D.; Voet, J. G. *Biochemistry*; Second ed.; John Wiley and Sons, INC.: New Jersey, 1995.

(56) Jacques, V.; Desreux, J. F., New classes of MRI contrast agents. *Topics in Current Chemistry* **2002**, *221*, 123-164.

(57) Meade, T., Seeing is believing. *Academic Radiology* **2001**, *8*, 1-3.

(58) Meade, T. J.; Taylor, A. K.; Bull, S. R., New magnetic resonance contrast agents as biochemical reporters. *Current Opinions in Neurobiology* **2003**, *13*, 597-602.

(59) Urbanczyk-Pearson, L. M.; Femia, F. J.; Smith, J.; Parigi, G.; Eckermann, A. L.; Duimstra, J. A.; Luchinat, C.; Meade, T. J., Mechanistic Investigation of ¾-Galactosidase-Activated MR Contrast Agents. *Inorganic Chemistry* **2008**, *47*, 56-68.

(60) Duimstra, J. A.; Femia, F. J.; Meade, T. J., A gadolinium chelate for detection of beta-glucuronidase: A self-immolative approach. *Journal of the American Chemical Society* **2005**, *127*, 12847-12855.

(61) Nivorozhkin, A. L.; Kolodziej, A. F.; Caravan, P.; Greenfield, M. T.; Lauffer, R. B.; McMurry, T. J., Enzyme-activated Gd3+ magnetic resonance imaging contrast agents with prominent receptor-induced magnetization enhancement. *Angewandte Chemie International Edition* **2001**, *40*, 2903-2906.

(62) Lauffer, R. B.; McMurry, T. J.; Dunham, S. O.; Scott, D. M.; Parmelee, D. J.; Dumas, S. In *WO patent 9736619*, 1997.

(63) Chang, Y. T.; Cheng, C. M.; Su, Y. Z.; Lee, W. T.; Hsu, J. S.; Liu, G. C.; Cheng, T. L.; Wang, Y. M., Synthesis and Characterization of a New Bioactivated

Paramagnetic Gadolinium(III) Complex [Gd(DOTA-FPG)(H2O)] for Tracing Gene Expression. *Bioconjugate Chemistry* **2007**, *18,* , 1716–1727.

(64) Bhorade, R.; Weissleder, R.; Nakakoshi, T.; Moore, A.; Tung, C. H. *Bioconjugate Chemistry* **2000**, *11*, 301.

(65) Pirko, I.; Johnson, A.; Ciric, B.; Gamez, J.; Macura, S. L.; Pease, L.; Rodriguez, M. In vivo magnetic resonance imaging of immune cells in the central nervous system with superparamagnetic antibodies. *In vivo MRI of Immune Cells in the CNS*, 179-181.

(66) Unger, E. C.; Totty, W. G.; Nuefeld, D. M.; Otsuka, F. L.; Murphy, W. A.; Welsh, M. S.; Connett, J. M.; Philpott, G. W. *Investigative Radiology.* **1985**, *27*, 829.

(67) Khaw, B. A.; Gold, H. K.; Goldman, K., In *WO patent* 4859450, 1989 .

(68) Curtet, C.; Bourgoin, C.; Bohy, J.; Strand, M.; Lempert, T. E.; Rosenbaum, A. E.; Joseph, P. M. *Journal of Nuclear Medicine* **1986**, *27*, 693.

(69) Kornguth, S. E.; Turski, P. A.; Perman, W. H.; Schultz, R.; Kalinke, T.; Reale, R.; Raybaud, F. *Journal of Neurosurgery* **1987**, *66*, 898.

(70) Anderson, S. A.; Rader, R. K.; Westlin, W. F.; Null, C.; Jackson, D.; Lanza, G. M.; Wickline, S. A.; Kotyk, J. J. *Magnetic Resonance in Medicine* **2000**, *44*, 433.

(71) Lanza, G. M.; Wallace, K. D.; Scott, M. J.; Cacheris, W. P.; Abdenschein, D. R.; Christy, D. H.; Sharkey, A. M.; Miller, J. G.; Gaffney, P. J.; Wickline, S. A. *Circulation* **1996**, *95*.

(72) Lee, J.; Zylka, M. J.; Anderson, D. J.; Burdette, J. E.; Woodruff, T. K.; Meade, T. J., A Steroid-Conjugated Contrast Agent for Magnetic Resonance Imaging of Cell Signaling. *Journal of the American Chemical Society* **2005**, *127*, 13164-13166.

(73) Muhler, A. *J. Magnetic Resonance Imaging* **1995**, *5*, 7.

(74) Bolskar, R. D.; Benedetto, A. F.; Husebo, L. O.; Price, R. E.; Jackson, E. F.; Wallace, S.; Wilson, L. J.; Alford, J. M., First Soluable M@C60 derivatives provide enhanced access to metallofullerenes and permit in vivo evaluation of Gd@C60[C(COOH)2]10 as a MRI contrast agent. *Journal of the American Chemical Society* **2002**, *125*.

(75) Kato, H.; Kanazawa, Y.; Okumura, M.; Taninaka, A.; Yokawa, T.; Shinohara, H., Lanthnoid endohedral metallofullernols for MRI contrast agents. *Journal of the American Chemical Society* **2003**, *125*, 4391-4397.

(76) Toth, E.; Bolskar, R. D.; Borel, A.; Gonzalez, G.; Helm, L.; Merbach, A. E.; Sitharaman, B.; Wilson, L. J., Water-Soluable Gadofullerenes: Toward high relaxivity pH-responsive MRI contrast agents. *Journal of the American Chemical Society* **2005**, *127*, 799-805.

(77) Hajela, S.; Botta, M.; Giraudo, S.; Xu, J.; Raymond, K. N.; Aime, S., A tris-hydroxymethyl-substituted derivative of Gd-TREN-Me-3,2-HOPO: An MRI relaxation agent with improved efficiency. *Journal of the American Chemical Society* **2000**, *122*, 11228-11229.

(78) Xu, J.; Churchill, D. G.; Botta, M.; Raymond, K. N., Gadolinium(III) 1,2-hydroxypridonate-based complexes: Toward MRI contrast agents of high relaxivity. *Inorganic Chemistry* **2004**, *43*, 5492-5494.

(79) Raymond, K. N.; Pierre, V., Next generation, high relaxivity gadolinium MRI agents. *Bioconjugate Chemistry* **2005**, *16*, 3-8.

(80) Allen, M. J.; Raines, R. T.; Kiessling, L. L., Contrast agents for magnetic resonance imaging synthesized with ring-opening metathesis polymerization. *Journal of the American Chemical Society (Communications)* **2006**, *128*, 6534-6535.

(81) Dong, Q.; Hurst, D. R.; Weinmann, H. J.; Chenevert, T. L.; Londy, F. J.; Prince, M. R. *Investigative Radiology* **1998**, *33*, 699.

(82) Gustafsson, B.; Youens, S.; Louie, A., Development of contrast agents targeted to macrophage scavenger receptors of MRI of vascular inflammation. *Bioconjugate Chemistry* **2006**, *17*, 538-547.

(83) Martina, M.; Fortin, J.; Menager, C.; Clement, O.; Barratt, G.; Grabielle-Madelmont, C.; Gazeau, F.; Cabuil, V.; Lesieur, S., Generation of superparamagnetic liposomes revealed as highly efficient MRI contrast agents for in vivo imaging. *Journal of the American Chemical Society* **2006**, *127*, 10676-10685.

(84) Kim, D. K.; Mikhaylova, M.; Wang, F. H.; Kehr, J.; Bjelke, B.; zhang, Y.; Tsakalakos, T.; Mujammed, M., Starch-coated superparamagentic nanoparticles as MR contrast agents. *Chemical of Materials* **2003,** *15,* 4343-4351.

(85) Gandon, Y.; Olivie, D.; Guyader, D.; Aube, C.; Oberti, F.; Sebille, V.; Deugnier, Y., Non-invasive assessment of hepatic iron stores by MRI. *The Lancet* **2004**, *363*, 357-362.

(86) Aime, S.; Geninatti, S.; Crich, S. G.; Gianolio, E.; Giovenzana, G. B.; Teia, L.; Terreno, E., High sensitivity lanthanide(III) based probes for MR-medical imaging. *Coordination Chemistry Reviews* **2006**, *250*, 1562-1579.

Chapter 2:

(1) Davidson, E. H. *Gene activity in early development*; Third ed.; Academic Press: New York, NY, 1986.

(2) Wilson, E. B. *The cell in development and inheritance*; Macmillan: New York, NY, 1986.

(3) Hoeijmakers, J. H. J., Genome maintenance mechanism for preventing cancer. *Nature* **2001**, *411*, 366-374.

(4) Zlokarnik, G.; Negulescu, P. A.; Knapp, T. E.; Mere, L.; Burres, N.; Feng, L.; Whitney, M.; Roemer, K.; Tsien, R. Y., Quantitation of transcription and clonal selection of single living cells with beta-lactamase as reporter. *Science* **1998**, *279*, 84-88.

(5) Alam, J.; Cook, J. L. Reporter Genes: Application to the study of mammalian gene transcription. *Analytical Biochemistry* **1990**, *188*, 245-254.

(6) Guarente, L.; Ptashne, M., Fusion of Escherichia coli lacZ to the cytochrome c gene of Saccharomyces cervisiae. *Proceeding of the National Academy of Sciences of the United States of America* **1981**, *78*, 2199-2203.

(7) Weiss, D. J.; Liggitt, D.; Clark, J. G., Histochemical discrimination of endogenous mammalian beta-galactosidase activity from that resulting from lac-Z gene expression. *Histochemical Journal* **1999**, *31*, 231-236.

(8) Hoffman, R. M., Green fluorescent protein for metastasis research. *Methods in Molecular Medicine* **2001**, *58*, 285-298.

(9) Tjuvajev, J. G.; G., S.; Desai, R.; Uehara, H.; K., W.; B., G.; Blasberg, R. G., Imaging the expression of transfected genes in vivo. *Cancer Research* **1996**, *55*, 6126-6132.

(10) Blankenberg, F. G., Molecular Imaging: the latest generation of contrast agents and tissue characterization techniques. *Journal of Cellular Biochemistry* **2003**, *90*, 443-453.

(11) Deconinck, F., Nuclear imaging in the realm of medical imaging. *Nuclear Instruments and Methods in Physics Research* **2003**, *509*, 213-228.

(12) Ciobanu, L.; Pennington, C. H., 3D micron-scale MRI of single biological cells. *Solid State Nuclear Magnetic Resonance* **2004**, *25*, 137-141.

(13) Gillies, R. J. *J. Cell.,* In vivo molecular imaging. *Journal of Cellular Biochemistry Supplement* **2002**, *39*, 231-238.

(14) Caravan, P.; Ellison, J. J.; McMurry, T. J.; Lauffer, R. B., Gadolinium chelates as MRI contrast agents: Structure, Dynamics, and Applications. *Chemical Review* **1999**, *92*, 2293-2352.

(15) Caravan, P., Strategies for increasing the senstivity of gadolinium based MRI contrast agents. *Chemical Society Reviews* **2006**, *35*, 512-523.

(16) Clarkson, R. B., Blood-Pool MRI contrast agents: Properties and characterization. *Topics in Current Chemistry* **2002**, *221*, 202-232.

(17) Toth, E.; Helm, L.; Merbach, A. E., Relaxivity of MRI contrast agents. *Topics in Current Chemistry* **2002**, *221*, 62-98.

(18) Gries, H., Extracellular MRI contrast agents. *Topics in Current Chemsitry* **2002**, *221*, 2-23.

(19) Lauffer, R. B., Paramagnetic metal complexes as water proton relaxation agents for NMR imaging: Theory and Design. *Chemical Review* **1987**, *87*, 901-927.

(20) Meade, T. J.; Taylor, A. K.; Bull, S. R., New magnetic resonance contrast agents as biochemical reporters. *Current Opinions in Neurobiology* **2003**, *13*, 597-602.

(21) Frullano, L.; Meade, T. J., Multimodal MRI Contrast Agents. *Journal of Biological Inorganic Chemistry* **2007**, *12*, 939-949.

(22) Lowe, M. P., Activated MR Contrast Agent. *Current Pharmaceutical Biotechnology* **2004**, *5*, 519-528.

(23) Moats, R. M.; Fraser, S. E.; Meade, T. J., A Smart Magnetic Resonance Imaging Contrast Agent That Reports on Enzymatic Activity. *Angewandte Chemie International Edition* **1997**, *36*, 726.

(24) Louie, A.; Huber, M.; Ahrens, E.; Jacobs, R. E.; Fraser, S. E.; Meade, T. J., In-vivo Visualization of Gene Expression by Magnetic Resonance Imaging. *Nature Biotechnology* **2000**, *18*, 321-325.

(25) Urbanczyk-Pearson, L. M.; Femia, F. J.; Smith, J.; Parigi, G.; Eckermann, A. L.; Duimstra, J. A.; Luchinat, C.; Meade, T. J., Mechanistic Investigation of ¾-Galactosidase-Activated MR Contrast Agents. *Inorganic Chemistry* **2008**, *47*, 56-68.

(26) Asp, N. G.; Dahlqvist, A. *Analytical Biochemistry* **1971**, *42*, 275-278.

(27) Yamamoto, A.; Adachi, S.; Kawamura, S.; Takahashi, M.; Kitani, T., Localized beta-galactosidase deficiency. Occurrence in cerebellar ataxia with myoclonus epilepsy and macular cherry-red spot--a new variant of GM1-gangliosidosis?. *Archives of Internal Medicine* **1974**, *134*, 627-634.

(28) Duimstra, J. A.; Femia, F. J.; Meade, T. J., A gadolinium chelate for detection of beta-glucuronidase: A self-immolative approach. *Journal of the American Chemical Society* **2005**, *127*, 12847-12855.

(29) Guerquin-Kern, J.; Volk, A.; Chenu, E.; Lougerstay-Madec, R.; Monneret, C.; Florent, J.; Carrez, D.; Croisy, A., Direct in vivo observation of 5-fluorouracil release from a prodrug in human tumors heterotransplanted in nude mice: a magnetic resonance study. *NMR in Biomedicine* **2000**, *13*, 306-310.

(30) Swift, T. J.; Connick, R. E. J., NMR-Relaxation Mechanisms of O^{17} in Aqueous Solutions of Paramagnetic Cations and the Lifetime of Water Molecules in the First Coordination Sphere. *Journal of Chemical Physics* **1962**, *37*, 307.

(31) Fowler, A. V.; Zabin, I., The amino acid sequence of beta-galactosidase of Escherichia Coli. *Proceedings of the National Academy of Sciences of the United States of America USA* **1977**, *74*, 1507-1510.

(32) Aich, S.; Delbaere, L. T. J.; Chen, R., Continuous Spectrophotometric Assay for beta-Glucuronidase. *Biotechniques* **2001**, *30*, 846-850

(33) Voet, D.; Voet, J. G. *Biochemistry*; Second ed.; John Wiley and Sons, INC.: New Jersey, 1995.

(34) Supkowski, R. M.; Horrocks, W. D., On the determination of the number of water molecules, q, coordinated to europium(III) ions in solution from luminsecence decay lifetimes. *Inorganica Chemica Acta* **2002**, *340*, 44-48.

(35) Bruce, J. I.; Dickins, R. S.; Govenlock, L. J.; Gunnlaugsson, T.; Lopinski, S.; Lowe, M. P.; Parker, D.; Peacock, R. D.; Perry, J. J. B.; Aime, S.; Botta, M., The selectivity of reversible oxy-anion binding in aqueous solution at a chiral europium and terbium center: Signaling of carbonate chelation by changes in the form and circular polarization of luminescence emission. *Journal of the American Chemical Society* **2000**, *122*, 9674-9684.

(36) Bretonniere, Y.; Cann, M. J.; Parker, D.; Slater, R., Design, synthesis and evaluation of ratiometric probes for hydrogencarbonate based on europium emmission. *Organic and Biomolecular Chemistry* **2004**, *2*, 1624-1632.

(37) Parker, D. *In Crown Compounds: Towards Future Applications*; VCH: New York, NY, 1992.

(38) Supkowski, R. M.; Horrocks, W. D., Displacement of inner-sphere water molecules from Eu3+ analogues of Gd3+ MRI contrast agents by carbonate and

phosphate anions: Dissociation constants from luminescence data in the rapid-exchange limit. *Inorganic Chemistry* **1999**, *38*, 5616-5619.

(39) Dickins, R. S.; Gunnlaugsson, T.; Parker, D.; Peacock, R. D., Reversible Anion Binding in aqueous solution at cationic heptacoordinate lanthanide centre: selective bicarbonate sensing by time-delay luminescence. *Chemical Communication* **1998**, 1643-1644.

(40) Toth E.; Dhubhaill, O.M,; Besson, G.; Helm, L.; Merbach, A.E., Coordination equilibrium - a clue for fast water exchange on potential magnetic resonance imaging contrast agents?. *Magnetic Resonance in Chemistry* **1999**, *37*, 701-708.

(41) Aime, S.; Barge, A.; Botta, M.; Howard, J. A.; Kataky, R.; Lowe, M. P.; Moloney, J. M.; Parker, D.; de Sousa, A. S., Dependence of the relaxivity and luminescence of gadolinium and europium amino-acid complexes on hydrogencarbonate and pH. *Chemical Communication* **1999**, 1047-1048.

(42) Aime, S.; Botta, M.; Geninatti Crich, S.; Giovenzana, G.; Pagliarin, R.; Sisti, M. Terreno, E., NMR relaxation Studies of Gd(III) complexes with hetadentate macrocyclic ligands. *Magnetic Resonance in Chemistry* **1998** S200-S208.

(43) Laus, S.; Ruloff, R.; Toth, E.; Merbach, A. E., Gd(III) complexes with fast water exchange and high thermodynamic stability: potential building blocks for high - relaxivtiy MRI contrast agent. *Chemistry: A European Journal* **2003**, *9*, 3555-3566.

(44) Baggett, N.; Case, M.; Barby, P. R.; Gray, C. J., 7-beta-D-Galactopyranosyloxycoumarin-4-acetic acid and its methyl ester as substrates for the beta-D-galactosidase of Escherichia Coli. *Carbohydrate Research* **1990**, *197*, 295-301.

(45) Alauddin, M. M.; Louie, A. Y.; Shahinian, A.; Meade, T. J.; Conti, P. S., Receptor mediated uptake of a radiolabeled contrast agent sensitive to beta-galactosidase activity. *Nuclear Medicine and Biology* **2003**, *30*, 261-265.

(46) Kim, Y. R.; Savellano, M. D.; Savellano, D. H.; Weissleder, R.; Bogdanov, A. A., Measurement of tumor interstitial volumne fraction: method and implication for drug delivery. *Magnetic Resonance in Medicine* **2004**, *52(3),* 485-494.

Chapter 3:

(1) Fisher, E.H.; Charbonneau, H.; Tonks, N.K., Protein tyrosine phosphatases: a diverse family of intracellular and transmembrane enzymes. *Science* **1991**, *253*, 401-406.

(2) Cyert, M. S.; Thorner, J., Putting it on and taking it off: phosphoprotein phosphatase involvement in cell cycle regulation. *Cell* **1989**, *57*, 891.

(3) Stoker, A. W., Isoforms of a novel cell adhesion molecule-like protein tryosine phosphatase are implicated in neural development *Mechanisms of Development* **1994**, *46*, 201.

(4) Ostman, A.; Hellberg, C.; Bohmer, F. D., Protein-tyrosine phosphatases and cancer. *Nature Reviews* **2006**, *6*, 307-320.

(5) Alexander, D. R., The role of phosphatases in signal transduction. *New Biologist* **1990**, *2*, 1049.

(6) Myers, J. K.; Cohen, J. D.; Widlanski, T. S., Substituent effects on the mechanism-based inactivation of prostatic acid phosphatase. *Journal of the American Chemical Society* **1995**, *117*, 11049-11054.

(7) Lauffer, R. B.; McMurry, T. J.; Dunham, S. O.; Scott, D. M.; Parmelee, D. J.; Dumas, S. In *WO patent 9736619*, 1997.

(8) Lowe, M. P., Activated MR Contrast Agent. *Current Pharmaceutical Biotechnology* **2004**, *5*, 519-528.

(9) Woods, M.; Kiefer, G. E.; Bott, S.; Castillo-Muzquiz, A.; Eshelbrenner, C.; Michaudet, L.; McMillan, K.; Mudiguda, S. D.; Orgin, D.; Tircso, G.; Zhang, S.; Zhao, P.; Sherry, D. A., Synthesis, relaxometric, and photophysical properties of a new pH-responsive MRI contrast agent: The effect of other ligating groups on

dissociation of a p-nitrophenolic pendant arm. *Journal of the American Chemical Society* **2004**, *126*, 9248-9256.

(10) Li, W. H.; Parigi, G.; Fragai, M.; Luchinat, C.; Meade, T., Mechanistic studies of a calcium-dependent MRI contrast agent. *Inorganic Chemistry* **2002**, *41*, 4018-4024.

(11) Li, W. H.; Fraser, S. E.; Meade, T. J., A calcium-sensitive magnetic resonance imaging contrast agent. *Journal of the American Chemical Society* **1999**, *121*, 1413-1414.

(12) Lowe, M. P.; Parker, D.; Reany, O.; Aime, S.; Botta, M.; Castellano, G.; Gianolio, E.; Pagliarin, R., pH-Dependent Modulation of Relaxivity and Luminescence in Macrocyclic Gadolinium and Europium Complexes Based on Reversible Intramolecular Sulfonamide Ligation. *Journal of the American Chemical Society* **2001**, *123*, 7601-7609.

(13) Bretonniere, Y.; Cann, M. J.; Parker, D.; Slater, R., Design, synthesis and evaluation of ratiometric probes for hydrogencarbonate based on europium emmission. *Organic and Biomolecular Chemistry* **2004**, *2*, 1624-1632.

(14) Parker, D. *In Crown Compounds: Towards Future Applications*; VCH: New York, NY, 1992.

(15) Supkowski, R. M.; Horrocks, W. D., On the determination of the number of water molecules, q, coordinated to europium(III) ions in solution from luminsecence decay lifetimes. *Inorganica Chemica Acta* **2002**, *340*, 44-48.

(16) Bruce, J. I.; Dickins, R. S.; Govenlock, L. J.; Gunnlaugsson, T.; Lopinski, S.; Lowe, M. P.; Parker, D.; Peacock, R. D.; Perry, J. J. B.; Aime, S.; Botta, M., The selectivity of reversible oxy-anion binding in aqueous solution at a chiral europium and terbium center: Signaling of carbonate chelation by changes in the form and circular polarization of luminescence emission. *Journal of the American Chemical Society* **2000**, *122*, 9674-9684.

(17) Caravan, P.; Ellison, J. J.; McMurry, T. J.; Lauffer, R. B., Gadolinium chelates as MRI contrast agents: Structure, Dynamics, and Applications. *Chemical Review* **1999**, *92*, 2293-2352.

(18) Aime, S.; Barge, A.; Botta, M.; Howard, J. A.; Kataky, R.; Lowe, M. P.; Moloney, J. M.; Parker, D.; de Sousa, A. S., Dependence of the relaxivity and luminescence of gadolinium and europium amino-acid complexes on hydrogencarbonate and pH. *Chemical Communication* **1999**, 1047-1048.

(19) Swift, T. J.; Connick, R. E. J., NMR-Relaxation Mechanisms of O^{17} in Aqueous Solutions of Paramagnetic Cations and the Lifetime of Water Molecules in the First Coordination Sphere. *Journal of Chemical Physics* **1962**, *37*, 307.

Chapter 4:

(1) Merbach A,E,; Toth, E.; *The Chemistry of Contrast Agents in Medical Magnetic Resonance Imaging*, John Wiley & Sons, Ltd. New York, **2001**.

(2) Caravan, P.; Ellison, J. J.; McMurry, T. J.; Lauffer, R. B., Gadolinium chelates as MRI contrast agents: Structure, Dynamics, and Applications. *Chemical Review* **1999**, *92*, 2293-2352.

(3) Wulfsberg, G.; *Inorganic Chemistry*, University Science Books. Sausalito, **2000**.

(4) Aime, S.; Geninatti, S.; Crich, S. G.; Gianolio, E.; Giovenzana, G. B.; Teia, L.; Terreno, E., High sensitivity lanthanide(III) based probes for MR-medical imaging. *Coordination Chemistry Reviews* **2006**, *250*, 1562-1579.

(5) Li, W.; Fraser, S.E.; Meade, T.J., A calcium-sensitive magnetic resonance imaging contrast agent. *Journal of the American Chemical Society* **1999**, *121*, 1413-1414.
Li, W.; Parigi, G.; Gradai, M.; Luchinat, C.; Meade T.J., Mechanistic studies of a calcium-dependent MRI contrast agent. *Inorganic Chemistry* **2002**, *41*, 4018-4024.

(6) Hanaoka, K.; Kikuchi, K.; Urano Y.; Nagano, T. Selective Sensing of Zinc ions with Novel Magnetic Renonance Imaging Contrast agent. *Journal of the Chemical Society: Perkin Transactions* **2001**, *2*, 1840-1843.
Hanaoka, A.; Kikuchi, K.; Urano, Y.; Narazaki, M.; Yokawa, T.; Sakamoto, S.; Yamaguchi, K.; Nagano, T., Design and Synthesis of a Novel Magnetic Resonance Imaging Contrast agent for Selective sensing of Zinc Ion. *Chemistry and Biology* **2002**, *9*, 1027-1032.

(7) Louie, A.; Huber, M.; Ahrens, E.; Jacobs, R. E.; Fraser, S. E.; Meade, T. J., In-vivo Visualization of Gene Expression by Magnetic Resonance Imaging. *Nature Biotechnology* **2000**, *18*, 321-325.

(8) Moats, R. M.; Fraser, S. E.; Meade, T. J., A Smart Magnetic Resonance Imaging Contrast Agent That Reports on Enzymatic Activity. *Angewandte Chemie International Edition* **1997**, *36*, 726.

(9) Merbach A,E,; Toth, E.; *The Chemistry of Contrast Agents in Medical Magnetic Resonance Imaging*, John Wiley & Sons, Ltd. New York, **2001**.

(10) Guerquin-Kern, J.; Volk, A.; Chenu, E.; Lougerstay-Madec, R.; Monneret, C.; Florent, J.; Carrez, D.; Croisy, A., Direct in vivo observation of 5-fluorouracil release from a prodrug in human tumors heterotransplanted in nude mice: a magnetic resonance study. *NMR in Biomedicine* **2000**, *13*, 306-310.

(11) Meade, T., Seeing is believing. *Academic Radiology* **2001**, *8*, 1-3

Addendum:

(1) Edwards, B. K.; Howe, H. L.; Ries, L. A.; Thun, M. J.; Rosenberg, H. M.; Yancik, R.; Wingo, P. A.; Jemal, A.; Feigal, E. G., Annual report to the nation on the status of cancer, 1973–1999, featuring implications of age and aging on U.S. cancer burden. *Cancer Research* **2002**, *94*, 2766-2792.

(2) Edwards, B. K.; Howe, H. L.; Reichman, M. E.; Kohler, B. A.; Ajani, U. A.; Cardinez, C. J.; King, J. B.; Stewart, S. L.; Thompson, T. D.; Weir, H. K.; Anderson, R. N. *U.S. Department of Health and Human Services; Centers for Disease Control and Prevention and National Cancer Institute* **2007**.

(3) Parkin, D. M.; Bray, F.; Ferlay, J.; Pisani, P., Estimating the world cancer burden: Globocan 2000. *International Journal of Cancer* **2001**, *94* 153 - 156.

(4) Robbins, S. L.; Cotran, R. S. *Pathologic Basis of Disease*; 7th ed.; Elsevier Saunders: Philadelphia, Pennsylvania, 2005.

(5) Matsumoto, T.; Mugishima, H., Signal transduction via vascular endothelial growth factor (VEGF) receptors and their roles in atherogenesis. *Journal of Atherosclerosis and Thrombosis* **2006**, *13*, 130-135.

(6) Deryugina, E. I.; Quigley, J. P., Matrix metalloproteinases and tumor metastasis. *Cancer and Metastasis Review.* **2006**, *25*, 9-34.

(7) Voet, D.; Voet, J. G. *Biochemistry*; Second ed.; John Wiley and Sons, INC.: New Jersey, 1995.

(8) Hirsch, J., An anniversary for cancer chemotherapy. *Journal of the American Medical Association* **2006**, *296*.

(9) Joensuu, H., Systemic chemotherapy for cancer: from weapon to treatment. *Lancet Oncology* **2008**, *9*, 304.

(10) Goodman, L. S.; Wintrobe, M. M.; Dameshek, W.; Goodman, M. J.; Gilman, A.; McLennan, M. T., Nitrogen mustard therapy. *Journal of the American Medical Association* **1946**, *132*, 26-32.

(11) Goodman, L. S.; Wintrobe, M. M.; Dameshek, W.; Goodman, M. J.; Gilman, A.; McLennan, M. T., Nitrogen mustard therapy. *Journal of the American Medical Association* **1946**, *132*, 26-32.

(12) Hartley, J. A.; Bingham, J. P.; Souhami, R. L., DNA sequence selectivity of guanine-N7 alkylation by nitrogen mustards is preserved in intact cells . *Nucleic Acids Research* **1992**, *20*, 3175-3178.

(13) Duchovic, R. J.; Vilensky, J. A., Mustard Gas: Its Pre-World War I History. *Journal of Chemical Education* **2007**, *84*, 944.

(14) Bauer, G. B.; Povirk, L. F., Specificity and kinetics of interstrand and intrastrand bifunctional alkylation by nitrogen mustards at a G-G-C sequence. *Nucleic Acids Research* **1997**, *25*, 1211–1218.

(15) Lawley, P. D.; Brookes, P., Cytotoxicity of Alkylating Agents *Biochemical Journal* **1968**, *109*, 433-447.

(16) Caravan, P.; Ellison, J. J.; McMurry, T. J.; Lauffer, R. B., Gadolinium chelates as MRI contrast agents: Structure, Dynamics, and Applications. *Chemical Review* **1999**, *92*, 2293-2352.

(17) Aime, S.; Botta, M.; Fasano, M.; Terreno, E., Lanthanide (III) chelates for NMR biomedical applications. *Chemical Society Review* **1998**, *27*, 19-29

(18) Toth, E.; Helm, L.; Merbach, A. E., Relaxivity of MRI contrast agents. *Topics in Current Chemistry* **2002**, *221*, 62-98.

(19) Merbach, A. E.; Toth, E., Eds. *The Chemistry of Contrast Agents in Medical Magnetic Resonance Imaging*; 1 ed.; John Wiley & Sons, LTD.: West Sussex, England, 2001.

Appendix:

Swift-Connick Equation used in Origin to determine τ_M:

```
F=90;s=3.5;univ=8.31;wi=6.28e6*F*0.13557;ws=6.28e6*F*658.21;tm=((tm0^(-
1)*x/298.15)*exp((Hm/univ)*(0.003354-(1/x))))^-1;tr=((tr0^(-
1)*x/298.15)*exp((Hr/univ)*(0.003354-(1/x))))^-1;tv=((tv0^(-
1)*x/298.15)*exp((Hv/univ)*(0.003354-(1/x))))^-1;T1e=((1/25)*delta*tv*(4*s^2+4*s-
3)*((1/(1+ws^2*tv^2))+(4/(1+4*ws^2*tv^2))))^-1;T2e=((0.02*(4*s^2+4*s-
3)*tv*delta*(3+(5/(1+(ws^2*tv^2)))+(2/(1+(4*ws^2*tv^2))))))^(-1);tc1=(T1e^(-1)+tr^(-
1)+tm^(-1))^(-1);tc2=(T2e^(-1)+tr^(-1)+tm^(-1))^(-1);te1=(T1e^-1+tm^-1)^(-
1);te2=(T2e^(-1)+tm^(-1))^(-
1);cont=(1/3)*s*(s+1)*acc^2*(te1+(te2/(1+ws^2*te2^2)));dip1=((1/15)*4.535671e-
33*s*(s+1))/(r^6);dip2=4*tc1;dip3=(13*tc2)/(1+ws^2*tc2^2);dip4=(3*tc1)/(1+wi^2*tc1
^2);dip9=1.6995e14*0.32;dip5=(0.2*tr)/(1+wi^2*tr^2);dip6=(0.8*tr)/(1+4*wi^2*tr^2);di
p7=(2/5)*(wi^2*1.1890597e-79*s^2*(s+1)^2)/(9*1.9063324e-
32*x^2*r^6);dip8=(3*tc1)/(1+wi^2*tc1^2);dip=dip1*(dip2+dip3+dip4);quad=dip9*(dip5
+dip6);cur=dip7*dip8;diptot=dip+cur+quad;T2m=(cont+diptot)^-
1;gauss=F*1e6/4255.319;dwm=(1.856953e-20*s*(s+1)*acc*gauss)/(3*1.3807e-
16*x);num=(T2m^-2)+(T2m*tm)^-1+dwm^2;denom=(tm^-1+T2m^-
1)^2+dwm^2;scam=num/denom;pm=n*conc/55.56;y=pm*scam/tm
```